VILNIUS UNIVERSITY
CENTER FOR PHYSICAL SCIENCES AND TECHNOLOGY

Akvilė
ZABILIŪTĖ-KARALIŪNĖ

Spectral Engineering of Phosphor Converted Light-Emitting Diodes

DOCTORAL DISSERTATION
Technological sciences
Materials engineering 08 T

VILNIUS 2019

This dissertation was written between 2013 and 2019 at Vilnius University, Institute of Photonics and Nanotechnology. The research was supported by the Research Council of Lithuania.

Academic supervisor:
Prof. Habil. Dr. Artūras Žukauskas (Vilnius University, Technological sciences, Materials engineering, 08 T)

Acknowledgement

First of all I would like to thank my supervisor prof. habil. dr. Artūras Žukauskas for giving me the opportunity to work in this interesting field and helping to improve my scientific and writing skills. I would also like to give my gratitude to dr. Pranciškus Vitta, who helped me to carry the photoluminescence decay measurements in frequency domain, gave me valuable advices and consulted during the studies.

I thank dr. Skirmantė Butkutė, who was my collaborator and performed the synthesis as well as structural and morphological analysis of the samples that were investigated in this work. I am also grateful to prof. Rimantas Vaicekauskas, who has performed the computer optimization and modelling, which was very useful for my work.

I would also like to thank prof. dr. Roland Tomašiunas who supervised my work during the bachelor and master studies, taught me a lot of useful things and gave me many valuable advices. I am grateful to prof. Živilė Lukšienė for providing Perkin Elmer fluorimeter used for the photoluminescence measurements.

The work was done much faster due to the help of my students. I want to give a special thanks to Henrikas Dapkus, who contributed a lot to the production of solid state luminary prototypes. I also want to thank Justina Aglinskaitė and Vladislovas Čižas who made the long (or short) working hours more interesting by discussing or chatting.

Thanks a lot to my colleagues, who at some point helped me, consulted me, gave me advices, had valuable scientific discussions or simple chats, which are: Andrius Petrulis, dr. Arūnas Tuzikas, Laurynas Dabašinskas, and Justas Trimailovas. A special thanks for Paulius Baronas who helped me to carry out the PL measurements with Edinburgh spectrometer.

I also want to give my gratitude to our PhD lunch club, which made lunch breaks much more fun: dr. Jonas Jurkevičius, dr. Lina Skardžiūtė, dr. Steponas Raišys, Donatas Meškauskas, dr. Vytautas Klimavičius, and dr. Tomas Serevičius.

Thanks so much for my rock band, for supporting me and forgiving me for all the rehearsals I have skipped during the dissertation writing process:

Krešas, Pričkus, Falšas, Tango, and Inkaras. Thanks for musical artists all around the world for creating music. Listening to Daft Punk, Muse, the Clash, Thievery Corporation, and Morcheeba made the writing process of the dissertation much more pleasant.

Sitting in the office and writing or working in the dark lab all day is sure tiring. Therefore, I want thank Vilnius University Kendo Club where I could have a rest from science, do some sports and practice kendo. For this opportunity I am grateful for my kendo friends: Raminta, Roberta, Vaida, Egidija, Mona, Viktorija, Edvardas, Jurgita, Danas, Pawel, Liza, Gytis, Mindaugas, Aurimas; Instructors: Mykolas, Marius, Vytenis, Kastytis; and of course for our teacher Haga-sensei.

I would like to thank my childhood, school, and university friends for their support: Eglė – aka kaimynka, Kamilė, Gabija, Diana, Justina, and Muckus. Special thanks to my dear friend dr. Laura Vilkaitė for scientific discussions, support and understanding. I also thank my teachers, who have taught me and shown, that physics is a very interesting science. I am also very grateful to my FiDi mates, because FiDi makes studies much more exciting and fun.

Thanks a lot to my family for the support: my grandparents, my mother-in-law, sisters-in-law and their families. A special thanks for my dear parents Nijolė and Bronius for helping me during my studies and for the belief in me. I am also very grateful for my big sister dr. Emilija Zabiliūtė, who would always cheer me up and share the #hownottostresswhilewritingthesis type of advices.

A special thanks for my beloved husband and son: dr. Mindaugas Karaliūnas and Kostas. Your love and support was the main engine pushing me forward.

Finally, I would like to thank a lot for all participants that attended the psychophysical experiment. You are a part of science now.

This research was partly funded by grants (DOK-17209, P-DOC-17-144, P-DAP-18-140) from the Research Council of Lithuania.

The major part of this work was done using the open source software: Ubuntu, Lubuntu, GNU Octave, Qti Plot, Libre Office, Engauge Digitizer, TEX studio; This dissertation was prepared using LATEX.

Contents

List of abbreviations

BAM	Barium magnesium aluminate, $BaMgAl_{10}O_{17}$
CAF	Circadian action factor
CCT	Correlated colour temperature
CDI	Colour dulling index
CFI	Colour fidelity index
CIE	International Commission on Illumination
CQS	Colour quality scale
CRI	Colour rendering index
CSI	Colour saturation index
EL	Electroluminescence
FWHM	Full width at half maximum
GGG	Gadolinium gallium garnet, $Gd_3Ga_5O_{12}$
GSGG	Gadolinium scandium gallium garnet, $Gd_3Sc_2Ga_3O_{12}$
HDI	Hue distortion index
HID	High intensity discharge lamp
HPS	High pressure sodium lamp
LD	Laser diode
LDI	Luminance distortion index
LED	Light-emitting diode
LER	Luminous efficacy of radiation
LGG	Lutetium gallium garnet, $Lu_3Ga_5O_{12}$
MesoLED	Mesopic light-emitting diode
pcLED	Phosphor converted light-emitting diode
PL	Photoluminescence
PLE	Photoluminescence excitation
PMMA	Poly(methyl methacrilate)
PrefLED	Light-emitting diode of colour preference
PVC	Polyvinyl chloride
RHT	Retinohypothalamic tract
QE	Quantum efficiency
SCN	Supraciasmatic nucleus
SEM	Scanning electron microscope
SiAlON	Oxonitridoaluminosilicate
SiON	Oxonitridosilicate
SPD	Spectral power distribution
UV	Ultraviolet
XRD	X-ray diffraction
YAG	Yttrium aluminium garnet, $Y_3Al_5O_{12}$
YGG	Yttrium gallium garnet, $Y_3Ga_5O_{12}$
YMASG	Yttrium magnesium aluminium silicon garnet $Y_3Mg_2AlSi_2O_{12}$

Introduction

Due to the constantly increasing world energy demand, air and water pollution, and the decreasing amount of fossil fuels, scientists keep searching for the ways to save energy. Around 19% of energy consumed in the world is used for lighting applications [1]. For this reason, the old inefficient light sources are rapidly being changed by new and energy saving ones. Since the efficiency of light-emitting diodes (LEDs) has already surpassed that of other luminaries such as incandescent or fluorescent lamps, LEDs became the most attractive sources for new lighting installations [2]. Moreover, LEDs have many efficiency non-related advantages over other light sources – they are compact, robust, resistant to cold, can be dimmed or rapidly switched on and off, thus being suitable for Li-Fi (also known as light fidelity) applications [3]. Nevertheless, probably one of the main advantages of LED technology is the ability to engineer the shape of their spectral power distribution (SPD) regarding to the applications [2, 4, 5]. For this reason, LEDs are widely applied as the indicator lamps on electronic devices, exit signs in the buildings, car turn lights, traffic signals and lights, design elements in architecture or interior, etc. [4, 5]. A schematic drawing of a direct emission LED is presented in Fig. 0.1 (a). The LED chip (1) placed inside a reflector (2) is connected to metal terminals (3) via wires (4) and encapsulated in epoxy resin (5). This kind of LEDs emit only a single colour of light (6). As a result, in order to get white light, clusters of different colour direct emission LEDs are used. The most popular one is the RGB cluster which consists of a red, green and blue chips. Although widely applied for computers or TV screens back-lights, these clusters are not suitable for the general lighting applications due to increased colour saturation [6].

Another way to obtain white light is to combine LEDs with light converting photoluminescent materials called phosphors. Such LEDs are known as phosphor-converted LEDs (pcLEDs) [7]. A schematic drawing of a white partial conversion pcLED is presented in fig 0.1 (b). Here it is seen that a part of the blue light (6) is absorbed by phosphor particles (7) (e.g. yttrium aluminium garnet doped with Ce^{3+} (YAG)) within silicone or epoxy resin (8) and converted to yellow light (9). The remaining blue light (10) is scat-

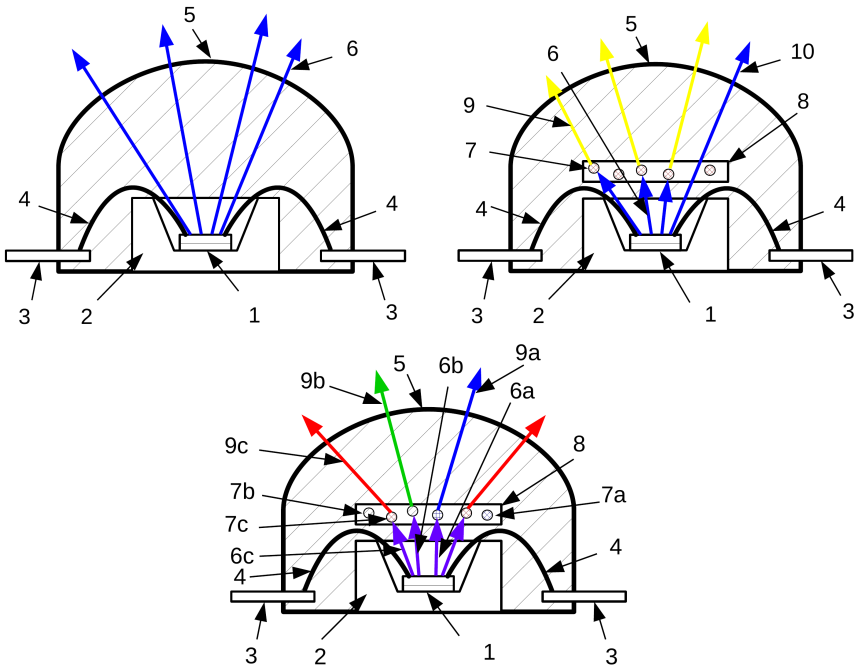

Figure 0.1: Schematic drawings of: (a) direct emission LED; (b) partial conversion pcLED; (c) full conversion pcLED [**VI,VII**].

tered and diffused by phosphor particles and mixes with yellow photoluminescence (PL) emitted by the phosphor thus creating white light. However, the SPD of such light source consists of only two components; therefore, it is characterized by a high correlated colour temperature (CCT), low colour rendition properties and colour dulling [4]. Nowadays in order to overcome this problem, phosphor blends of 2 different phosphors are applied for general lighting applications. Such light sources can be of different CCT values and render colours with high fidelity [5].

White light also can be generated via full conversion using an ultraviolet (UV) LED and three different phosphors. This type of LED is called full conversion pcLED and its schematic drawing is presented in fig. 0.1 (c). Here, the emitted UV light (6 a,b, and c) is absorbed by blue (7a), green (7b), and red (7c) phosphor particles and converted to a blue (9a), green (9b), and red (9c) light, respectively. The mix of these three components is perceived as white light. Despite the good colour rendition parameters caused by the broad PL components composing SPDs of such light sources, this technology is not widely applied for general lighting due to the small efficiency of UV LEDs, reabsorption of phosphor PL in other phosphors, losses arising from the Stokes shift as well as the degradation of phosphor

binding materials and plastic encapsulant [4]. Full conversion is applied in niche applications to produce lime and amber LEDs in order to fill the *green gap* arising from the lack of the materials suitable for efficient electroluminecence (EL) in the green-yellow spectral region [8]. pcLEDs have many advantages over the direct emission LED clusters – they are characterized by better colour rendition parameters, are easier to install, do not require complicated optics for colour mixing and, unlike direct emission LEDs where different wavelength emitters need different driving current, can be driven by a single current source.

The ability to compose different SPDs of solid state light sources creates challenges in finding the optimal ones. Current SPD engineering of LEDs is usually focused on achieving a high colour fidelity score R_f [9] or high colour rendering index (CRI) R_a [10] as well as the luminous efficacy of radiation (LER) due to energy saving reasons [11]. However, it is widely known that people tend to choose lighting with a slight colour saturation ability [6, 12, 13, 14]. Superior LEDs could be produced by enriching their SPDs with different colour components. The visual parameters of such light sources should be evaluated not only in terms of colour fidelity, but other colour rendition parameters like colour saturation, dulling or preference, have to be taken into account. These parameters were already optimized for the clusters of direct emission LEDs [15].

LEDs characterized by colour saturation, could be used for medical application whereas those of preferential colour rendition would be perfect for home, work or commercial lighting. However, due to a significant amount of blue light in their SPDs, such LEDs cause light pollution thus negatively affecting human health and environment [16] and for these reasons are not suitable for nocturnal applications such as street lighting. The connection between blue light and human physiological activity was already known in the last century, and in the year 2001 Brainard and Thapan have proven that the blue light detected by the ganglion cells in the eye and transferred to brain, suppresses the production of melatonin, which is sleep hormone and oncostatic agent [17, 18]. This means that the exposure to blue rich light in the evenings or at night may cause the disruption of the human circadian rhythm, i.e. the internal biological clock. Moreover, research shows that the improper lighting, shift work or other actions that supresses the melatonin secretion may cause various diseases such as insomnia, depression, or even cancer [19, 20]. The importance of human circadian rhythm was highlighted in 2017, as the Nobel prize in Physiology or Medicine was awarded jointly to Jeffrey C. Hall, Michael Rosbash and Michael W. Young “for their discov-

eries of molecular mechanisms controlling the circadian rhythm" [21]. For this reason, it is of importance to take human physiology into account while designing light sources, especially those used during the evening or at night.

Solid state light sources find the application not only in general lighting but also in other areas. As the world food demands grow, greenhouses are getting more popular and direct emission or pcLEDs could easily find application in this area [22, 23, 24]. Recently the most popular light sources in greenhouses still are the high pressure sodium (HPS), high-intensity discharge (HID) or fluorescent lamps [25, 26]. However, they have many disadvantages over LEDs: first, they are less efficient; second, their SPDs cannot be modified and, therefore, they emit light in unnecessary spectral regions which is not absorbed by plant pigments. Moreover, most of these lamps create more dangerous working conditions since they require high driving voltage, are fragile and toxic. Solid state light sources are more advantageous since they are tiny and robust what makes it easier to create optimal lighting systems for plants. Also they are characterized by a longer lifetimes and require less maintenance than other type of light sources. Probably the main advantage is the one mentioned before – the ability to create an optimal SPD which contains only spectral components that are necessary for plants [4, 22, 23, 24, 27].

It is known that each kind of plant needs unique growing conditions, including lighting [28]. However in general, there are three main photophysiological processes in plants called phototropism, photosynthesis and photomorphogenesis which are responsible for the movement, nutrition and development of plant and require blue (400-500 nm), red (620-680 nm), as well as red and far-red (700-760 nm) light, respectively. Blue InGaN and red AlGaInP LEDs are known as well established, stable light sources and are widely used for horticultural lighting. However, far-red AlGaAs ones contain high amounts of aluminium and for this reason they are sensitive to humidity and temperature variations; besides they are characterized by fast degradation [29]. An organic LED composed of poly(N-vinylcarbazole) doped with Pt-tetraphenyltetrabenzoporphyrin was proposed as an alternative to inorganic far-red LEDs [30]. However, the peak of its SPD is shifted too much towards the infra-red (IR) part thus making the spectrum not optimal for horticultural applications. Another way to get far-red light is to use a partial or full conversion LEDs with phosphors. A good phosphor suitable for solid state lighting applications is usually defined by six criteria [31], briefly – the luminescence and excitation spectra should meet the requirements for lighting; the phosphor must show high efficiency and be

chemically, mechanically, and thermally stable. As a result, a phosphor for the plant photomorphogenesis should be characterized as an efficient material, excited by blue light and exhibiting a relatively broad PL band in the far-red region. Moreover, it should withstand the unfriendly greenhouse environment, i.e. be resistant to high humidity levels as well as temperature variations. Some common far-red phosphors are: $Ca_3MgSi_2O_8$:Eu^{2+},Mn^{2+}, $LiAlO_2$:Fe^{3+}, CaS:Yb^{2+}, and $CaGa_2S_4$:Mn^{2+} [32, 33]. However, most of them have PL excitation maxima in the UV region whereas $CaGa_2S_4$:Mn^{2+} is known to be unstable in water [32]. Meanwhile, garnet phosphors doped with different activators are known to exhibit strong luminescence in various wavelength ranges. Moreover, they are characterized by mechanical, chemical, and thermal stability [34]. A good example of a far-red garnet phosphor is yttrium aluminium garnet ($Y_3Al_5O_{12}$, YAG) doped with Cr^{3+} ions. This phosphor is described by efficient PL in the far-red region which is even enhanced by co-doping with Ce^{3+} ions [35, 36]. However, the PL spectrum of this particular phosphor is in the range between 680 and 720 nm which does not match the absorption spectrum peak of the far-red phytochrome – the plant pigment responsible for the process of photomorphogenesis. For this reason a phosphor host characterized by a weaker crystal field leading to a slightly longer PL wavelength is desirable.

This work consists of three parts dedicated to the application of pcLEDs in different areas: horticultural lighting, street lighting and lighting characterized by different colour rendition properties. In the first part, a concept of phosphor-converted solid state sources of light for greenhouses is discussed. Literature review gives the background of plant photobiology, briefly describes the synthesis methods of garnet materials and presents the PL mechanisms of different gallium garnets activated with Cr^{3+} ions. In this part the morphological and PL properties of gadolinium, gadolinium scandium, yttrium and lutetium garnets doped with different amounts of Cr^{3+} and annealed at different temperatures are presented and discussed. In the end of this part a prototype luminary meeting the photomorphogenetic needs of plants is presented.

The second part describes the non-visual effect of light on human circadian rhythm and presents an introduction to colour science. In this part a concept of photobiologically friendly mesopic sources for street lighting is presented which is based on the modelling and characterization of theoretical spectra. The chapter is finalized with a presentation of a patented pcLED prototype characterized by minimized circadian action.

The last part gives a more comprehensive analysis of the visual param-

eters of light and discusses different colour quality evaluation metrics. Here, a model for creating theoretical pcLED SPDs as well as their optimization in respect to different colour rendition properties (colour fidelity, colour saturation, colour dulling and colour preference) and LER is presented. The model is confirmed by composing theoretical SPDs using PL spectra of real commercial phosphors as well as by a patented prototype validated by a psychophysical experiment.

Goal of the dissertation

The goal of the dissertation is to develop theoretical SPDs of pcLEDs for niche applications such as greenhouse lighting, photobiologically friendly outdoor lighting and general lighting of preferential colour rendition as well as to design and characterize such pcLED luminary prototypes.

Tasks of the work

In order to reach the goal of the scientific work the following tasks were set:

1. To measure and investigate the PL properties of gadolinium, gadolinium scandium, yttrium and lutetium gallium garnet phosphors doped with Cr^{3+} and calcined at different temperatures.

2. To develop and characterize a pcLED luminary prototype for the control of plant photomorphogenesis with the spectral power distribution containing a far-red component in the 700-760 nm range.

3. To model and characterize theoretical SPDs of pcLED with low circadian action as well as to design and characterize a photobiologically friendly firelight pcLED prototype for outdoor lighting.

4. To verify the theoretical optimization model of pcLED SPDs characterized by high fidelity, colour saturation or colour preference by determining the colour rendition properties of the composite SPDs with the spectral components provided by commercial phosphors.

5. To design and characterize a pcLED luminary of preferential colour rendition and to validate it by means of a psychophysical experiment.

Novelty and importance of the work

The novelty of this work lies in the in the optimization and engineering of the SPD of pc LEDs for three application fields: horticulture, street lighting, and general lighting.

At the time of performing the research there were many solid state lighting options for the use in greenhouses such as HID, HPS, or direct emission LEDs. However, there were no greenhouse lighting solutions based on pcLEDs. The novelty of this part relies on the synthesis method of Cr^{3+} doped gallium garnets and their characterization as well as on the proposed new field of application – horticultural lighting with controlled photomorphogenesis of plants.

The novelty of the second part is the concept of a healthy street lighting which can be accomplished by finding the trade-off between non-visual effect on humans, on one hand, and the LER and colour quality, on the other hand. The novelty of this part is also verified by the patent of the Republic of Lithuania **VI**; as well as by an international PCT patent application **VII**.

The novelty of the third part is based on the verification of the theoretical optimization of SPDs of pcLEDs characterized by different colour rendition properties. The novelty also lies in the design of a pcLED luminary with preferential colour rendition properties, verified by a US patent and international PCT patent application **VIII**.

Key statements for defence

1. Sol-gel derived gadolinium, gadolinium-scandium, yttrium and lutetium gallium garnets doped with Cr^{3+} can be efficiently excited by blue light and exhibit a broad PL band in the far-red region. Moreover, no thermal quenching is observed in these phosphors at least up to 90 °C, meaning that they can be successfully applied for phosphor-converted light-emitting diodes meeting the photomorphogenetic needs of plants.

2. The two-component blue-orange spectral power distributions of the modelled light-emitting diodes and designed prototypes are characterized by small correlated colour temperatures, low circadian action factors, relatively high mesopic colour rendition indices and, therefore, are favourable for the use in photobiologically friendly mesopic outdoor lighting.

3. The modelling of composite spectral power distributions consisting of photoluminescence spectra of Eu^{2+} doped phosphors has shown that theoretical Gaussian shape spectral components can be used for the optimization purposes of phosphor converted light-emitting diodes characterized by high fidelity, colour saturation and colour preference.

4. The developed and psychophysically validated phosphor converted light-emitting diode luminaire of colour preference can be used in certain niche applications, which require enhanced attractiveness of illuminated objects.

Layout of the dissertation

Due to the broad topic of scientific work, the dissertation is divided into three chapters each covering a different application field and consisting of separate sections called Literature review, Experimental method and Results. The dissertation begins with the Introduction which shortly introduces to the research, defines the main terms and presents the significance ofthe topic. The first chapter "Phosphor converted light-emitting diodes for plants" is dedicated to the pcLEDs application in greenhouses. It describes the photobiological processes in plants, explains and presents the PL of far-red gallium garnet phosphors and introduces the pcLED luminary meeting the photomorphogenetic needs of plants. The second chapter "Phosphor converted light-emitting diodes with low circadian action for outdoor lighting" covers the non-visual effects of light on human circadian rhythm. It explains the basics of human physiology related to lighting and presents the solutions for photobiologically friendly street lighting. The chapter is finalized with the patented *firelight* pcLED prototype for street lighting characterized by low circadian action. The third chapter even is more devoted for colour science and compares various colour quality evaluation metrics. It presents the modelled SPDs of pcLEDs characterized by different colour rendition properties, i.e. high fidelity, colour saturation, colour dulling, and colour preference. The model is validated by a patented PrefLED prototype and a psychophysical experiment presented in the end of this chapter. The work is finalized with the Conclusions that summarize the entire work.

Contribution of the author

The author has made a major part of the experiments, calculations and analysis of the results. To begin with, the author has performed the diffuse reflection, PL excitation, PL, quantum efficiency, decay time, and PL dependence on the temperature measurements of gallium garnets. The cuvettes used as the holders for PL measurements were also produced by the author. The author has measured the PL spectra of commercial phosphors and performed the SPD modelling as well as the characterization of *firelight* and *preference* phosphor converted LEDs. The author has digitized over fifty PL spectra of various phosphors, and by calculating their peak wavelengths and full widths at half maximum has verified the theoretical model describing phosphor PL bands by Gaussian shape. The author has also designed and characterized the *firelight* and *preference* pcLED prototypes, organized the psychophysical experiment and analysed the results.

Besides the mentioned scientific work, the author has made a number of conference presentations, prepared the manuscripts of four research papers (**II, III, V, IX**), gathered and processed data for two research papers (**I, IV**) and has written the text, drew a part of the figures and made the translations of patents and patent applications (**VI, VII, VIII**).

However, a part of this research was done with the help of some colleagues and the supervisor. Besides consulting the author of this dissertation and providing with some useful advices or ideas, the supervisor prof. Artūras Žukauskas has contributed to the text and reviewed all publications and patent applications, as well as conference works prepared by the author.

The chemical synthesis, structural, and morphological analysis (XRD and SEM) of gallium garnets was performed at Vilnius University Faculty of Chemistry and Geosciences by dr. Skirmantė Butkutė during her Ph.D studies. The PL decay measurements of phosphors were carried out with the help of dr. Pranciškus Vitta from the Institute of Photonics and Nanotechnology, Vilnius University.

The PL measurements of YGG pellets, the development of pcLED luminaire for plants, the second *firelight* pcLED prototype and a big part of the phosphor concentration optimization for the prefLED prototype was done in collaboration with Henrikas Dapkus during his bachelor studies in the Faculty of Physics, Vilnius University.

The blue InGaN LED used for the first *firelight* pcLED prototype was designed by dr. Ignas Reklaitis in the Institute of Photonics and Nanotechnology, Vilnius University.

The computer optimization of the SPDs of pcLEDs characterized by different colour rendition properties was performed at the Faculty of Mathematics and Informatics, Vilnius University by prof. Rimantas Vaicekauskas.

Approbation of the research results

This section presents the lists of papers, patents and conferences related to the dissertation. In the doctoral dissertation the following papers are referred by Roman numbers in square brackets.

List of papers and patents related to the dissertation

I A. Žukauskas, R. Vaicekauskas, P. Vitta, A. Zabiliūtė, A. Petrulis, and M. Shur, Colour rendition engineering of phosphor-converted light-emitting diodes, Opt. Express **21**(22), 26642–26656 (2013).

II A. Zabiliūtė, A. Žukauskas, R. Vaicekauskas, P. Vitta, Phosphor converted LEDs with low circadian action for outdoor lighting, Opt. Lett. **39**(3), 563–566 (2014).

III A. Zabiliūtė, S. Butkutė, A. Žukauskas, P. Vitta, A. Kareiva, Sol-gel synthesized far-red Cr-doped garnet phosphors for phosphor-conversion LEDs that meet the photomorphogenetic needs of plants, Appl. Opt. **53**(5), 907–914 (2014).

IV S. Butkutė, A. Zabiliūtė, R. Skaudžius, P. Vitta, A. Beganskienė, A. Žukauskas, A. Kareiva, Sol–gel synthesis, characterization and study of substitution effects in different gallium-containing garnets, J. Sol-Gel Sci. Technol. **76**(1), 210–219 (2015).

V A. Zabiliūtė-Karaliūnė, H. Dapkus, R. P. Petrauskas, S. Butkutė, A. Žukauskas, A. Kareiva, Cr^{3+} Doped Yttrium and Gallium Garnet Phosphor for Phosphor-Conversion Light Emitting Diodes, Lith. J. Phys. **55**(3), 200–207 (2015).

VI A. Zabiliūtė, A. Žukauskas, R. Vaicekauskas, P. Vitta, "Fotobiologiškai draugiškas konversijos fosfore šviestukas", patent of Republic of Lithuania, No. 6215 (2015).

VII A. Zabiliūtė, A. Žukauskas, R. Vaicekauskas, P. Vitta, Photobiologically Friendly Phosphor Converted Light-Emitting Diode, PCT Patent App. No EP3060624 A1 (2016).

VIII A. Žukauskas, R. Vaicekauskas, P. Vitta, A. Tuzikas, A. Zabiliūtė, A. Petrulis, Solid-state sources of light for preferential colour rendition, USA Patent US9370072 B2, PCT Patent Appl. EP2962530 A1 (2016).

IX A. Zabiliūtė-Karaliūnė, H. Dapkus, P. Vitta, A. Petrulis, A. Žukauskas, Phosphor-Converted Light-Emitting Diodes of Preferential Color Properties, *Proceedings of 13th AIC Congress 2017* (Jeju, South Korea, 16th–20th, October, 2017) OS21. Conference paper.

List of conference contributions related to the dissertation

1. A. Zabiliūtė, R. Vaicekauskas, P. Vitta, A. Tuzikas, A. Petrulis, A. Žukauskas "Spektrinio galios skirstinio inžinerija konversijos fosfore šviestukuose, pasižyminčiuose įvairiomis spalvų atgavos savybėmis", The fourth conference of young scientists "Fizinių ir technologijos mokslų tarpdalykiniai tyrimai" (Vilnius, 11th, February, 2014) p. 46. Oral presentation.

2. A. Zabiliūtė, R. Vaicekauskas, P. Vitta, A. Tuzikas, A. Petrulis, and, A. Žukauskas, "Phosphor-Converted Light-Emitting Diodes with Advanced Color Rendition Properties" Conference on LED and Its Industrial Application "LEDIA'14", (Yokohama, Japan, 22–24th, April, 2014) p. 24p-LEDp6-32.

3. A. Zabiliūtė, S. Butkutė, A. Žukauskas, P. Vitta, A. Kareiva, "Far-Red Cr-Doped Garnets for the Control of Photomorphogenesis in Plants Using Phosphor-Conversion LEDs" Conference on LED and Its Industrial Application "LEDIA'14", (Yokohama, Japan, 22–24th, April, 2014) p. 22p-LED2-2. Oral presentation.

4. A. Zabiliūtė, S. Butkutė, A. Žukauskas, P. Vitta, A. Kareiva,"Far-Red Cr-doped Garnet Phosphor-Conversion LEDs that Meet the Photomorphogenetic Needs of Plants", 16th Int. Conf.-Scool "Advanced Materials and Technologies" Book of Abstracts (Palanga, Lithuania, 21–31st, August, 2014) p. 97. Best poster presentation award

5. H. Dapkus, A. Zabiliūtė-Karaliūnė, R. P. Petrauskas, S. Butkutė, A. Žukauskas, A. Kareiva, "Cr^{3+} Doped Ytrium and Gallium Garnet Phosphor for Phosphor-Conversion Light Emitting Diodes", 58th Scientific Conference for Young Students of Physics and Natural Sciences "Open Readings". Programme and Abstracts (Vilnius, 24–27, March, 2015) p. 228.

6. H. Dapkus, A. Zabiliūtė-Karaliūnė, P. Vitta, A. Žukauskas, "The Development and Characterization of Phosphor Converted LED Lamps for Niche Applications", 18th Int. Conf.-Scool "Advanced Materials and Technologies" Book of Abstracts (Palanga, Lithuania,27–31st, August, 2016) p. 82.

7. A. Zabiliūtė-Karaliūnė, H. Dapkus, P. Vitta, "Konversijos fosfore šviestukų, skirtų nišiniams taikymams, prototipavimas", The conference for Ph.D. students and young researchers "FizTeCh" (Vilnius, Lithuania, 26–27th, October, 2016) Oral presentation. Best presentation award.

8. H. Dapkus, A. Zabiliūtė-Karaliūnė, P. Vitta, "Development and characterization of phosphor converted LED lamps for niche applications," 60th Scientific Conference for Young Students of Physics and Natural Sciences "Open Readings". Programme and Abstracts (Vilnius, 14–17th, March, 2017) p. 72. Oral presentation.

9. A. Zabiliūtė-Karaliūnė, H. Dapkus, P. Vitta, A. Petrulis, A. Žukauskas, "The Design and Characterization of Phosphor-Converted LED Luminary of Preferential Colour properties", 19th Int. Conf.-School "Advanced Materials and Technologies" Book of Abstracts (Palanga, Lithuania, 27–31th, August, 2017) p. 81.

10. A. Zabiliūtė-Karaliūnė, H. Dapkus, P. Vitta, A. Petrulis, A. Žukauskas, "Pirmenybinėmis spalvinėmis savybėmis pasižyminčio konversijos fosfore šviestuko prototipavimas ir charakterizavimas" The 42nd Lithuanian National Conference of Physics, Programme and abstracts book, (Vilnius, 4–6th, October, 2017) p. S3-24.

11. A. Zabiliūtė-Karaliūnė, H. Dapkus, P. Vitta, A. Petrulis, A. Žukauskas, "Phosphor-Converted Light-Emitting Diodes of Preferential Color Properties", 13th AIC Congress "AIC 2017" Book of Abstracts (Jeju, South Korea, 16th–20th, October, 2017) p. 159. Oral presentation.

1 Phosphor converted light-emitting diodes for plants

This chapter is dedicated for the topic of solid state horticultural lighting. The literature review gives the information on the photobiological processes of plants and explains the PL mechanisms of garnet phosphors used for pcLEDs. Experimental part introduces the techniques that were used for this work, including the chemical synthesis of the samples, photoluminescence measurements and description of the design process of the solid state luminary for the plant growth. The last section gives the results of the work, such as properties of the investigated garnet materials and presents the characterization of the luminary prototype. The information and results provided in this chapter are based on Papers **III**, **IV**, and **V**.

1.1 Literature review

In this section a theoretical background necessary for understanding the photobiological processes in plants as well as the synthesis and working principles of light converting phosphors is presented. The first subsection introduces the main photobiological processes like photosynthesis, phototropism and photomorphogenesis and briefly discusses their importance for the growth and development of higher plants. Further goes the introduction on the synthesis methods of phosphor materials and the description of their chemical and physical properties with the emphasis on Cr(III) doped gallium garnets, which were studied in this research.

1.1.1 Photophysiological processes in plants

Greenhouses are an important facility for the human population, especially in Nordic countries, since they enable to grow fruit and vegetables despite the season or latitude and to harvest more than once a year. Moreover, the constantly growing population of humanity increases the demand for food, water, energy and other goods provided by our planet. There is no place to grow crops in densely populated cities and the transportation of food

from the outskirts is unsustainable, due to the "horizontal sprawl" of the world largest cities [37]. For this reason a "vertical farm" is becoming a very attractive concept. As defined by the ecologist D. Despommier, "the vertical farm is the mass cultivation of plant and animal life for commercial purposes in skyscrapers. Using advanced greenhouse technology such as hydroponics and aeroponics, the vertical farm could theoretically produce fish, poultry, fruit, and vegetables" [24]. An innovative lighting technology is also a very important component for the successful farming [37]. In the year 2009 LEDs were claimed to be a promising light source for the greenhouses [23] and they are still being research today letting for HPS and HID to lead in the area of horticultural lighting [25]. However, a recent study has shown that LEDs are ideal in luminous efficiency, life span and electricity usage if compared do HPS and CFL lamps [27] for this reason they are the main candidates for niche areas such as the vertical or space farming [37, 38].

In order to optimize the growth conditions it is important to customize the lighting according to the needs of plants. The light is absorbed by a number of various pigments in a plant that afterwards initiate different photophysiological processes. Three main such processes are phototropism – that is responsible for the movement of plants, photosynthesis – which supplies the plant with necessary carbohydrates, and photomorphogenesis – which is responsible for the development of plant. The pigments initiating these processes are, respectively, phototropin that absorbs light in the blue region (400–500 nm), chlorophyll that absorbs red light (620–680 nm), and phytochromes P_r and P_{fr} that absorb red and far-red (700–760 nm) light, respectively [39]. Much research has been done in order to determine the optimal SPDs of light sources for plants [23, 29, 40, 41] and the results are varying for each species. However, approximately optimal SPD for plants should consist of 75-87% of red light, 10-20% of blue light and 3-5% of far-red light [4]. Although the percentage of far-red light is negligible and seems unnecessary, it was shown that if an SPD of a light source lacks the far-red component, the plants are smaller, thinner and do not develop roots [29, 40]. Moreover, the same study has shown that by modifying the amount of far-red light the shape of plants can be controlled [29]. For this reason, in order to optimize the plant growth conditions, it is important to compose the right SPD containing all necessary components.

1.1.2 Synthesis of garnets

Depending what form of the phosphors are desired (single crystal, powder or ceramic), garnets can be synthesized by different methods. Single crystal materials are usually grown by Czochralski method. They are characterized by outstanding thermal properties since these type of light converters do not contain epoxy or silicone which are sensitive to high temperatures and UV radiation. However, the production of single crystal phosphors is expensive and to date they are mostly applied for white laser diodes (LDs) [42]. Due to the lower output power and chip temperature than that of LDs, phosphor converters for LEDs can be produced of phosphor powder and silicone or epoxy resin mixture [1]. The well known methods for the garnet phosphor powder synthesis are the solid state reaction, co-precipitation or sol-gel methods [7, 43]. Phosphor powders are usually characterized by poorer quality than the crystal samples, nevertheless they are the most popular choice for light converters due to the significantly lower production cost [44]. The thermal properties of the powder phosphors can be improved by producing ceramic phosphors. They are usually made by applying a high pressure and temperature on phosphor powders [45]. However, due to the required additional equipment and the increased production time, ceramic phosphors as well as single crystals are mostly considered only for high power LED or LD applications [46].

Czochralski process

The Czochralski process was invented by a polish chemist Jan Czochralski and is used for the manufacture of single crystals. It is the most popular method for the growth of silicon single crystals for wafer production [47], but is also applied for the making of high quality garnet phosphors [42, 48, 49]. During this method the seed of a single crystal is immersed to a crucible full of a hot stoichiometric solution and slowly pulled upwards. Due to the temperature gradient the solution crystallises on the seed, thus forming a high quality single crystal [47]. However, the process is slow, expensive and requires special equipment. Moreover this method is not the best option for the growth of gallium garnet crystals due to the volatility of one of the starting materials Ga_2O_3 which prevents the ability to keep the stoichiometry of the solution [43].

Solid state reaction

The solid state reaction is the simplest, cheapest and the most widely applied method of the powder phosphor synthesis [7]. During the solid state reaction, the dry precursors are mixed, heated at 1000-1500 °C and ground. However, the simplicity of this process has its drawbacks – it requires multiple heating and grinding, moreover the obtained powder consists of large (several tens of microns) dispersed size crystallites, containing defects and impurities which reduces the luminescence efficiency [7].

Co-precipitation method

Co-precipitation method is classified as a solution-based chemical synthesis. The main advantage of this method is the ability to control the resulting particle size. During the co-precipitation method, the oxides of garnet composites are dissolved in the nitric acid and mixed together with ammonium bicarbonate. The precipitates form after 20 hours which then are filtered, washed, heated to decompose a precursor and calcined to form crystallites [43]. However, in order to completely remove the residues of precursor salts the repeated washing is necessary, which makes the whole process complicated and time consuming [7].

Sol-gel method

The beginning of the sol-gel method is very similar to that of the co-precipitation. However, during this process instead of ammonium bicarbonate a complexing agent tris(hydroxymethyl)–aminomethane is mixed to the solution which turns to a *sol*. The sol is heated to 65 °C and evaporated until it becomes a gel. The gel is further dried at 110 °C and the temperature of the hot plate is raised gradually until a self-combustion of the gel is initiated. The ashes are heated for 4 h in 800 °C until metal oxides are formed and carbonate composites are removed. To form garnet phase materials, these compounds are heated for 10 h at 1000 °C. The obtained material consists of high quality and purity crystallite particles in the nanometre-micrometre range [7]. The sol-gel method is one of the most attractive methods for garnet synthesis, because it is simple and non-time consuming, yet yielding a high quality material.

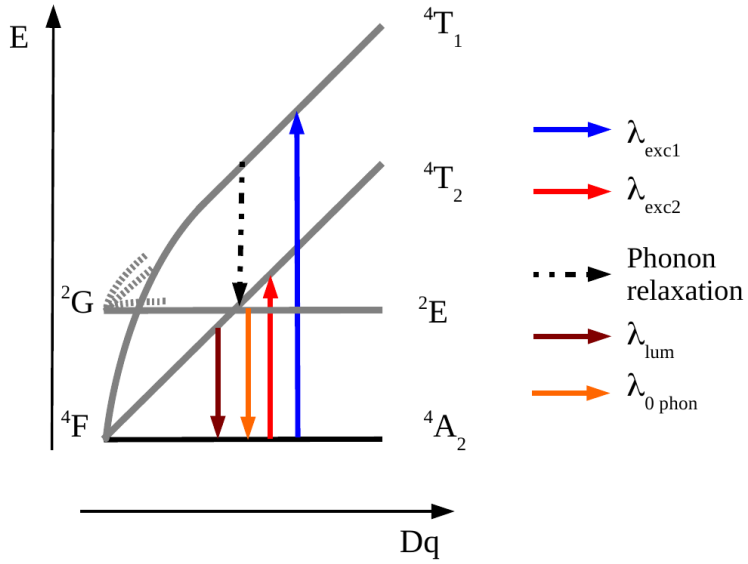

Figure 1.1: Simplified Tanabe-Sugano diagram for the d^3 configuration. x axis represents the crystal field strength (Dq), y axis represents the energy (E). Adapted from [54].

1.1.3 Physical and chemical properties of gallium garnets

Garnet crystal structure materials are characterized by specific chemical and physical properties. They are inert and resistive to humidity, temperature variations and even most of the acids. The crystal lattice of garnets is cubic and has a complicated structure with 160 ions composing a unit cell [50]. The general formula of garnet compound is $A_3B_2C_3D_{12}$, here the element A occupies dodecahedral, B – octahedral, C – tetrahedral, sites and D is situated between elements A, B, and C on the top of polyhedra [51]. In the case of gadolinium, lutetium, and yttrium gallium garnets (GGG, LGG, and YGG, respectively), the D site is taken by oxygen, B and C by gallium and A by gadolinium, lutetium, or yttrium, respectively. In the case of gadolinium scandium gallium garnet (GSGG), B site is occupied by scandium and A site is occupied by gadolinium. When garnets are doped with Cr^{3+} it occupies B position ending up in the octahedral site [48].

In the periodic table chromium belongs to the transition metals block. When chromium looses three electrons, Cr^{3+} ions get the d^3 configuration. 3d orbital is not screened and becomes strongly influenced by the external crystal field [52, 53]. The energy level diagram of Cr^{3+} of d^3 configuration in octahedral site was calculated by Tanabe and Sugano and can be found in refs. [53, 54, 55].

A simplified energy diagram showing only the ground state and part of the second excited state is presented in Fig. 1.1. Here the x axis represents the crystal field strength Dq and the y axis – the energy E. As it is seen in the diagram, a degenerate ground state of a free ion of d^3 configuration is labelled as ^4F and in the octahedral field it is split into a ground state $^4A_2$ and two excited states $^4T_2$ and $^4T_1$ [55]. The degenerate excited states in the same manner are split in a number of components. The absorption bands of Cr^{3+} ions are due to the $^4A_2 \rightarrow {}^4T_1$ and $^4A_2 \rightarrow {}^4T_2$ transitions and the photoluminescence (PL) occurs due to the $^4T_2 \rightarrow {}^4A_2$ or $^2E \rightarrow {}^4A_2$ transitions depending on the crystal field strength. For a weak crystal field the energy difference ΔE between ^2E and $^4T_2$ energy levels is small and at room temperature, they are in a thermal equilibrium thus the spin allowed $^4T_2 \rightarrow {}^4A_2$ transition is dominant. However, for a stronger crystal field ΔE increases and transition $^2E \rightarrow {}^4A_2$ takes place [48, 55, 56]. The crystal field strength is varied by changing the elements composing the lattice and thus increasing or decreasing its parameter. E.g. due to the greater diameter of Gd ion, the crystal field in GGG:Cr is weaker than in YGG:Cr or LGG:Cr [48, 55, 57]. Moreover, as it is seen in Fig. 1.1 the distance between the energy levels depends on the crystal field strength, therefore, by changing the lattice parameter it is also possible to tune the PL peak wavelength [48, 55, 56].

1.1.4 Quantum efficiency

The quantum efficiency (QE) is a very important parameter of luminescent materials. For liquid solutions (e.g. polymers) the internal QE is defined as the ratio of photons emitted to photons absorbed by the phosphor. It also can be expressed as the ratio of radiative transition rate to the sum of radiative and non-radiative transition rates [58]. The external QE can be defined as the internal QE multiplied by the light extraction, which is the number of photons emitted by the sample to the total number of converted photons. The main factor limiting the light extraction is the reabsorption. For this reason it is very important to make sure that the samples are thin and uniform [58, 59].

However, for phosphor powders the definition of internal and external QE is slightly different, according to ref. [44] "the internal QE is how much light (photons) absorbed by the phosphor is converted into luminescence. The external quantum efficiency denotes the ratio of the number of photons of the emitted light to that of the incident light on a phosphor" and is

expressed as follows:

$$\eta_{\text{int}} = \frac{\int \lambda \cdot P(\lambda)\mathrm{d}\lambda}{\int \lambda \cdot E(\lambda)\mathrm{d}\lambda - \int \lambda \cdot R(\lambda)\mathrm{d}\lambda}, \quad \eta_{\text{ext}} = \frac{\int \lambda \cdot P(\lambda)\mathrm{d}\lambda}{\int \lambda \cdot E(\lambda)\mathrm{d}\lambda}, \tag{1.1}$$

here $P(\lambda)$, $E(\lambda)$ and $R(\lambda)$ are the spectra of PL, excitation light and reflection, respectively [44]. The internal QE is usually limited by the lattice defects, impurities or concentration quenching [60, 61].

The PL QE is not the only factor limiting the efficiency of phosphors – some energy is lost due to the Stokes shift which simply is the wavelength conversion loss. As a photon with a shorter wavelength has higher energy than the one having a longer wavelength, the total energy loss ΔE is expressed as:

$$\Delta E = E_1 - E_2 = \frac{hc}{\lambda_1} - \frac{hc}{\lambda_2}, \tag{1.2}$$

thus the wavelength conversion efficiency is calculated by the following equation:

$$\eta_\lambda = \frac{h\nu_2}{h\nu_1} = \frac{\lambda_1}{\lambda_2}, \tag{1.3}$$

here λ_1, λ_2 are the weighted wavelengths and ν_1, ν_2 are the frequencies of the excitation and PL, respectively [5]. The overall limiting radiant efficiency of a partial conversion LED caused only by the Stokes shift is expressed as:

$$\eta_0 = p_1 + p_2\eta_\lambda, \tag{1.4}$$

where p_1 and p_2 are the proportions of the excitation and PL components composing the SPD.

1.1.5 PL decay time

When the PL excitation (PLE) light is switched of, the PL does not stop instantly, but rather decays gradually, this process is called the luminescence decay and is described by a PL decay time τ. PL decay time usually depends on the host lattice, its quality, the amount of dopant ions or impurities that cause different recombination processes. For the most simple case when there is only one recombination process the decrease of PL intensity $I(t)$ is described by the following equation:

$$I(t) = I_0 \exp(-t/\tau), \tag{1.5}$$

here I_0 is the PL intensity at the initial moment, t – is time. As it can be understood from eq. 1.5, the decay time τ defines the period of time, after

which the intensity of PL is reduced e times. However, usually the materials are more complex and there are several recombination mechanisms, in this case the PL decay is described by a multiexponential decay law:

$$I(t) = \sum_i \alpha_i \exp(-t/\tau_i), \tag{1.6}$$

here α_i describes the relative input of each recombination centre to the whole decay law. Input of a certain process to the integral PL signal is found from the following relation:

$$f_i = \frac{\alpha_i \tau_i}{\sum_i \alpha_i \tau_i}, \tag{1.7}$$

where f_i is the weight function for each recombination process [62]. It is worth mentioning that for a biexponential decay it is enough to calculate only f_1 since these coefficients are linearly dependent: $f_2 = 1 - f_1$ [63].

1.2 Experimental methods

In this section the synthesis and characterization methods of the samples are presented. The synthesis and structural analysis of the garnet phosphors was performed at the faculty of Chemistry and Geosciences by dr. S. Butkutė and co-workers. The comprehensive analysis of the synthesis and chemical properties of phosphors are described in dr. S. Butkutė's doctoral dissertation [64]. Here, a brief description of the synthesis and morphological analysis of the samples is presented. The section also describes the sample preparation for the PL measurements and the description of PL, PLE, PL QE, and PL decay time measuring techniques. Finally a design process of the far-red luminary meeting the photomorphogenetic needs of plants is discussed.

1.2.1 Synthesis of the samples

The schematic drawing of the sol-gel combustion method is presented in Fig. 1.2. The garnet structure powder phosphors $Gd_3Ga_5O_{12}$:,Cr^{3+} (GGG:Cr) and $Gd_3Ga_5O_{12}$:Ce^{3+},Cr^{3+} (GGG:Ce,Cr) doped with chromium (Cr = 0.25, 0.5, 1, 3, 5 and 10 mol%), and equimolar amounts of cerium and chromium (Ce + Cr = 0.25, 0.5, 1, 3, 5 and 10 mol%), respectively calcined at 1000 °C as well as $Gd_3Ga_5O_{12}$:Cr^{3+} (GGG:Cr), $Y_3Ga_5O_{12}$:Cr^{3+} (YGG:Cr), $Gd_3Sc_2Ga_3O_{12}$:Cr^{3+} (GSGG:Cr), and $Lu_3Ga_5O_{12}$:Cr^{3+} (LGG:Cr) with chromium concentrations of 3, 5, and

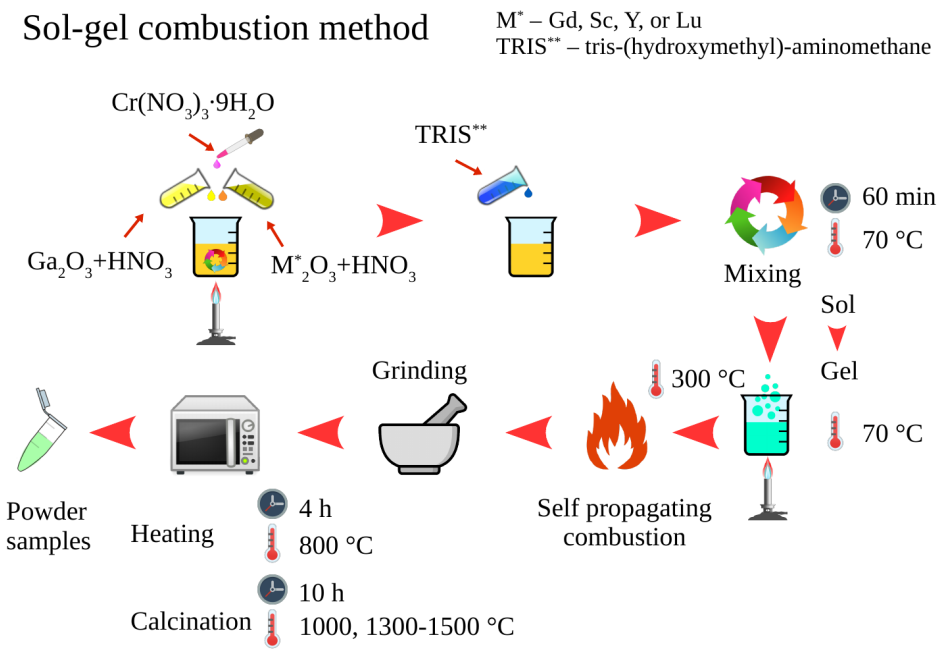

Figure 1.2: Schematic drawing of the sol-gel combustion method.

8 mol% were synthesized by a sol-gel combustion method. The starting materials Gd_2O_3, Ga_2O_3, Y_2O_3, Sc_2O_3, and Lu_2O_3 were dissolved in concentrated hot nitric acid and by a molar ratio mixed with a chromium nitrate nonahydrate dissolved in distilled water ($Cr(NO_3)_3 \cdot 9\,H_2O$). Afterwards the complexing agent tris(hydroxymethyl)–aminomethane (TRIS) was added in a molar ratio 1:1 with metal ions and the solution was continually stirred for 1 h at ∼70 °C and slowly evaporated. Then the hot-plate temperature was raised to 300 °C thus initiating the self-propagating combustion. In order to remove the carbon compounds, the obtained ashes were preheated for 4 h at 800 °C. The materials were calcined at 1000 °C for 10 h. After the PL QE measurements, the optimal concentrations of Cr^{3+} for different garnet phosphors were established and the synthesis process was repeated adding the determined optimal amount of Cr^{3+} and performing the calcination at 1300, 1400 and 1500 °C. Pure GGG calcined at 1000 °C was prepared for reference.

The YGG:Cr phosphor for the pellets was prepared by the same method as described above. The resulting powder was pressed into pellets and heated for 10 h at 1000, 1100, 1200, 1300, and 1400 °C temperatures with a heating rate of 3 °C. The pellets were intended to be doped with 8 mol% of Cr^{3+}. However, the further analysis of the material has revealed that the

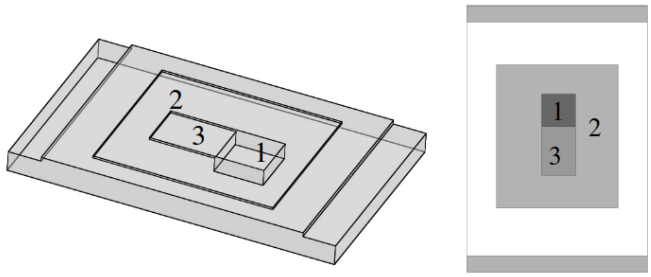

Figure 1.3: 3D and 2D drawing of the phosphor case used for the measurements of PL and QE.

concentration was 8.7 mol%

The XRD analysis of powder phosphors was performed using a Rigaku MiniFlex II diffractometer working in the Bragg–Bretano ($\theta/2\theta$) geometry. The data was collected using the CuKα (λ = 1.54060 Å) line within the 2θ angle from 10 ° to 70 ° and the scan speed was kept at 10 °/min. The microscope images of the samples were taken using Hitachi SU-70 SEM.

1.2.2 Photoluminescence experiments

Sample preparation for PL measurements

In order to perform correct PL and QE measurements, avoid the reabsorption and be able to compare the PL properties of different samples it was important to ensure the thin and even thickness of phosphor powder samples. For this reason special poly(methyl methacrylate) (PMMA) cases designed by *FreeCAD* 3D modeling software were engraved using *ROLAND Modela 4 MDX-40* milling machine. The 3D and 2D drawings of the case is presented in Fig. 1.3.

The cavity No. 1 is filled with phosphor powder and covered by a microscope glass that is glued to the surface No. 2. Afterwards the case is softly shaken and the powder falls to the 200 µm thickness cavity No. 3 thus forming a thin and uniform layer.

Measurements of diffuse reflection, PLE and PL

Due to the opaque nature of garnet phosphor powder it is impossible to measure the transmission spectra. White colour phosphor powder particles scatter the light to all directions. In order to collect scattered light the diffuse reflection spectra were measured using *Perkin Elmer Lambda 950* spectrometer equipped with an integrating sphere. The diffuse reflection

was measured in the intervals between 350 and 800 nm, as well as 200 and 800 nm, for phosphor powders and pellets, respectively; *Spectralon*® white standard was used as a reference.

The PL spectra of GGG:Cr and GGG:Cr,Ce during the optimization of garnets were measured with a *Hamamatsu PMA-11* spectrometer. A blue LED (peak wavelength 445 nm) was used as an excitation source. Due to the very weak PL signal a red-pass filter (cut-off 600 nm) was used in front of the spectrometer fibre.

The PLE and PL spectra were measured using *Perkin Elmer LS55* fluorescence spectrometer. During the PLE measurements PL was monitored at different wavelengths for each sample depending on the PL band peak value position (720 nm for GGG:Cr, 710 nm for YGG:Cr, 758 nm for GSGG, and 705 nm for LGG). The PL was measured upon 450 nm excitation since PLE bands of all samples peaked around this value. Moreover, most of the commercial blue InGaN LEDs are characterised by a peak wavelength of this value.

The PL intensity dependence on the ambient temperature was measured using a *LabSphere* Peltier element in the –5–85 °C range. The PL was detected with *Hamamatsu PMA-11* spectrometer.

Measurement of quantum efficiency

The measurements of QE were performed by the *J. C. de Mello* proposed method described in [59]. The experimental scheme is presented in Fig. 1.4. Here the light source is a halogen lamp placed in a black box 1. The light comes out through a diaphragm and is focused to a monochromator with a convex lens 2. 450 nm blue light comes out of the monochromator, passes the blue-pass filter 3 (cutoff 500 nm) and is focused with another convex lens (4) to an integrating sphere 5 (*Sphere Optics*, *Spectralon*® white standard). Screen 6 protects the detector from the direct excitation light. The light is collected with a fibre 7 and is transferred to a spectrometer (*Hamamatsu PMA-11*) which further sends the data to the computer. The inner part of the sphere is covered by a white barium sulphate layer which reflects and diffuses the incident light.

In order to calculate QE values, the measurements are performed under three different configurations: A, B, and C that are depicted on the right hand side of Fig. 1.4. Under the A configuration only the excitation light is measured so the sphere is empty. Afterwards the sample is placed into the sphere yet the excitation light is not focused to it (B). This way during the later calculations PL induced by the light reflected from the sphere walls is

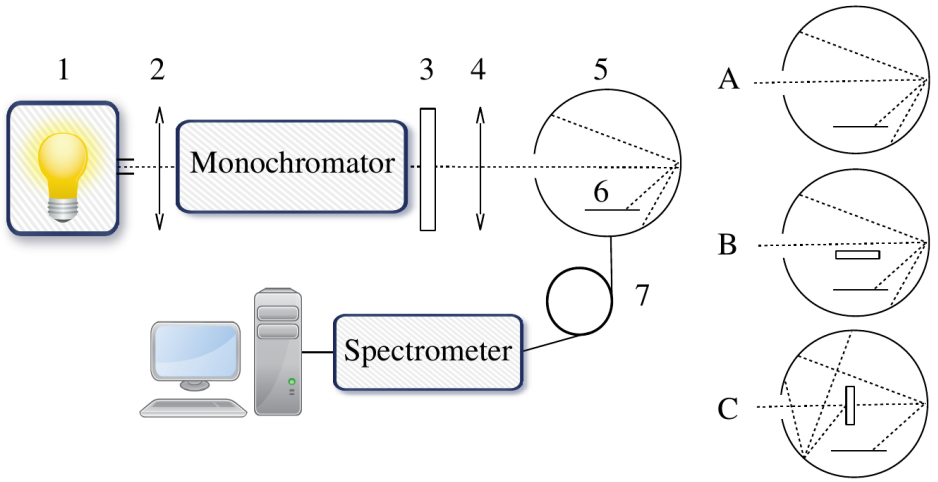

Figure 1.4: Experimental setup of the QE measurements.

neglected. Under the last C configuration the excitation light is focused to the sample. When spectra of the three described configurations are collected the QE is calculated using the following equation:

$$QE = \frac{P_C - \frac{L_C}{L_B} P_B}{L_A(1 - \frac{L_C}{L_B})}, \tag{1.8}$$

here P_B and P_C are integrated PL spectra measured under B and C configurations, respectively, L_A, L_B and L_C are integrated spectra of the excitation light measured under A, B and C configurations, respectively.

Measurement of PL decay time

In order to measure the PL decay times, two different methods can be employed – time domain (TD) and frequency domain (FD) [62]. Due to a more simple experimental set up and the possibility to use a blue LED as an excitation source the latter was chosen for this research. The principle of the FD method is presented in Fig. 1.5 [63]. During this method the excitation signal is modulated with an angular frequency ω and modulation depth M. Due to the finite PL decay time ($\tau > 0$), the sample PL signal is delayed. As a result the phase shift ϕ occurs and the modulation depth m is reduced. In general case the phase shift and the reduction of the modulation μ have the following expressions:

$$\phi = \arctan \frac{N_\omega}{D_\omega}, \quad \mu = \frac{m}{M} = \sqrt{N_\omega^2 + D_\omega^2}, \tag{1.9}$$

here N_ω and D_ω are sine and cosine intensity transformations of the frequency domain that under the multiexponential conditions have the following expressions:

$$N_\omega = \frac{\sum_i \frac{\alpha_i \omega \tau_i^2}{1+\omega^2\tau_i^2}}{\sum_i \alpha_i \tau_i}, \quad D_\omega = \frac{\sum_i \frac{\alpha_i \tau_i}{1+\omega^2\tau_i^2}}{\sum_i \alpha_i \tau_i}. \tag{1.10}$$

In general, the phase shift and modulation depth are measured in the broad interval of frequencies and the parameters are calculated by fitting the best non-linear function using the least square method. E.g. for the biexponential case we obtain the parameters τ_1, τ_2, and α_1. The parameter α_2 is not mentioned since it linearly depends on α_1: $\alpha_2 = 1 - \alpha_1$ [63].

During the experiment the blue InGaN LED (peak wavelength 445 nm) excitation light was sinusoidally modulated in the frequency range between 1 Hz and 25 kHz. The excitation light passed the blue-pass filter (cutoff 500 nm) and was focused to the sample. The PL signal emitted by the sample was filtered with a red-pass filter (cutoff 600 nm). The PL was detected by a photomultiplier *Hamamatsu H6780-01*, the modulation depth and the phase shift were measured using a digital lock-in amplifier *Signal Recovery 7265*. The electronic noise was evaluated by replacing the sample with a metal plate and repeating the measurement. The optical noise of the environment was evaluated by performing the measurement with a covered excitation light source.

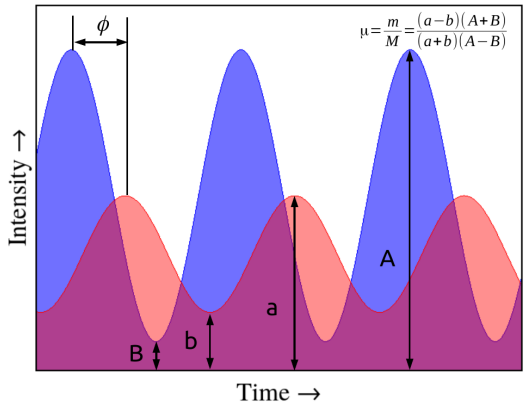

Figure 1.5: Blue excitation signal modulated by a sinusoidal shape and the following far-red PL. Here ϕ is a phase shift and μ is the reduction of a modulation depth (after [63]).

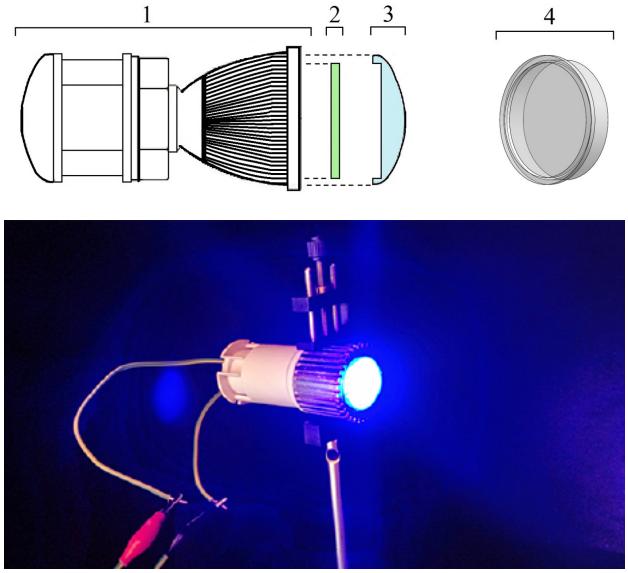

Figure 1.6: Up: drawing of the far red luminary for plant photomorphogenesis; down: photo of the far-red luminary for plant photomorphogenesis. Driving current 350 mA [**V**].

1.2.3 Design process of the luminary

The design process of the pcLED luminary for the plant photomorphogenesis is described in Paper **V**. Although the phosphor pellets exhibit better PL properties they still cause some technological difficulties for the application in pcLED luminary. For this reason the phosphor converter was made of YGG:Cr^{3+} 8 mol% powder, calcined at 1300 °C, mixed with a transparent sanitary silicone with phosphor concentrations of 5.3 wt% and 5.7 wt%. PMMA cases of different depths – 0.5, 1 and 1.5 mm were used as molds for converters. The cases were milled with the milling machine described in subsection 1.2.2, their 3D model is presented in the upper part of figure 1.6 as No. 4. The solidified converters were examined and the one of 1.5 mm thickness and 5.7 wt% phosphor concentration was found to be optimal for the luminary design. The drawing of the far-red luminary is presented in figure 1.6. The excitation source – *Philips Lumileds* Rebel Royal Blue (peak wavelength 452 nm) was mounted inside the *HortiLED* greenhouse luminary housing with a radiator 1, the 5.7 wt% 1.5 mm thickness phosphor-silicone converted 2 was placed inside the engraved PMMA lens 3. The picture of the designed far-red luminary is presented in Fig. 1.6

1.3 Results

This section presents the morphological, photoluminescence and temperature properties of gallium garnets doped with Cr^{3+}. In the end the characterization of the designed far-red pcLED luminaire satisfying the photophysical needs of plants is provided.

1.3.1 Structure and morphology of gallium garnets

Powder samples

The synthesised phosphor samples were in the form of white powder with a greenish hue, which was more pronounced for higher calcination temperatures.

Figure 1.7 shows the XRD patterns of gallium garnets doped with Cr^{3+} and calcined at 1000 °C. It is seen that all patterns match the standard data (ICDD) shown as straight vertical lines which means that the synthesised phosphors are of the desired garnet crystal phase.

The morphology of phosphor powder strongly depends on the calcination temperature. Figures 1.8–1.10 present the SEM images of GGG:Cr, GSGG:Cr, LGG:Cr, and YGG:Cr, respectively, that are calcined at 1000, 1300, 1400, and 1500 °C temperatures. It is seen in the figures that all samples calcined at 1000 °C temperature consist of small submicron platelike particles with a high level of agglomeration. Raising the calcination temperature yields the formation of larger particles and reveals the crystal shape of phosphor particles. Figures 1.8–1.10 (d) show that for 1400 °C annealing temperature micron range crystallites are formed.

Pellets

The YGG:Cr 8.7 mol% phosphor pellets as the powder samples were of white colour with a greenish hue being more pronounced for higher annealing temperatures. The XRD pattern was very similar to that of the powder samples and confirmed the garnet phase. The SEM images of the pellets calcined at 1200 and 1400 °C are presented in Fig. 1.12. As in the case of powder samples it is seen that the size and crystallinity of the particles increases with the calcination temperature.

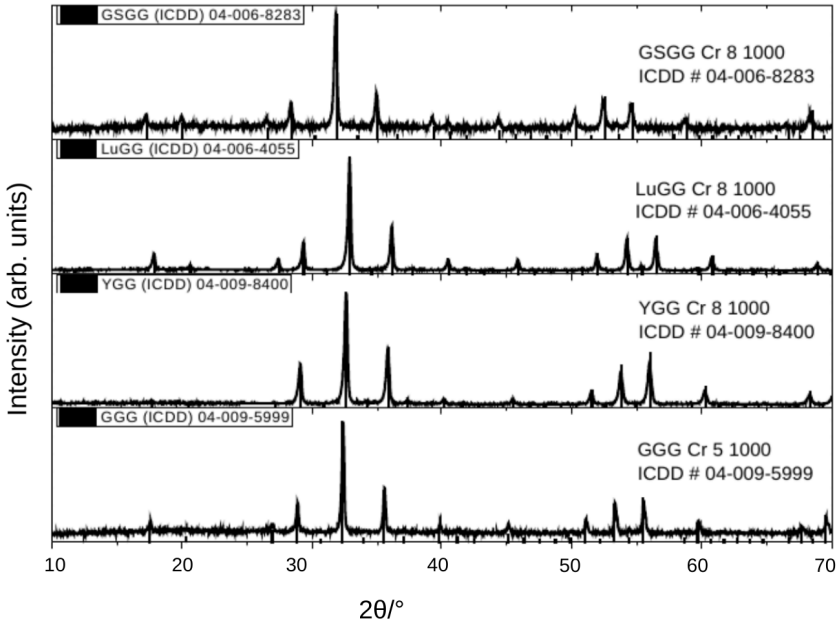

Figure 1.7: XRD patterns of Cr^{3+} activated gallium garnets calcined at 1000 °C. Vertical lines represent standard data (ICDD).

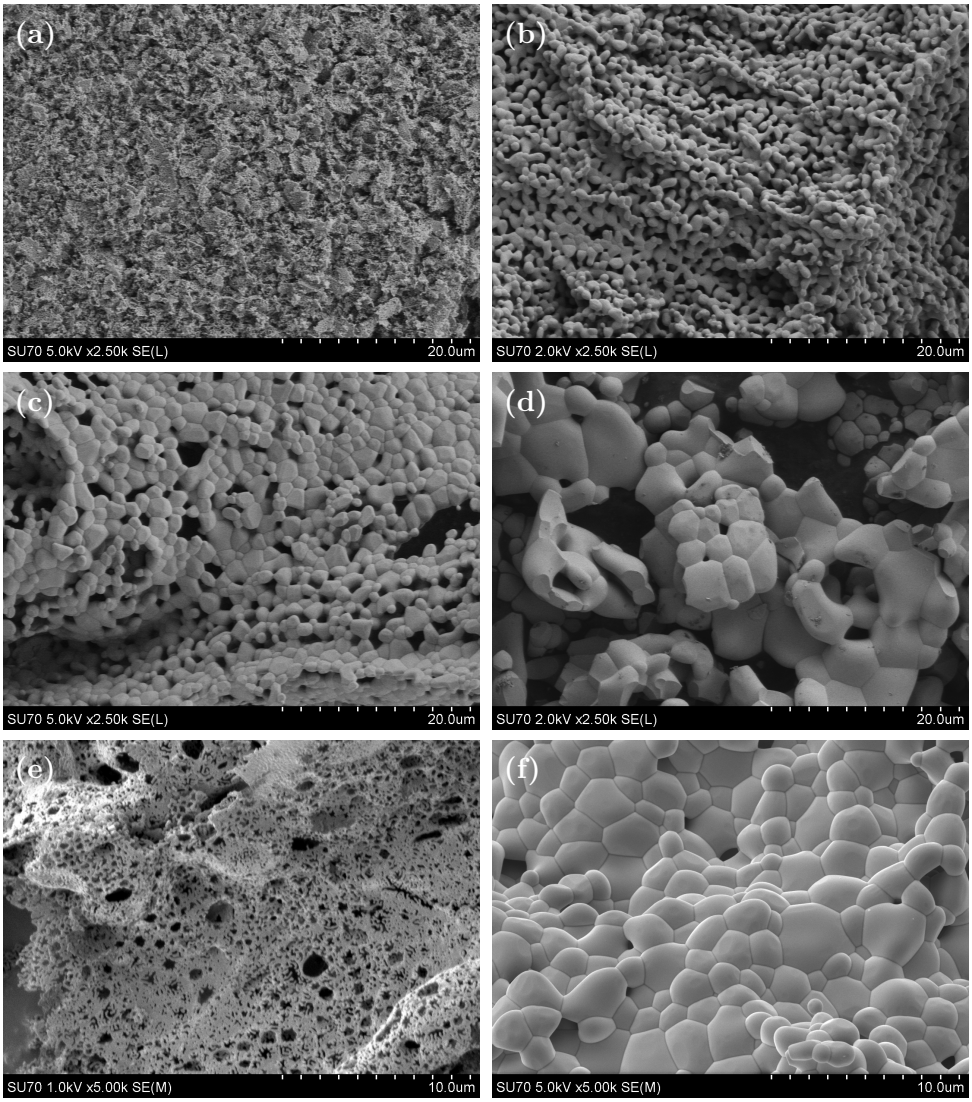

Figure 1.8: SEM images of GGG:Cr 5 mol% powder samples calcined at a) 1000 °C, b) 1300 °C, c) 1400 °C, and d) 1500 °C temperatures. The scale step corresponds to 2 µm. Figures e) and f) show the enlarged SEM images of GGG:Cr 5 mol% calcined at 1000 and 1400 °C, respectively. The scale step corresponds to 1 µm. Figure f) was used for the front cover of Applied Optics **53**(5), (2014) [**III**].

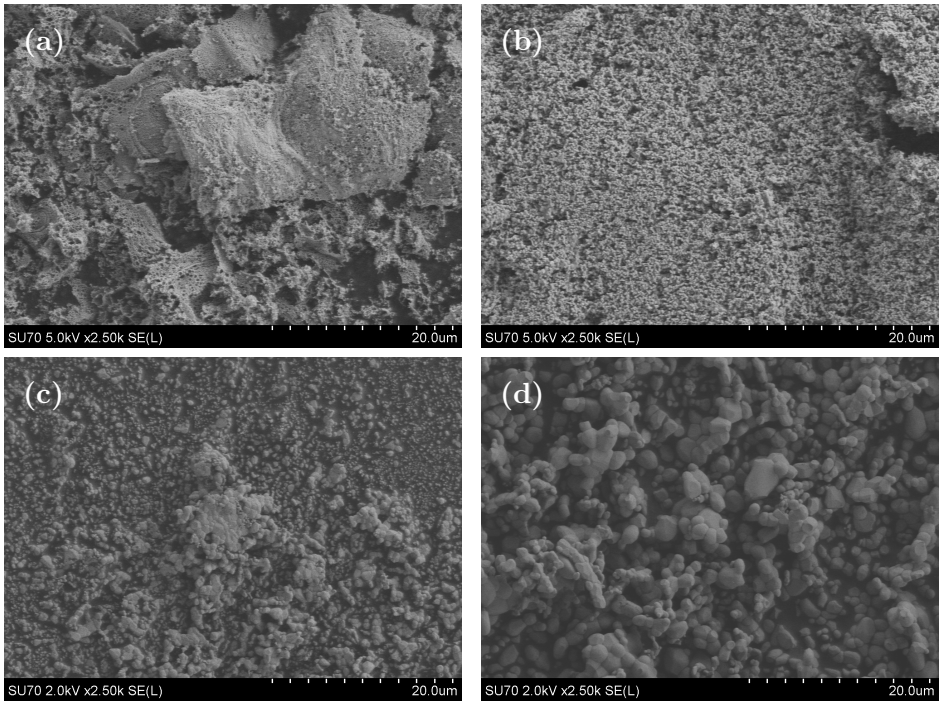

Figure 1.9: SEM images of GSGG:Cr 8 mol% powder samples calcined at (a) 1000 °C, (b) 1300 °C, (c) 1400 °C, (d) 1500 °C temperatures.

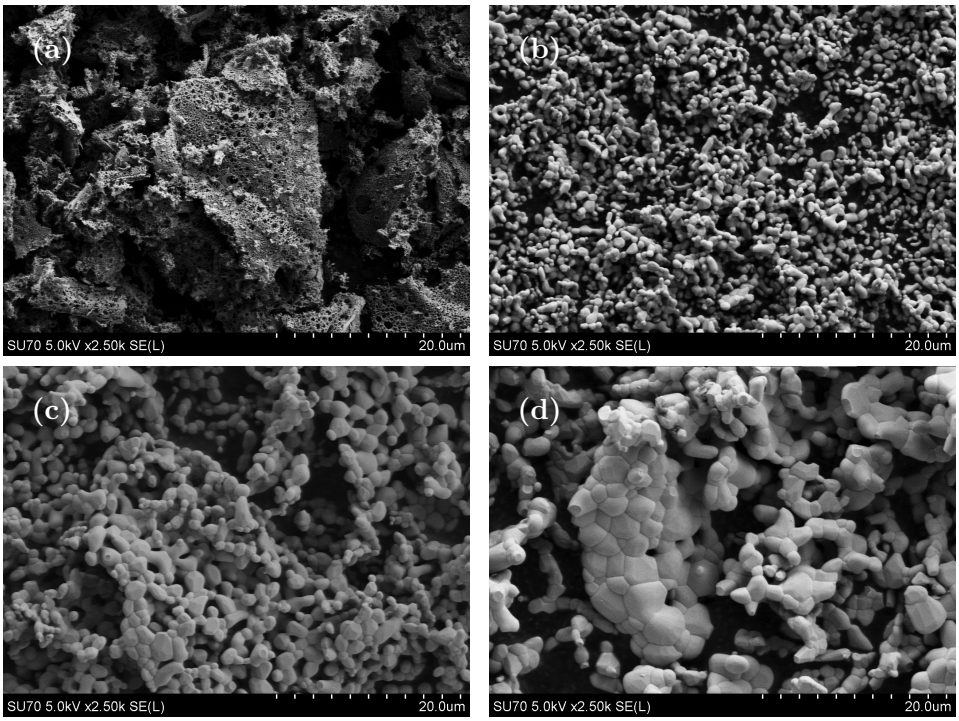

Figure 1.10: SEM images of LGG:Cr 3 mol% powder samples calcined at (a) 1000 °C, (b) 1300 °C, (c) 1400 °C, (d) 1500 °C temperatures.

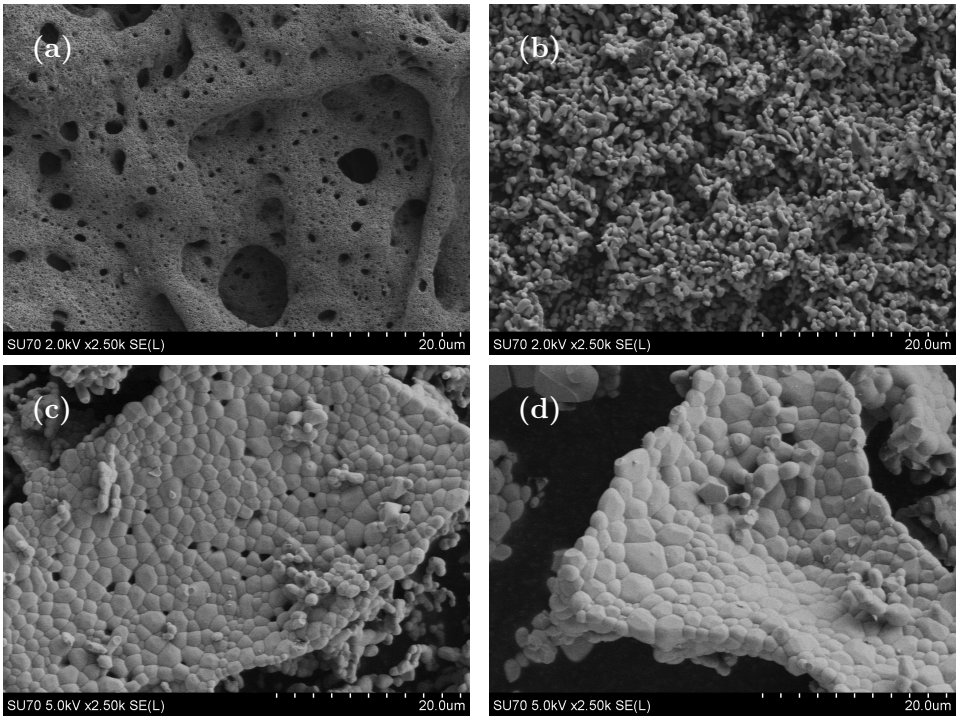

Figure 1.11: SEM images of YGG:Cr 8 mol% powder samples calcined at (a) 1000 °C, (b) 1300 °C, (c) 1400 °C, (d) 1500 °C temperatures.

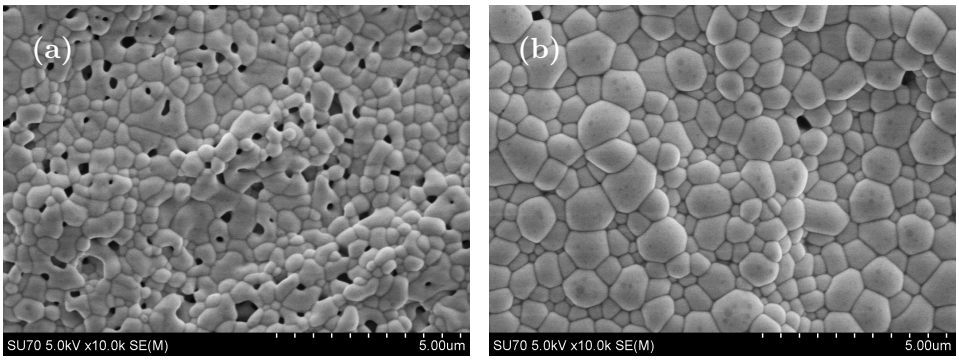

Figure 1.12: SEM images of YGG:Cr 8.7 mol% phosphor pellets calcined at (a) 1200 °C and (b) 1400 °C [**V**].

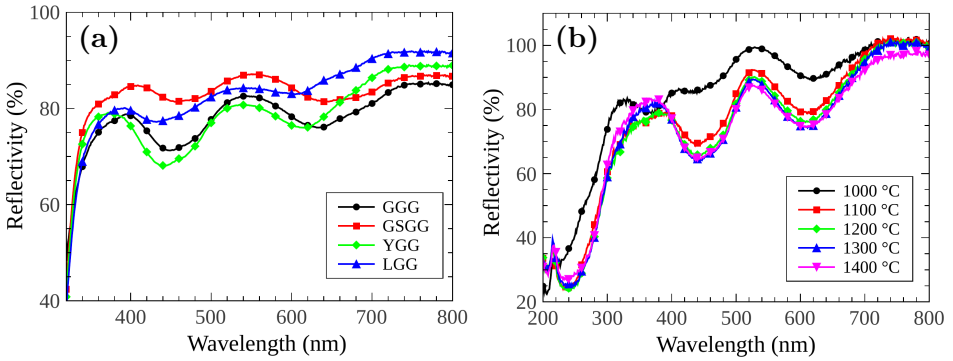

Figure 1.13: (a) Diffuse reflection spectra of GGG 5 mol% Cr^{3+}, GSGG 8 mol% Cr^{3+} , LGG 3 mol% Cr^{3+}, and YGG 8 mol% Cr^{3+} calcined at 1400 °C [**III**]; b) the diffuse reflection spectra of YGG 8.7 mol% Cr^{3+} calcined at 1000–1400 °C temperatures [**V**].

1.3.2 PL properties of gallium garnets

Diffuse reflection spectra

Figure 1.13 (a) presents the diffuse reflection spectra of GGG:Cr 5 mol%, GSGG:Cr 8 mol%, YGG:Cr 8 mol%, and LGG:Cr 3 mol% calcined at 1400 °C [**III**]. The spectra were measured from 320 nm due to the glass cover which absorbs UV radiation and makes the measurements in the spectral region below 300 nm irrelevant. The spectra reveal a relatively high reflectivity of the samples in the region from 340 up to 800 nm which is above 50%, therefore, the samples weakly absorb light in the visible spectral region. However, a strong absorption is observed in the UV region below 340 nm which is enhanced by the glass cover absorption. Two reflection minima are observed around 450 nm and 630 nm for all samples except for the LGG, which has a less pronounced minima in the red region. These two bands occur due to the $^4A_2 \rightarrow {}^4T_1$ and $^4A_2 \rightarrow {}^4T_2$ transitions, respectively, that are typical for Cr^{3+} ions in octahedral crystal field [65].

Figure 1.13 (b) presents the diffuse reflection spectra of YGG:Cr 8.7 mol% calcined at 1000, 1100, 1200, 1300, and 1400 °C temperatures [**V**]. If compared to the powder samples, the pellets are characterized by a lower absorption due to the higher density of the material. The diffuse reflection spectra reveal that at 1000 °C calcination temperature the absorption in the blue and red regions is not well pronounced. This is probably due to the residual concentrations of the impurities and lower crystal quality of the materials, since for higher calcination temperatures the absorption in the blue and red spectral regions increases. Due to the solid nature of pellets,

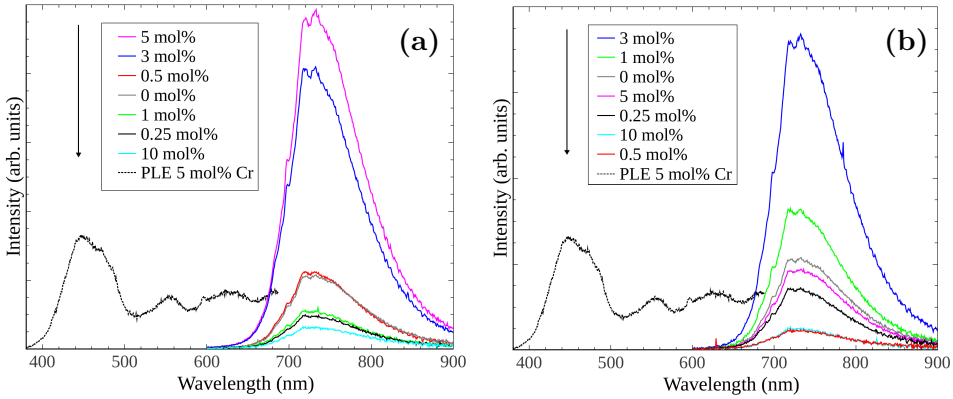

Figure 1.14: PLE ($\lambda_{lum} = 730$ nm) of GGG:Cr 5 mol% calcined at 1000 °C and PL ($\lambda_{exc} = 460$ nm) spectra of (a) GGG:Cr and (b) GGG:Ce,Cr calcined at 1000 °C temperature and doped with different amounts of Cr and Ce [**IV**].

the glass cover during the diffuse reflection measurements was unnecessary, therefore, the absorption band in the UV region of the spectra is ascribed to the optical absorption edge of the host lattice [65].

Luminescence spectra and the optimization of garnets

Figure 1.14 presents the PLE spectrum of GGG:Cr 5 mol% calcined at 1000 °C as well as PL spectra of, (a) GGG:Cr and (b) GGG:Cr,Ce calcined at 1000 °C and doped with 0.25, 0.5, 1, 3, 5, and 10 mol% of Cr and Cr,Ce, respectively. PLE in the blue ($\lambda_b = 450$ nm) and red ($\lambda_r = 630$ nm) regions is caused by the $^4A_2 \rightarrow {}^4T_1$ and $^4A_2 \rightarrow {}^4T_2$ transitions respectively, as are the absorption bands observed in the diffuse reflection spectra. The PLE spectrum also contains a band in the yellow region ($\lambda_y = 550$ nm) which diminishes for the samples calcined at higher temperatures and is, therefore, attributed to some sort of impurities or defects. The broad PL band of both sets of the samples in the far-red region ($\lambda_{peak} = 720$ nm) is caused by the $^4T_2 \rightarrow {}^4A_2$ transition of Cr^{3+} ions. The figures reveal that Ce^{3+} ions cause a srong quenching of Cr^{3+} ions PL. The PL band of Ce^{3+} ions was not observed due to the red-pass filter used during the PL measurements.

The decreased PL efficiency caused by the codoping of Ce^{3+} ions to the material is also observed in the optimization tab. 1.1, where the measured internal QE values of various gallium garnets doped with different concentrations of activators and calcined at 1000 °C are presented.

The optimization tab. 1.1, presents that in the most cases QE increases with the activator concentration due to the fact that activators create radia-

Table 1.1: Optimization table of gallium garnets calcined at 1000 °C. The materials in the same host group exhibiting the highest PL QE values were chosen for further investigation (marked in bold) Paper **III**.

Phosphor	**Doping**	**QE,%** λ_{exc} = 445 nm	λ_{lum}, nm
GGG:Ce,Cr	1 mol%	2.6	
	3 mol%	3.6	718
	5 mol%	1.4	
GGG:Cr	3 mol%	7.4	
	5 mol%	**8**	718
	8 mol%	5	
GSGG:Cr	3 mol%	0.6	720
	5 mol%	1.3	734
	8 mol%	**1.6**	737
YGG:Cr	3 mol%	13	
	5 mol%	12	711
	8 mol%	**18**	
LGG:Cr	**3 mol%**	**11**	
	5 mol%	6.5	706
	8 mol%	3.6	

tive recombination centres. However, at some point the activator concentration reaches the critical value and concentration quenching takes place which is caused by energy transfer between activator ions and leads to the increase of the non-radiative transition probability [61]. Table 1.1 presents that for GGG:Cr and LGG:Cr the quenching effect arises above 5 and 3 mol%, respectively. Later research has shown that for GSGG:Cr and YGG:Cr this effect takes place above 8 mol% Cr(III) concentration [66]. Materials within the same phosphor host group having the highest QE values (marked in bold in table 1.1) were investigated in the further research.

PLE and PL spectra of chromium doped gallium garnet powders calcined at 1000, 1300, 1400, and 1500 °C temperatures are presented in Fig. 1.15. Subfigs. (a), (b), (c), and (d) present GGG:Cr 5 mol%, GSGG:Cr 8 mol%, YGG:Cr 8 mol%, and LGG:Cr 3 mol%, respectively. PLE spectra, presented as dashed lines with open symbols, of all samples consist of two bands in the blue (around 450 nm) and red (around 620 nm) regions caused by the $^4A_2 \rightarrow {}^4T_1$ and $^4A_2 \rightarrow {}^4T_2$ transitions, respectively. The exact peak wavelength values of PLE are given in the characterization tab. 1.2. As Fig. 1.15 shows, the intensity of PLE increases with the calcination temperature, this can be explained by the increased crystallinity or particle size of powder samples for higher annealing temperatures as was observed in figs. 1.8 – 1.10.

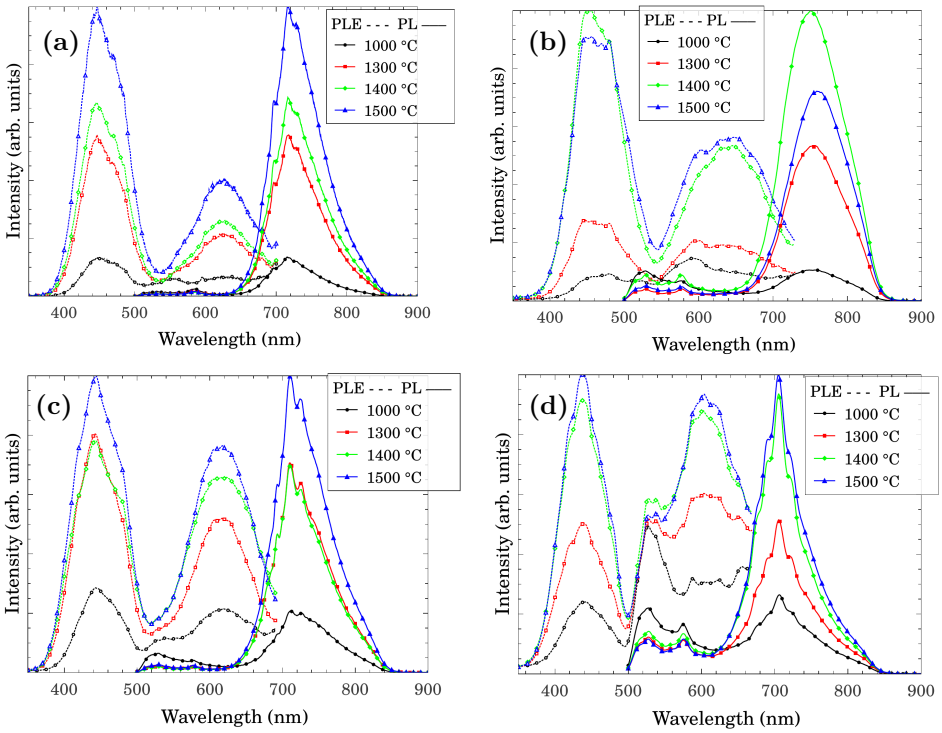

Figure 1.15: PLE (dashed line, open symbols) and PL (line, solid symbols) spectra of gallium garnets calcined at different temperatures: (a) GGG:Cr 5 mol%; (b) GSGG:Cr 8 mol%; (c) YGG:Cr 8 mol%; (d) LGG:Cr 3 mol%. The PL was measured upon 450 nm excitation; PLE was recorded at $\lambda_{lum} = 720, 758, 710$ and 705 nm for (a), (b), (c), and (d), respectively.

Figure 1.15 also demonstrates that upon 450 nm excitation the samples are characterized by a broad PL band in the far-red region with the peak wavelength values around 718, 756, 710 and 705 nm for GGG:Cr, GSGG:Cr, YGG:Cr, and LGG:Cr, respectively. The exact values are given in the gallium garnets characterization table 1.2 [**III**]. This broad PL band in a far-red region is attributed to the $^4T_2 \rightarrow {}^4A_2$ transition in Cr^{3+} ions. The reason for different peak wavelengths of gallium garnets is the differences of crystal field strength as discussed in subsec. 1.1.3. The crystal field strength is the highest in LGG:Cr and gradually decreases for YGG:Cr, GGG:Cr, and GSGG:Cr [48, 57]. As it is seen in Fig. 1.1 the distance between $^4T_2$ and $^4A_2$ energy levels increases with the crystal field strength, and, therefore, the PL peak wavelength gradually increases from LGG:Cr to GSGG:Cr. Moreover, due to the weaker coupling between $^2E_2$ and $^4T_2$ energy levels in the materials of a larger crystal field, sharp zero-phonon line caused by the

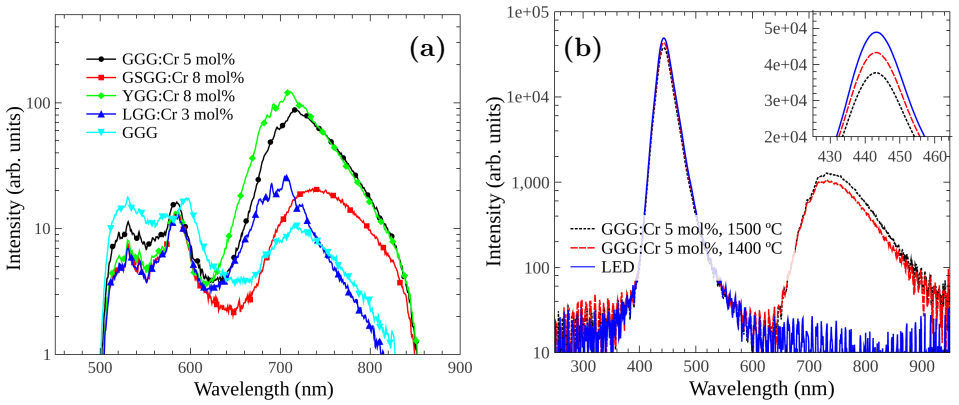

Figure 1.16: (a) PL spectra of GGG 5 mol% Cr^{3+}, GSGG 8 mol% Cr^{3+}, LGG 3 mol% Cr^{3+}, YGG 8 mol% Cr^{3+}, and pure GGG at 1000 °C in a logarithmic scale upon 450 nm excitation [**III**]; (b) The PL spectra of GGG 5 mol% Cr^{3+}, calcined at 1400 and 1500 °C and the excitation light spectra in the integrating sphere [**III**].

$^2E_2 \rightarrow {}^4A_2$ transition can be resolved for YGG:Cr and LGG:Cr [67, 56].

The PLE and PL spectra of YGG:Cr 8.7 mol% pellets were very similar to those of the powder samples shown in Fig. 1.15 (c).

Figure 1.16 (a) from Paper **III** demonstrates the PL spectra of Cr(III) doped gallium garnets and pure GGG upon 450 nm excitation in the logarithmic scale. A weak luminescence in the 400–600 nm region clearly observed in fig 1.16 is the most pronounced for the undoped GGG sample. Moreover, as Fig. 1.15 shows, it diminishes with the calcination temperatures and is thus attributed to various defects or impurities in the host material [67].

Values of internal quantum efficiency

The internal QE values of phosphor powders for 1300-1500 °C calcination temperatures are presented in tab. 1.2. The highest QE values are 30, 21, 20 and 46% for GGG:Cr 5 mol%, GSGG:Cr 8 mol%, LGG:Cr 3 mol% calcined at 1400 °C and YGG:Cr 8 mol% calcined at 1300 °C, respectively. If compared to the QE values provided in the tab. 1.1 it is seen that the PL efficiency increases for higher calcination temperatures. However, when 1500 °C temperature is reached the PL QE values decrease for GGG:Cr, GSGG:Cr, and LGG:Cr, and for YGG:Cr it decreases even at 1400 °C calcination temperature. The correlation mismatch between the PL intensity and efficiency can be explained by the larger crystallite size of powders an-

Table 1.2: PL properties of gallium garnets doped by different amounts of Cr^{3+} and calcined at 1300–1500 °C temperatures [**III**].

Host	**Doping mol% Cr^{3+}**	**Calcination temp., °C**	**QE, %**	λ_{lum}, **nm**	λ_{exc}, **nm**	τ_1, **ms**	τ_2, **ms**	f
GGG	5	1300	24	718	446	0.15	4.4 µs	0.59
		1400	30	717	447	0.14	4.8 µs	0.68
		1500	28	716	447	0.14	7.3 µs	0.76
GSGG	8	1300	19	750	456	0.10	0.50	0.96
		1400	21	759	457	0.09	0.47	0.98
		1500	19	756	448	0.09	0.73	0.99
YGG	8	1300	46	710	442	0.15	0.32	0.26
		1400	33	711	443	0.10	0.27	0.31
		1500	32	711	444	0.09	0.25	0.35
LGG	3	1300	19	706	438	0.21	0.74	0.26
		1400	20	706	438	0.18	0.68	0.24
		1500	17	705	437	0.21	0.63	0.44

nealed at higher temperatures, which increases the reabsorption. This is illustrated in Fig. 1.16 (b) which shows the excitation light in the empty integrating sphere (A configuration), labelled as LED, and spectra obtained when the excitation light is focused to the GGG:Cr 1400 °C and GGG:Cr 1500 °C samples (C configuration) **III**. As it is seen phosphor PL is more intense in the second case. However, the inset of Fig. 1.16 (b) shows that the excitation light is absorbed stronger by the GGG:Cr 1500 °C sample which leads to the lower QE values. The same effect was observed for other gallium garnets, investigated in this work, as well as for YAG phosphor, reported by others [68].

The QE values of YGG:Cr pellets were 23, 49, 53, 55 and 55% for calcination temperatures of , 1000, 1100, 1200, 1300, and 1400 °C, respectively. Probably the pressing of powder samples to pellets increase the crystallinity of the material which yields a more efficient PL.

PL decay time measurements

The PL decay times were measured using a frequency domain method which was described in subsec. 1.2.2. A typical frequency response of the modulation depth and phase shift for GGG:Cr 5 mol% calcined at 1500 °C is shown in Fig. 1.17. The PL decay has shown a multi-exponential character and was fitted by the following bi-exponential function:

$$I(t) = f \exp(-t/\tau_1) + (1 - f) \exp(-t/\tau_2). \tag{1.11}$$

The measured decay times $\tau_{1,2}$ and the weight function f are presented

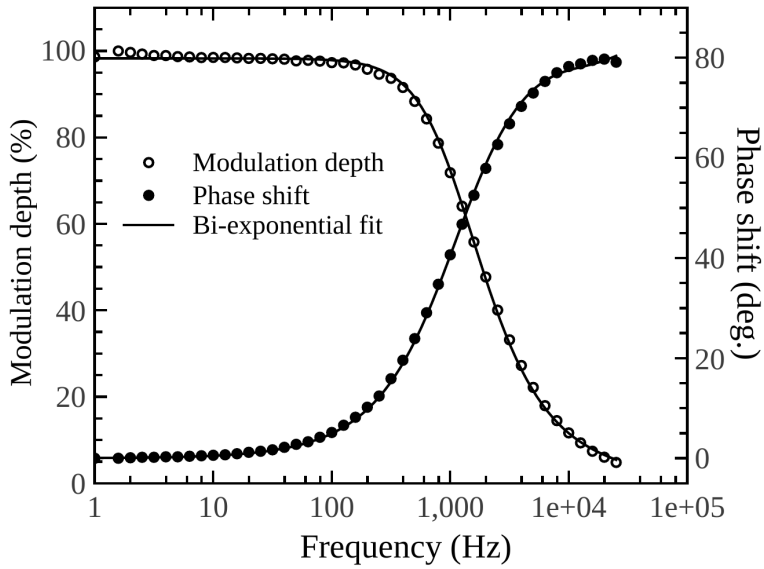

Figure 1.17: Frequency dependence of the PL modulation depth (open circles), phase shift (solid circles) and bi-exponential fits (solid lines) of GGG:Cr 5 mol% calcined at 1500 °C [**III**].

in tab. 1.2. Table 1.2 shows that the first PL decay time components for gallium garnet powders vary around 0.14–0.15, 0.09–0.10, 0.09–0.26 and 0.18–0.21 for GGG, GSGG, YGG and LGG powder phsophors, respectively. These values agree well with the ones for crystalline and ceramic GGG, GSGG, YGG samples [56, 49, 69] as well as for LGG powder prepared by a co-precipitation method [70]. The weight parameter f indicates that the first component is dominant for GGG and GSGG powders where Cr^{3+} ions experience a weaker crystal field. This leads to the conclusion that the first decay component is due to the broad PL band in the far-red region which is more pronounced in the materials exhibiting a weaker crystal field [48]. The second decay component ranges between 0.25–0.32 and 0.63–0.74 ms for YGG and LGG, respectively, and is likely due to the narrow PL line caused by the $^2E_2 \rightarrow {}^4A_2$ transition. For GSGG powder samples this decay component is negligible, nevertheless it varies between 0.47 and 0.73 ms. As for GGG powder, the second decay component is very short if compared to the other samples and varies between 4.4 and 7.3 µs. Since its significance is reduced with the calcination temperature, it could be related to lattice defects or impurities which are eliminated for higher quality material.

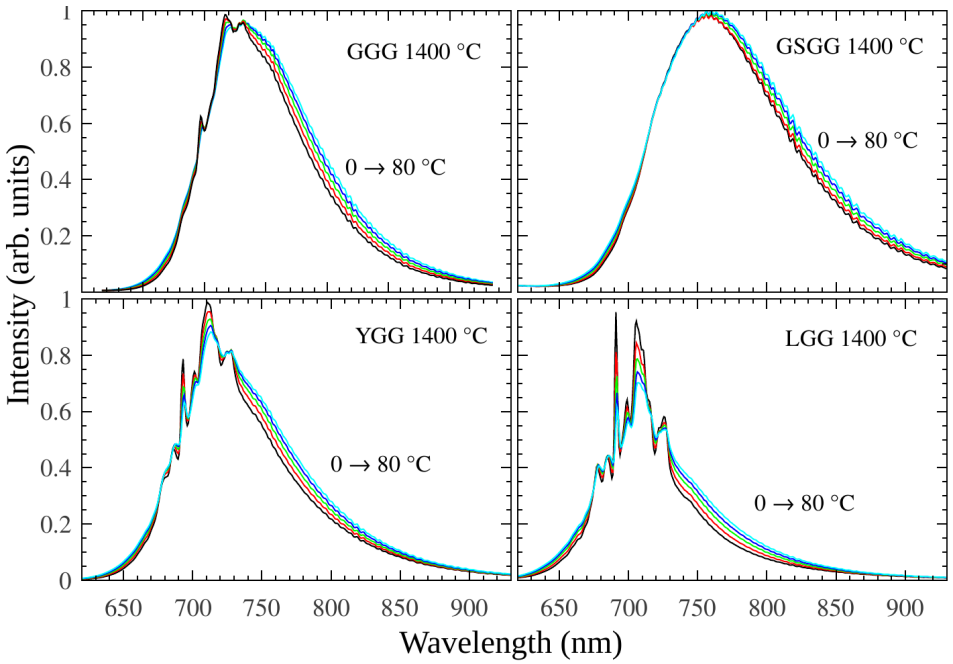

Figure 1.18: PL spectra of gallium garnet samples annealed at 1400 °C for ambient temperatures of 0, 20, 40, 60, and 80 °C upon 445 nm excitation [**III**].

1.3.3 Thermal properties of gallium garnets

Figure 1.18 presents the normalized PL spectra of powder samples calcined at 1400 °C temperature at ambient temperatures of 0, 20, 40, 60, and 80 °C. Here, due to the higher resolution of spectrometer, the effect of crystal field is observed even more clearly than in Fig. 1.15, since the sharp lines are be clearly distinguished in some of the spectra, in particular in that of LGG. This occurs due to the strong crystal field in LGG. As it was discussed in subsec. 1.1.3, for stronger crystal field $^2E_2 \rightarrow {}^4A_2$ transition is dominant and, therefore, sharp lines are observed in PL spectra. Since the crystal field strength gradually decreases for YGG, GGG and GSGG, the intensity of sharp lines also gradually decrease for these PL spectra, respectively.

The figure also shows that the intensity of sharp spectral lines lightly decreases with the increasing ambient temperature. However, as Fig. 1.19 demonstrates, no thermal quenching is observed, since for higher ambient temperatures the spectra become broader and the overall spectrally integrated PL intensity linearly increases even for 90 °C ambient temperature. This occurs due to the fact that for low temperatures the PL is dominated by the $^2E_2 \rightarrow {}^4A_2$ transition [71]. However, as the temperature is increased,

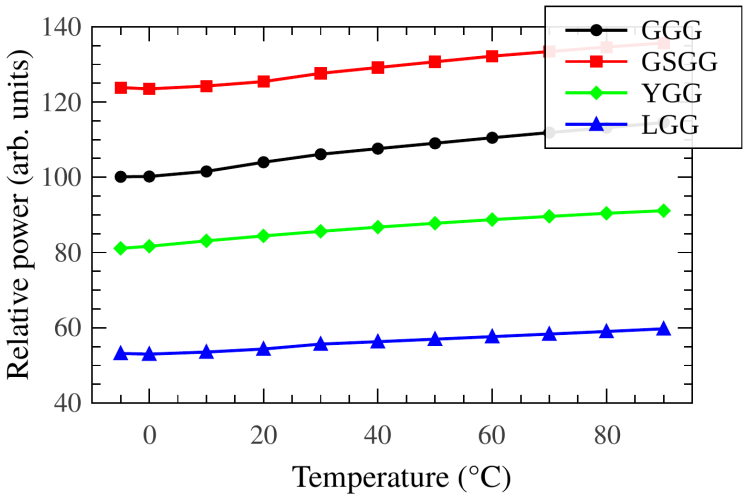

Figure 1.19: Dependence of spectrally integrated PL intensity on ambient temperature for samples annealed at 1400 °C [**III**].

the broad $^4T_2 \rightarrow {}^4A_2$ transition takes place. This effect was also observed for other garnet materials doped with Cr^{3+} ions [49, 69, 71].

The absence of thermal quenching up to 90 °C is an important advantage of the phosphors considered for the pcLED applications. In operation the junction temperature of LEDs reaches more than 100 °C and transfers part of the generated heat to a phosphor converter, thus causing a thermal quenching. As a result, materials characterized by a high thermal quenching temperature are desired for pcLED applications.

1.3.4 Characterization of far-red luminaire

Figure 1.20 presents the spectrum of the designed blue-far-red pcLED luminaire. It is seen that the SPD consists of two spectral components in the blue and far-red regions with the blue to far-red photon flux ratio of 4.6 which satisfies the requirements for phototropic and photomorphogenetic needs of plants [39]. However, in order to fully meet the photophysiological needs of plants the luminaire spectrum should be supplemented by a red component between 620 and 680 nm which is necessary for the process of photosynthesis and photomorphogenesis [28].

Table 1.3 gives the spectral properties of the luminaire for 350 mA driving current. The photon flux was calculated integrating the spectrum in the ranges of 400–520 nm and 650–850 nm for blue and red components, respectively. The efficiency of the converter was found to be 35% which is a satisfactory value taking into account that the internal QE of YGG:Cr

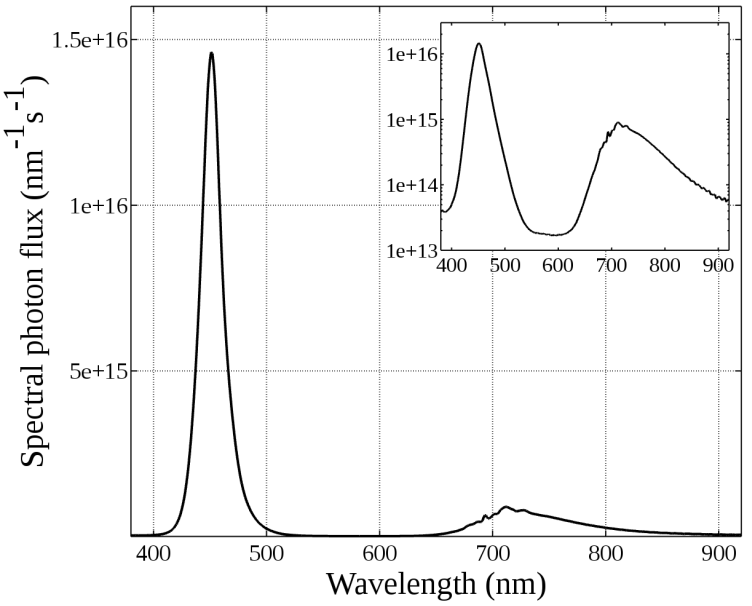

Figure 1.20: Emission spectrum of the blue–far-red pcLED lamp for agriculture. The inset shows the same spectrum in a logarithmic scale. The spectrum consists of two components in the blue and far-red regions that can satisfy phototropic and photomorphogenetic needs of plants [**V**].

8 mol% 1300 °C is 46%.

Table 1.3: Spectral properties of the designed blue–far-red pcLED luminaire for 350 mA driving current [**V**].

Condition	**Component**	**Photon flux**
Lamp covered by a lens	Blue	2.21 µmol/s
Lamp covered by a converter	Blue	0.64 µmol/s
Lamp covered by a converter	Far-red	0.14 µmol/s
Lamp covered by a converter	Sum	0.78 µmol/s
The efficiency of the converter		35%

1.4 Summary

During this part of work gadolinium, gadolinium scandium, yttrium and lutetium gallium garnets doped with various concentrations of Cr^{3+} and calcined at different temperatures were investigated. The PL measurements of GGG:Ce,Cr has shown that Ce causes the quenching of PL in a far-red spectral region, for this reason, the samples were further doped only with

Cr^{3+} ions. Gallium garnets with chromium ions occupying the octahedral site have shown a broad PL band in the far-red spectral region between 700 and 760 nm. The PL bandwidth was different for each garnet due to the effects of crystal field which influences the dominant transitions. As a result the widest PL spectrum was observed for GSGG:Cr where mostly $^4T_2 \rightarrow {}^4A_2$ transition takes place. The narrowest lines were clearly observed for LGG:Cr, where the $^2E_2 \rightarrow {}^4A_2$ transition is dominant.

All garnets have shown no thermal quenching up to 90 °C and were characterized by the increasing overall PL intensity integral with ambient temperature. This is explained by the increasing domination of $^4T_2 \rightarrow {}^4A_2$ transition over $^2E_2 \rightarrow {}^4A_2$ for higher temperatures.

YGG:Cr, 8 mol% calcined at 1300 °C was characterized by the highest QE which is 46% and, for this reason, was chosen for the production of the far-red pcLED luminaire prototype. The SPD of the designed prototype consisted of two spectral components in the blue and far-red regions with a blue to far-red photon flux ratio of 4.6. As a result, the far-red luminaire was declared as a light source meeting the photophysiological processes of plants and suitable for the application in greenhouses.

2 Phosphor converted light-emitting diodes with low circadian action for outdoor lighting

This chapter is devoted to the mesopic solid state sources of light which are to be used for outdoor lighting. The chapter starts with the introduction to the visual and non-visual effects of light to human following with the description of the experimental part as well as the modelling and design of photobiologically friendly mesopic solid state light sources. In the end the characterization of the *firelight* pcLED luminaire prototype is presented. The term *firelight* is defined as the light that has a low CCT ($<$ 2500 K) with the chromaticity that is similar to that of a black body radiation [**VI,VII**]. The results provided in this chapter are based on Paper **II** as well as Patent **VI** and Patent appl. **VII**.

2.1 Literature review

This section provides the reader with the knowledge necessary for understanding human vision during the daylight, in the evening and at night. It also presents the basics of colour science and introduces the main quantities used for the evaluation of colour rendering parameters of light sources. In the last subsection the reader is acquainted with the non-visual effect of light and a concept of circadian action factor.

2.1.1 Efficiency of light-emitting diodes

For the optimization of a light source it is very important to take into account its efficiency which depends on the SPD as well as on other parameters, such like the internal QE, light extraction, the contact resistance and even the manufacture cost. The rapidly developing LED technologies cause the constant increase of the mentioned parameters [1]. For this reason

during this research the efficiency of LEDs was evaluated by taking into account only the SPD and is described as the ratio of light (Φ_v) and radiance (Φ_e) fluxes and is called the luminous efficacy of radiation (LER) K:

$$K = \frac{\Phi_v}{\Phi_e} = K_0 \times \frac{\int_{380}^{780} V(\lambda)S(\lambda)\mathrm{d}\lambda}{\int_0^{\infty} S(\lambda)\mathrm{d}\lambda}, \tag{2.1}$$

where $S(\lambda)$ is the SPD of an LED, λ is the wavelength, $V(\lambda)$ is the spectral luminous efficiency function for photopic vision defined by the International Commission on Illumination (*fr – Commission internationale de l'éclairage*, CIE) in 1924 [72], K_0 is the maximum possible value of luminous efficacy, which for photopic vision equals 683 lm/W [73]. Photopic vision is typical for a daylight environment, i.e. when the average (adaptation) luminance is above 10 cd/m^2. Under such conditions the sense of vision is dominated by three types of photoreceptors in the eye retina (cones), thus the photopic vision is chromatic. At night, when the value of adaptation luminance is below 0.01 cd/m^2, the sense of vision is caused by one type of photoreceptors (rods), therefore under the conditions of low luminance humans lose the ability to distinguish colours. In this case the eye sensitivity function is described by the spectral luminous efficiency function of scotopic vision V'(λ), which was defined by the CIE in 1951 [74]. The maximum possible value of luminous efficacy for scotopic vision is 1700 lm/W [73]. The luminous efficiency functions are dimensionless and usually normalized to 1 or 100%. However, if they are multiplied by the luminous efficacy, they get lm/W dimension and are called the luminous efficacy functions. The spectral luminous efficacy functions for photopic and scotopic vision are presented in Fig. 2.1.

In the early morning or late evening when the adaptation luminance is in a so called mesopic region and varies between 0.01 and 10 cd/m^2 the sense of vision is determined by both cones and rods, the discrimination of colours is reduced, and the eye sensitivity is described by the mesopic spectral luminous efficiency function $\mathrm{V}_{mes}(\lambda)$ which depends on the luminance of the environment. The dependence of the spectral sensitivity of mesopic vision on adaptation luminance is complex and is described by various models. In this work the photometric system MES-2 recommended by the CIE [75] is referred. According to this system, the spectral luminous efficiency function is defined as:

$$V_{mes}(\lambda) = M^{-1}(m)[mV(\lambda) + (1-m)V'(\lambda)], \tag{2.2}$$

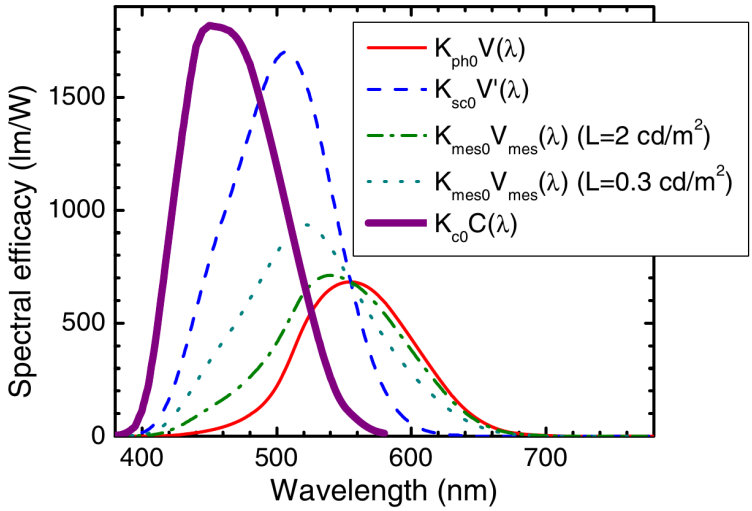

Figure 2.1: Solid, dashed, dotted, and dash-dotted thin lines: photopic, scotopic, and mesopic (for two mesopic adaptation luminances of 0.3, and 2 cd/m^2) luminous efficacy functions, respectively [75]; solid bold line, Gall's circadian action efficacy function normalized to 1817 (bio)lm/W [76] [**II**].

where $M(m)$ is the normalization function and m is the multiplier that depends on the luminance of the environment. In the case of mesopic vision, LER is estimated as:

$$K_{mes} = K_{mes0} \times \frac{\int_{380}^{780} V_{mes}(\lambda)S(\lambda)\mathrm{d}\lambda}{\int_{0}^{\infty} S(\lambda)\mathrm{d}\lambda}, \tag{2.3}$$

where the maximum possible mesopic luminous efficacy K_{mes0} depends on the luminance of the environment and varies from 1700 lm/W to 683 lm/W.

2.1.2 Chromatic parameters of light sources

It is well known that white sources of light can be described by number of properties, e.g. light can be of different chromaticity (red, yellow, purple, etc.), white light may be perceived as having different temperature, i.e. cool or warm, moreover it may saturate, dull or distort the colours of illuminated objects. However, it is not enough to describe the light sources only using the subjective terms above. In order to define white light and be able to quantitatively compare the visual and non-visual effects of different light sources it is of importance to determine the parameters characterizing the

chromaticity, colour temperature and colour quality of light. Further in this section a brief acquaintance with the most widely used parameters defining the light-sources is provided.

Chromaticity coordinates

Usually, the sources of white light used for the general lighting are defined as the light sources having SPDs with correlated colour temperatures (CCT) above 2500 K [7] and chromaticity that does not deviate from the black-body radiation (Planckian locus) more than $Duv = \pm 0.006$ [77]. However, prior the determination of CCT and other parameters, the chromaticity of a light source SPD has to be calculated. The first step in determining the chromaticity is to find the tristimulus X, Y, Z values:

$$\begin{aligned} X &= k \int_{380}^{780} \bar{x}(\lambda) S(\lambda) \mathrm{d}\lambda, \\ Y &= k \int_{380}^{780} \bar{y}(\lambda) S(\lambda) \mathrm{d}\lambda, \\ Z &= k \int_{380}^{780} \bar{z}(\lambda) S(\lambda) \mathrm{d}\lambda, \end{aligned} \tag{2.4}$$

here, k is the normalization multiplier, $\bar{x}(\lambda)$, $\bar{y}(\lambda)$, and $\bar{z}(\lambda)$ are the standard colour matching functions which approximately correspond to the eye sensitivity curves of the red, green and blue cones, respectively [5], and can be found in the literature [4, 78], and $S(\lambda)$ is the SPD of a light source. The tristimulus values X, Y, and Z correspond to colours lightness (light or dark), hue (red, orange, yellow, green, blue or purple), and saturation (pink-red, pastel-fluorescent, pastel blue-deep blue), respectively [44]. Afterwards the chromaticity coordinates can be calculated using the formulae bellow:

$$\begin{aligned} x &= \frac{X}{X+Y+Z}, \\ y &= \frac{Y}{X+Y+Z}, \\ z &= \frac{Z}{X+Y+Z} = 1 - x - y. \end{aligned} \tag{2.5}$$

As eq. 2.5 shows the z coordinate is linearly dependent, for this rea-

son the chromaticity can be described by two coordinates (x, y) in a two-dimensional Cartesian coordinate system. The most widely used colour space diagram CIE 1931 is presented in Fig. 2.2. As it is seen, the diagram

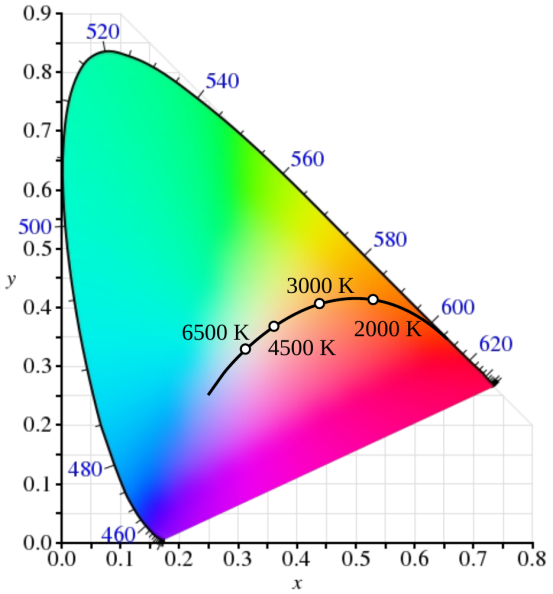

Figure 2.2: CIE 1931 chromaticity diagram. Bold line represents the Planckian locus with white points indicating the colour temperature of a black-body. Blue digits show the peak wavelength of a monochromatic light.

is composed of a horseshoe shaped monochromatic colour curve and a purple boundary [5]. The area covered by the diagram comprises the xy chromaticity coordinates of all real colours. A bold line in the figure is the Planckian or black-body locus which represents the chromaticities of blackbodies having different colour temperatures [44]. Although widely used, CIE 1931 chromaticity diagram has its drawbacks e.g. it is subjectively non-linear and non-uniform, since the subjects tend to distinguish less colours in the green region (the upper part of the diagram) than in the red (the lower right part) or the blue (the lower left part) ones, moreover, the colour differences even between two close points are very spatially non-uniform which causes a more rapid colour change in one direction than in another [79]. This was partly solved in 1960 when CIE has transformed the axes and created a Uniform chromaticity scale (UCS) where the non-uniformity was strongly reduced, although not eliminated [4]. In the UCS diagram the colour difference between two different points is directly proportional to the geometrical distance between those points [5]. The coordinates of this new system were

named uv and can be calculated from the following equations:

$$\begin{aligned} u &= \frac{4X}{X+15Y+3Z} = \frac{4x}{-2x+12y+3}, \\ v &= \frac{6Y}{X+15Y+3Z} = \frac{6y}{-2x+12y+3}. \end{aligned} \tag{2.6}$$

Duv and the correlated colour temperature

The colour coordinates of common light sources seldom exactly match the Planckian locus and usually there exists some offset; for this reason the test light source is described by correlated colour temperature. The CCT of the test light source cannot be calculated using graphical methods due to the non-uniformity of CIE 1931 colour space. As a result, the isothermal lines are introduced which cross the Planckian locus and indicate the geometrical spot of chromaticity coordinates having the same CCT [4]. The equation for the isothermal lines is as follows:

$$(y - y_T) = t_T(x - x_T), \tag{2.7}$$

here x_T and y_T are the coordinates of the intersection of Planckian locus and an isothermal line, and t_T is its inclination. The quantities x_T, y_T, t_T are tabulated in the literature [80].

The distance between the Planckian locus and colour coordinates of the test light source is called Duv and it tells how much does the test light source deviate from the black-body radiation. Duv is calculated as a geometrical distance between two points in a uv coordinate system:

$$Duv = \sqrt{(u - u_{ref})^2 + (v - v_{ref})^2}, \tag{2.8}$$

here u and v are the coordinates of a test light source, and u_{ref} and v_{ref} are the chromaticity coordinates of the black-body having the same colour temperature as the test light-source. In order to obtain a more precise value of Duv more complex triangular or parabolic methods can be applied [81].

Colour rendering index

Due to the differences of SPDs, light sources of similar chromaticity as well as exact CCT values, can have different colour rendering properties, e.g. they can be described by high fidelity, colour saturation, dulling or distortion. Different shape SPDs that are characterized by the same chromaticity

coordinates are called metamers. Different metamers can be distinguished by using parameters defining the colour rendering properties of the light sources. In 1965 CIE introduced the colour rendering index (CRI) R_a which quantitatively describes the ability of a light source to perceive real colours of different objects. During the R_a evaluating procedure, which was improved in 1995 [10] 8 or 14 test colour samples taken from Munsell palette are illuminated with a reference source (e.g. CIE A) which afterwards is switched by the test light source. The data for each colour sample is analysed and colour shifts for each sample are calculated. Then, the colour rendition indices are determined for each sample, and their mean value is called the general colour rendering index – R_a [4]. The maximum value of R_a is 100 and it is attained by incandescent or halogen lamps as well as CIE standard illuminants. However, the procedure described above is only valid for photopic conditions as in the mesopic region the ability to discriminate colours is reduced and, as a result, the mesopic general CRI is expressed as follows:

$$R_{a,mes} = 100 - \gamma(L_{mes})(100 - R_a), \tag{2.9}$$

here $\gamma(L_{mes})$ is the colour shift rescaling factor which depends on the adaptation luminance L_{mes} [73].

However, a small amount of colour samples and the lack of ability to distinguish the colour distortions of different types causes a wide critique towards general CRI. Moreover, due to narrow components comprising SPDs of solid state light sources it is especially not suitable for the evaluation of LEDs. In 2007, the CIE concluded that "the CIE CRI is generally not applicable to predict the colour rendering rank order of a set of light sources when white LED sources are involved in this set" [82]. Nevertheless, due to the simplicity of CRI, it is still widely used in everyday situations, especially in business. For this reason, and since the ability to discriminate colours is reduced under mesopic conditions, the general CRI was chosen as a suitable colour rendering parameter for the outdoor mesopic pcLED with a non-complex SPD consisting of only two spectral components described in this work.

2.1.3 Circadian rhythm of human

For the several past years LEDs drew lots off negative attention and were widely criticized due to the blue-enriched SPDs that cause the disruption of a human circadian rhythm [20, 83]. The light and circadian rhythm connection was known already in the past century. However, it was proven

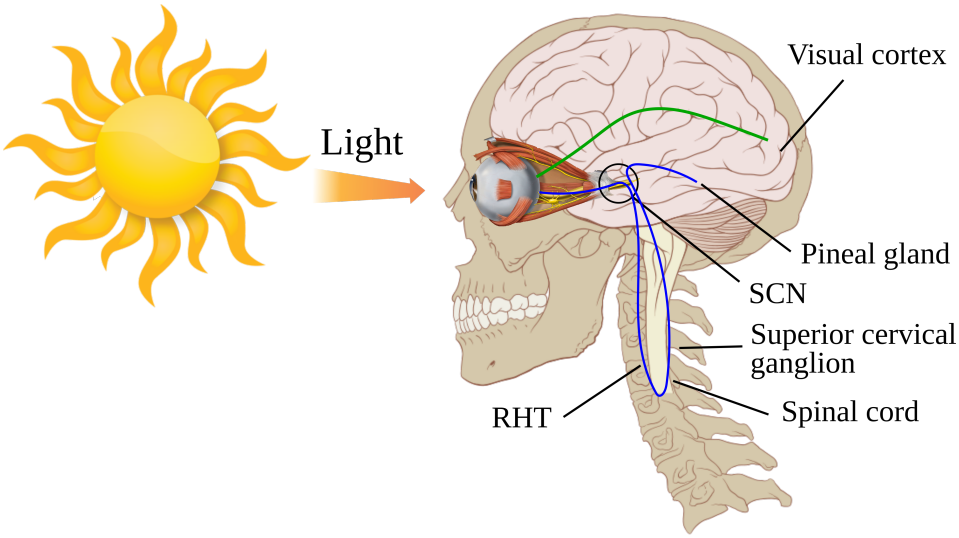

Figure 2.3: A visual path from the receptors in the eye via the optic nerve to the visual cortex in human brain (green), and a retinohypothalamic tract (RHT) from the ganglion cells in the eye via the suprachiasmatic nucleus (SCN), superior cervical ganglion in the spinal cord, back to the SCN and to the pineal gland (blue). Images composing the figure are from [85].

only in the year 2001, when Brainard and Thapan have shown that the ganglion cells in the eye retina together with a supraciasmatic nucleus (SCN) and pineal gland in human brain make a non-visual tract that controls the circadian rhythm [17, 18]. This non-visual path is explained and compared to a visual path in Fig. 2.3. The green line presents the visual path from the receptors in the eye via the optic nerve to the visual cortex in human brain. The blue line depicts the non-visual path, the so called retinohypothalamic tract (RHT). Firstly the blue light is detected by ganglion cells in human retina and the signal is sent to the SCN where it is processed, sent to the spinal cord and comes back to the SCN. Afterwards, the signal is sent to the pineal gland which then suppresses the secretion of sleep hormone and oncostatic agent melatonin [84]. For this reason, in the morning or during the daytime people feel active and energetic whereas in the evening, after the sunset they feel sleepy. It is proven that the disruption of circadian rhythm can cause various health problems such like insomnia, depression or even cancer [20, 19]; therefore, it is of importance to ensure a healthy evening outdoor lighting characterized by a low non-visual effect.

The impact of blue light for humans can be evaluated by calculating the non-visual effect of light. The ganglion cells that are responsible for

the circadian action of light are characterized by a spectral sensitivity in a similar way as the visual receptors. This spectral sensitivity is described by the circadian efficiency function $C(\lambda)$. $K_{c0}C(\lambda)$ is presented in Fig. 2.1 which demonstrates that the peak of this function is at about 460 nm, thus the circadian rhythm is mostly affected by the blue light [76]. The circadian efficacy of radiation (CER) K_c is expressed as:

$$K_c = K_{c0}\frac{\int_{380}^{780} C(\lambda)S(\lambda)\mathrm{d}\lambda}{\int_0^{\infty} S(\lambda)\mathrm{d}\lambda}. \tag{2.10}$$

Under mesopic conditions that are typical for artificial outdoor lighting, the non-visual circadian action of a light source is evaluated by calculating the mesopic circadian action factor (CAF) $a_{c,mes}$ [73]. This factor is defined as the ratio of the non-visual circadian efficacy of radiation to the mesopic LER:

$$a_{c,mes} = \frac{K_c}{K_{mes}} = \frac{K_{c0}\int_{380}^{780} C(\lambda)S(\lambda)\mathrm{d}\lambda}{K_{mes0}\int_{380}^{780} V_{mes}(\lambda)S(\lambda)\mathrm{d}\lambda}. \tag{2.11}$$

It should be noted that K_{c0} is set to 1817 (bio)lm/W, which is such that a_c is dimensionless and equals unity for the CIE standard illuminant A (2856 K blackbody radiation) at photopic conditions. The value of CAF is suitable for the comparison of the non-visual circadian action of different light sources. For lighting in the evening, as low as possible C_{mes} values are desired since, in this case, a higher luminous and a lower circadian efficacies are required. The previous theoretical study has shown that a dichromatic light source with a short wavelength component peaking in the range from 440 to 460 nm and with a long wavelength component peaking between 570 and 600 nm is characterized by a minimum CAF value [73].

2.2 Experimental methods

This part presents the commercial and in scientific papers described phosphors that were used for the pcLED SPD modelling. It also describes the experimental set-up for phosphor PL measurements. Afterwards it introduces the method for modelling the pcLED SPDs employing the colour mixing equations. In the end of this section the design process of two firelight pcLED prototypes is presented.

2.2.1 Model SPDs of photobiologically friendly pcLEDs

The main guidelines for the development of outdoor solid state sources of light with low CAF were made following the results of optimization presented in [73] and are as follows:

1. the SPD must have as low as possible CCT and must contain only two components;

2. the short-wavelength component is to be peaked in the range around 440 nm, and the complementary long-wavelength component is to be peaked in the orange range of the spectrum (such a selection of component peak wavelengths ensures the lowest mesopic CAF due to a low partial power of the short-wavelength component and a high mesopic LER of the compound SPD);

3. for outdoor lighting, the reduced photopic general CRI of such two-component SPDs can be tolerated due to the reduced colour-discrimination ability of human vision at mesopic adaptation luminances.

These guidelines, ensure the feasibility of low-CAF pcLEDs based on the technology of partial conversion of deep-blue emission generated in InGaN semiconductor chips within appropriate phosphors.

Phosphors used for the modelling

Theoretical mesopic photobiologically friendly pcLED SPDs were modelled using PL spectra of commercial garnet (BYW10A, HTY550, HTY560), nitride (HTR620), orthosilicate (BUVOR02, BUVY03, O5446, O6040), and chalcogenide (BUVY02) phosphors (*PhosphorTech* and *Intematix*) as well as of phosphors published in scientific papers: silicate $(Ba,Sr)_2SiO_4:Eu^{2+}$ [86], nitridosilicate $(Ba,Sr)_2Si_5N_8:Eu^{2+}$ [87], chalcogenide $(Ca,Sr)S:Eu^{2+}$ [88], oxonitridosilicate Ca–α–$SiAlON:Eu^{2+}$ [89], and garnet $Y_{3-x}Mg_2AlSi_2O_{12}:Ce^{3+}_x$ (YMASG) doped with different Ce^{3+} concentrations ($x = 0.015; 0.03; 0.045; 0.06$ – YMASG1-YMASG4, respectively) synthesized by the scientists of Vilnius and Münster Universities [60]. The EL spectrum of *Philips Lumileds* Rebel Royal Blue LED (peak wavelength 444 nm) was used as a blue component for model SPDs.

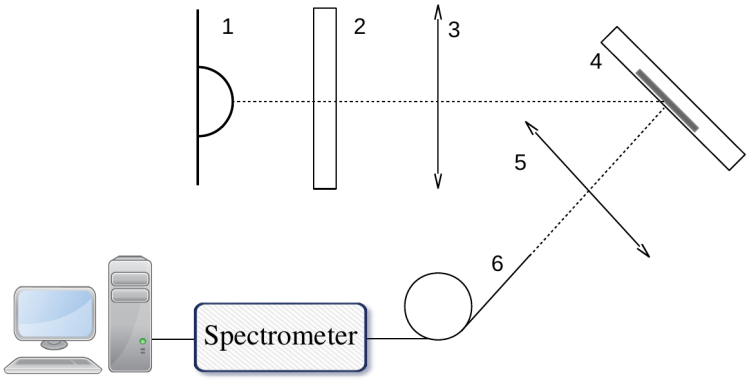

Figure 2.4: Experimental set up for the measurements of PL spectra.

Measurement of PL spectra

The PL spectra measurement scheme is presented in Fig. 2.4. The excitation light emitted by the blue LED passes the blue-pass filter 2 (cutoff 500 nm) and is focused by the convex lens 3 to the sample 4. The PL signal is collected by a convex lens 5 and focused to a fibre 6 which transmits the signal to the spectrometer.

Modeling of LED SPDs

The modelling of mesopic pcLED SPDs was performed using *GNU Octave* software. Firstly, the *xy* chromaticity coordinates of the blue LED EL and phosphor PL were calculated using the colour mixing equations 2.4 and 2.5. The *xy* chromaticity coordinates were used to determine the relative powers of the blue LED EL, and the long wavelength phosphor PL components required to get white light SPDs, characterized by *Duv* values between -0.006 and 0.006 [77]. The parameters (LER, CAF, general CRI) for the resulting SPDs were calculated for two mesopic adaptation luminance levels $L_1 = 0.3$ cd/m^2 and $L_2 = 2$ cd/m^2 that correspond to the illumination requirements for a low-class and high-class road, respectively.

2.2.2 Production of the mesopic firelight pcLED prototype

The detailed description of the prototype is disclosed in Patent **VI** and Patent App. **VII**. The schematic drawing and the picture of the prototype are presented in Fig. 2.5 (a) and (b), respectively. The blue LED chip (1) (peak wavelength 455 nm) grown on the sapphire substrate (2) by the MOCVD method at Vilnius University Institute of Applied Research

Table 2.1: Characteristics of blue-to-orange light converters used for the MesoLED prototype.

Phosphor	O5446	BUVOR02	YMASG
Phosphor concentration in the converter	21 wt%	21 wt%	19 wt%
The thickness of the converter	0.5 mm	1.5 mm	2 mm

(the growth technology and the parameters of the LED are described in Ref. [90]) was placed on a quartz prism (3) and driven by 6.24 V voltage and 20 mA current. The metal terminals (4) were connected via sharp wires (5) using an optical microscope. The emitted blue light (6) was bent by 90 ° towards the light converter (7) containing orange phosphor particles (8). Most of the photons were absorbed by the phosphor particles and converted to orange light (9). The remaining blue light (10) was diffused by the converter and mixed with the orange PL. The resulting firelight was registered with *Avantes* spectrometer. Three phosphor converters were made of three different phosphors – garnet YMASG [60] as well as orthosilicates BUVOR02 (*PhosphorTech*) and O5446 (*Intematix*) mixed with neutral silicone (*Macroflex*). The parameters of phosphor converters are presented in table 2.1. Due to a short lifetime of the lab-grown blue LED, the efficiency of converters could not be evaluated.

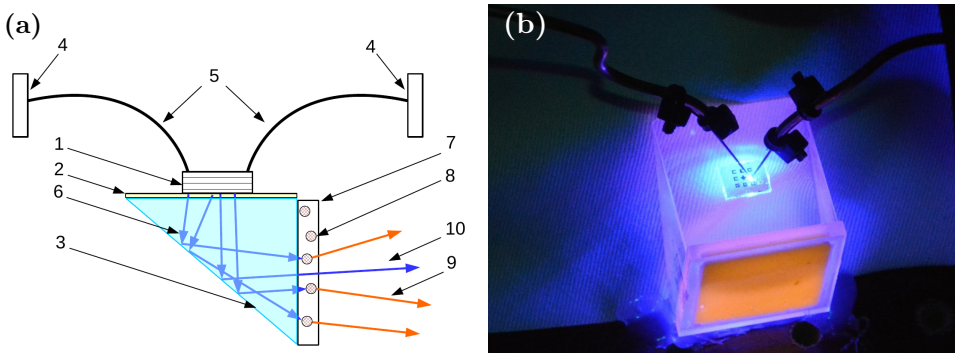

Figure 2.5: (a) Schematic drawing of the mesopic firelight pcLED prototype; (b) picture of a firelight pcLED prototype grown in Vilnius university Institute of Applied research. The remote phosphor presented in figure consists of silicone and orthosilicate phosphor.

Table 2.2: Characteristics of blue-to-orange light converters used for the second firelight LED prototype.

Phosphor	Concentration	Thickness	Efficiency
Intematix O6040	15 wt%	1.2 mm	27%
Intematix O5446	20 wt%	0.6 mm	42%
PTech BUVOR02	35 wt%	1.2 mm	33%

The second set of firelight pcLED prototypes was made using commercial *Philips Lumileds Luxeon Z* Royal blue LED (peak wavelength 450 nm) as an excitation and a blue light source as well as O5446, O6040 and BUVOR02 phosphors for the generation of orange spectral components. A detailed description of the luminaire design and optimization of the phosphor converter is presented in H. Dapkus bachelor thesis [91]. The drawing of the prototype is given in Fig. 2.6. The optimized light converter made of a phosphor and silicone mixture was cast in a PMMA mould no. 1. The blue LED was fixed in a white cone shaped PVC foam reflector 2 drilled by the milling machine, attached to a heatsink and covered by the phosphor converter case. Picture No. 3 shows the photo of the working prototype which is driven by 2.9 V and 1 A. The characteristics of the remote phosphor are presented in table 2.2.

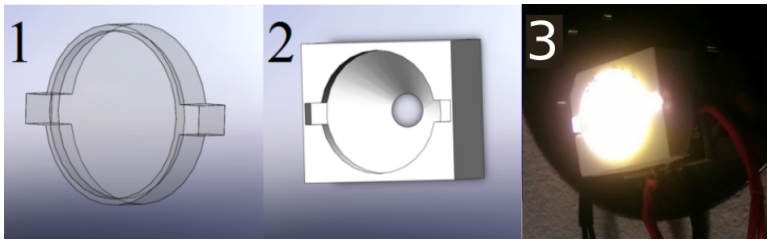

Figure 2.6: Drawing of the second firelight pcLED prototype made of commercial blue LED and an orange silicate phosphor [91].

2.3 Results

This section presents the modelled SPDs of firelight pcLEDs, their *xy* coordinates in the CIE 1931 chromaticity diagram, and photometric properties, such as: LER, CCT, CRI and CAF. In the end of the section the SPDs and spectral parameters of firelight pcLED prototypes are presented and compared. For a better understanding, the SPDs of modelled SPDs and the designed prototypes are compared to the conventional light sources, such as

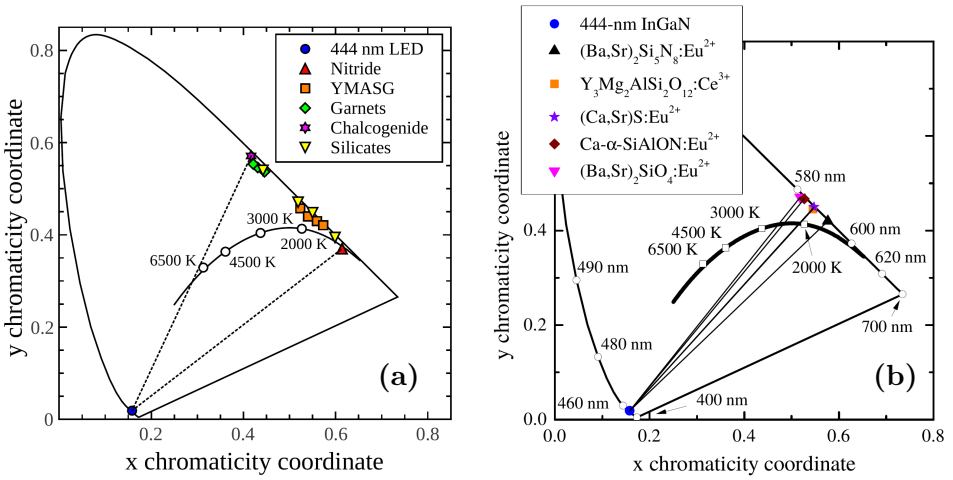

Figure 2.7: CIE 1931 diagrams showing the *xy* chromaticity coordinates of a) the blue LED as well as the commercial and YMASG phosphors used for the modelling. The dashed lines represent the confines of the possible *xy* coordinates of the resulting pcLEDs b) the InGaN emitter, five phosphors from scientific papers (symbols), and possible resulting pcLEDs (lines). Bold line represents the Planckian locus [**II**].

commercial dichromatic cool and white pcLEDs, HPS lamp, as well as the CIE standard illuminant A.

2.3.1 Modelling results

Figure 2.7 presents CIE 1931 chromaticity diagrams showing the *xy* coordinates of the blue 444 nm InGaN LED as well as of a) YMASG and commercial phosphors and b) phosphors described in scientific papers; that were used for the modelling. The bold line represents the Planckian locus, the dashed and the thin lines shows the possible chromaticities of the resulting pcLED. It is clearly seen in CIE 1931 diagram that a wide gamut of commercial phosphors was chosen. However, the results published in [73] and the modelling of SPDs comprising commercial phosphor PL bands have revealed that the SPDs of lower CCTs are characterized by smaller CAF values. For this reason, only phosphors exhibiting PL in the orange spectral region were chosen from the scientific papers for further modelling.

Figure 2.8 presents some of the modelled SPDs of LEDs with minimized CAF value. The SPDs presented on the left hand side were modelled using PL bands of commercial phosphors and those on the right hand side were modelled using PL bands of phosphors described in scientific pa-

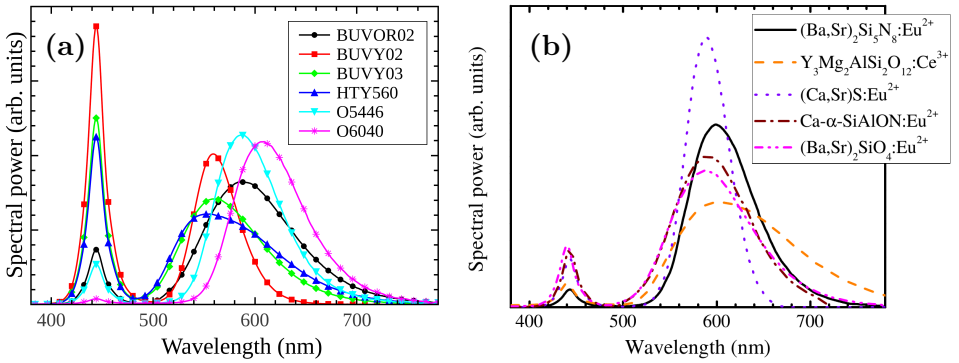

Figure 2.8: Some of the modelled SPDs of firelight LEDs with minimized circadian action factor. a) PL bands of commercial phosphors; b) PL bands of phosphors described in scientific papers; were used for the long wave components [**II**].

pers [**II**]. In order to make the figure more clear, similar shape SPDs containing the PL bands of HTY550, BYW01A as well as YMASG1, YMASG3 and YMASG4 phosphors were omitted in Fig. 2.8 a) and b) ,respectively. These SPDs are of a very similar shape to SPDs labelled as HTY560 and $Y_3Mg_2AlSi_2O_{12}$:Ce^{3+}, respectively. Figure 2.8 shows that all SPDs consist of two spectral components in the blue and orange regions where the blue dominates for higher CCT values, and the orange for the lower ones. Fig. 2.8 a) and b) also demonstrate that Ce^{3+} activated garnets exhibit the broadest PL spectra thus yielding the highest R_a values (see tab. 2.3) of the resulting LED SPDs, whereas the Eu^{2+} doped chalcogenides are characterized by the narrowest PL bands which are almost void in the range of 500 nm and therefore are characterized by the lowest R_a values.

Table 2.3 presents the spectral parameters of the modelled MesoLED SPDs and common light sources such as dichromatic cool and warm white LEDs, HPS lamp and CIE standard illuminant A. From left to right the columns display the names of phosphors used, the CCT value, the limiting radiant efficiency, η_0, which accounts for the Stokes shift of phosphor photoluminescence in respect to the primary blue emission [5, 92], the mesopic CAF, LER, and photopic general CRI (R_a) as well as its mesopic equivalent ($R_{a,mes}$) for two adaptation luminances (0.3 and 2 cd/m^2). The CRI equivalents were estimated with respect to [73] regarding the reduction of the colour discrimination ability at decreased mesopic adaptation luminance as is defined by equation 2.9.

Table 2.3 also shows that SPDs characterized by a high CCT ($\geq$ 4500 K) have relatively high CAF values ranging from 1.481 to 2.03 for

Table 2.3: Spectral parameters of pcLED SPDs for mesopic vision modelled using PL spectra of commercial phosphors and YMASG phosphor. Here $L_P > 10$ cd/m^2, $L_1 = 0.3$ cd/m^2 and $L_2 = 2$ cd/m^2.

Phosphor	**CCT, K**	η_0	**CAF**		**LER, lm/W**		**CRI**		
			L_1	L_2	L_1	L_2	L_P	L_1	L_2
Commercial phosphors									
BUVY02	8735	0.87	1.824	2.030	403	363	33	83	66
HTY550	7284	0.84	1.715	1.970	385	335	66	91	83
BYW01A	6185	0.84	1.546	1.737	387	344	64	91	82
BUVY03	5391	0.83	1.387	1.516	398	364	56	89	78
HTY560	5000	0.82	1.350	1.481	382	348	64	91	82
BUVOR02	2532	0.76	0.519	0.504	344	354	54	88	77
O5446	2148	0.75	0.337	0.315	358	384	34	83	66
O6040	1445	0.72	0.117	0.104	250	281	40	84	69
$Y_3Mg_2AlSi_2O_{12}$:Ce^{3+}									
YMASG1	2383	0.72	0.521	0.511	271	276	69	92	84
YMASG2[a]	2088	0.72	0.362	0.345	250	263	62	90	81
YMASG3	1876	0.70	0.270	0.251	222	239	59	89	79
YMASG4	1732	0.70	0.233	0.216	206	223	61	90	80
Other phosphors [II].									
$(Ba,Sr)_2SiO_4$:Eu^{2+}	2542	0.75	0.531	0.516	343	353	55	88	77
Ca$-\alpha-$SiAlON:Eu^{2+}	2425	0.76	0.479	0.462	356	369	53	88	76
(Ca,Sr)S:Eu^{2+}	2101	0.77	0.308	0.283	404	439	16	78	57
$(Ba,Sr)_2Si_5N_8$:Eu^{2+}	1704	0.73	0.186	0.169	298	329	39	84	69
Common light sources									
Cool white LED	5000	0.82	1.171	1.278	394	361	65	91	82
Warm white LED	3652	0.77	0.747	0.772	377	365	62	90	80
HPS lamp	1886	-	0.313	0.290	319	344	12	77	55
CIE A	2856	-	0.856	0.911	170	160	100	100	100

[a]Ploted as $Y_3Mg_2AlSi_2O_{12}$:Ce^{3+} in Fig. 2.8 b).

$L_2 = 2$ cd/m^2. For comparison, under the same luminance level the CAF of CIE A standard illuminant is only 0.911. It is also observed that CAF values of the proposed firelight SPDs are 1.6–4.2 times lower than that of the CIE A illuminant. These results reveal the correlation of human physiology, psychology and evolution, which is defined as Kruithof's rule and claims that the preferred CCT of a light source increases with luminance [93, 94]. It is also observed in the table that due to the increased overlap of the orange component with the mesopic luminous efficacy function (see Fig. 2.1) the CAF of each firelight slightly decreases when the luminance increases. Due to the void in the green region all firelight SPDs are characterized by a relatively low general CRI which ranges between 16 and 69. However, they satisfy the requirements for the street lighting applications since the mesopic CRI equivalent for luminance L_2 is in the range of 66–84 and greatly

surpasses the widely used HPS lamps ($R_{a,mes} = 55$). LER values of firelight sources vary between 206 and 439 lm/W and are slightly larger for SPDs containing orange spectral components with a shorter wavelength. This is explained by the larger overlap of a phosphor PL band and mesopic luminous efficacy function (see Fig. 2.1). For higher mesopic adaptation luminance the efficacy function shifts towards longer wavelengths, for this reason, the LER of firelight SPDs slightly increases with luminance. The highest LER value is achieved for the SPD modelled with (Ca,Sr)S:Eu^{2+} phosphor PL band and reaches 439 lm/W for L_2. This SPD is also characterized by a particularly small CAF $a_{c,mes} = 0.283$. However, its colour rendering ability is poor as the $R_{a,mes}$ is only 57 for L_2. The most promising and versatile phosphors for firelight sources are silicates, since they offer relatively high LER (343–369 lm/W), small CAF (0.531–0.462) and reasonable mesopic CRI (76–88) for L_1 and L_2, respectively. Despite of the lower LER, than that of a common warm white pcLED (365–377 lm/W), the significantly lower CAF values of the modelled SPDs give the advantage for firelight sources in the outdoor applications where a part of efficacy can be traded for photobiological safety and reduced light pollution, such as: pedestrian and residential areas, parking lots, old-town and fine architecture locations or parks.

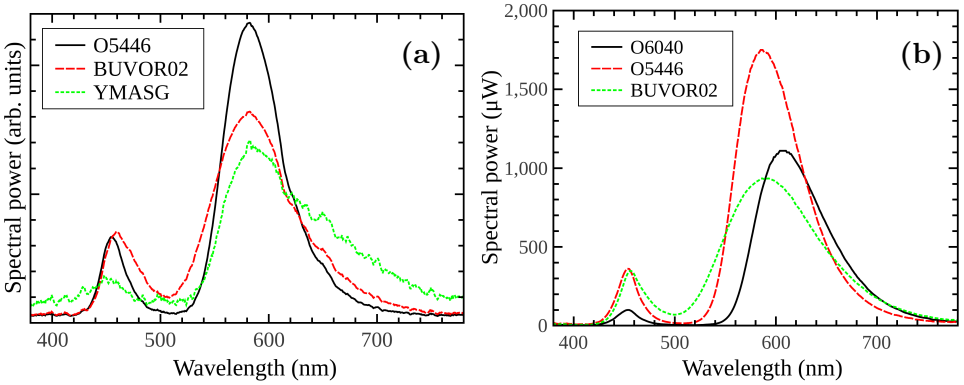

Figure 2.9: SPDs of the designed firelight prototypes. Phosphors were excited by: a) an InGaN LED ($\lambda_{peak} = 455$ nm) grown at VU TMI; b) a commercial Philips Lumileds Luxeon Z LED ($\lambda_{peak} = 445$ nm).

2.3.2 Characteristics of the designed luminary

The SPDs of prototypes containing the InGaN LED grown in the lab and a commercial LED are seen in Fig. 2.9 a) and b), respectively. The figure

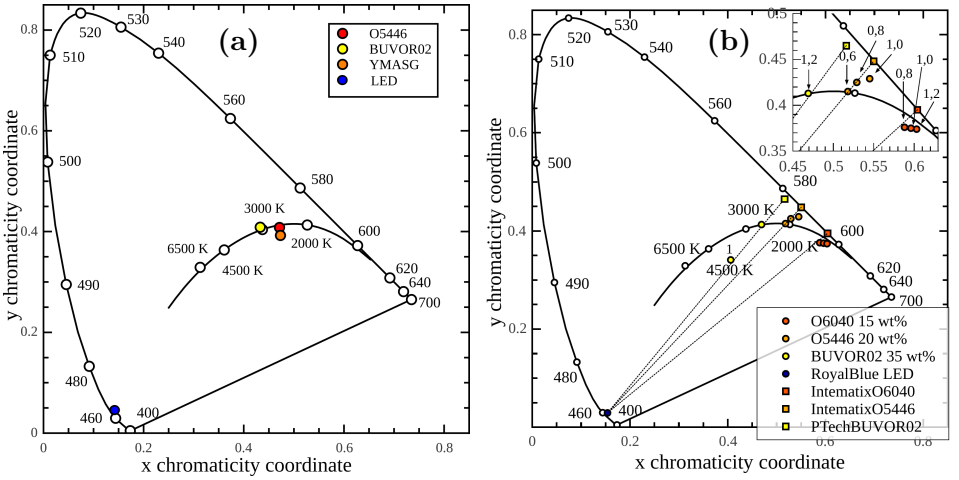

Figure 2.10: CIE 1931 chromaticity diagrams showing the *xy* coordinates of firelight pcLED prototypes SPDs. Phosphors were excited by a) the InGaN LED ($\lambda_{peak} = 455$ nm) grown at VU TMI; b) a commercial Philips Lumileds Luxeon Z LED ($\lambda_{peak} = 445$ nm).

shows that the shapes of these SPDs are very similar to the modelled ones and consist of an unpronounced blue and a dominant orange components. Due to the relatively low efficiency of YMASG phosphor converter the signal of this SPD is low and noisy. However, the signal to noise ratio varies around 8–14% thus the general shape of the SPD remains unchanged and its parameters are not influenced much. Figure 2.10 a) and b) depicts CIE 1931 chromaticity diagrams showing the *xy* coordinates of the first and second sets of the designed pcLED prototypes, respectively. It is seen that all SPDs are characterized by a low CCT and are located very close to the Planckian locus with D_{uv} values of a) 0.0036, -0.0023, and -0.0108

Table 2.4: Spectral parameters of pcLED prototypes for mesopic vision designed using lab-grown and commercial LEDs. Here $L_P > 10$ cd/m^2, $L_1 = 0.3$ cd/m^2 and $L_2 = 2$ cd/m^2.

Phosphor	**CCT, K**	η_0	**CAF**		**LER, lm/W**		**CRI**	**CRI**$_{mes}$	
			L_1	L_2	L_1	L_2	L_P	L_1	L_2
Lab-grown LED									
BUVOR02	3110	0.82	0.792	0.814	362	352	57	89	81
O5446	2533	0.79	0.568	0.551	370	383	32	82	66
YMASG	2389	0.81	0.697	0.690	256	259	57	89	78
Commercial LED									
BUVOR02	2585	0.77	0.600	0.596	336	338	61	90	80
O5446	2100	0.77	0.367	0.345	348	373	34	83	66
O6040	1345	0.73	0.223	0.199	229	257	34	83	66

for BUVOR02, O5446, and YMASG, respectively and b) 0.0002, -0.0015, and -0.0058 for BUVOR02, O5446, and O6040, respectively. The spectral parameters of designed prototypes are presented in tab. 2.4. Although two of the remote light converters were made of the same phosphors, the spectral parameters of different sets of prototypes vary due to the differences of lab-grown and commercial blue LEDs. As seen in Fig. 2.10 the lab-grown LED is characterized by a higher dominant wavelength. For this reason the CCTs of prototypes designed with this LED are higher. However, in both cases the tendencies remain similar as for the modelled SPDs – the low CCT prototypes are characterized by a low CAF, sufficient LER (if compared to "Common light sources" in tab. 2.3) as well as a satisfactory CRI_{mes}.

2.4 Summary

During this part of work the SPDs of dichromatic blue-orange pcLEDs operating in the firelight range of CCTs (1700–2500 K) were modelled and their photometric, photobiological, and colourimetric properties for mesopic conditions were assessed. The proposed theoretical pcLEDs are characterized by a low CAF and are advantageous in respect of common white pcLEDs for the use in photobiologically safe low-luminance outdoor lighting. Moreover, most of them have the mesopic equivalent of the general CRI comparable to the general CRI of common LEDs under photopic conditions.

Afterwards, two sets of firelight pcLED prototypes, based on the modelling results were designed. The first prototype, was designed using commercial phosphors and the blue InGaN LED grown in the Vilnius University Institute of Photonics and Nanotechnology, whereas for the second prototype a commercial blue InGaN LED was used as an excitation source. The first firelight pcLED prototype was characterized by a slightly higher CCT, CAF and LER due to the longer peak wavelength of the blue spectral component. Nevertheless, both prototypes were characterized by low CAF values (if compared to the common pcLEDs or CIE A standard illuminant) and reasonable mesopic CRI.

The firelight pcLEDs can find application in many outdoor environments (e.g., in pedestrian and residential areas, old-town and fine architecture locations, etc.), where a part of efficacy can be traded for photobiological safety, reduced light pollution, visual comfort and illumination design diversity.

3 Phosphor converted light-emitting diodes of preferential colour properties

In this chapter the optimisation and modelling of pcLED SPDs with different colour rendition properties: high fidelity, colour saturation, dulling and preference are presented. The second part of this chapter is focused to a pcLED characterized by colour preference (PrefLED) which has the ability to perceive a more appealing look of the illuminated objects. The chapter discusses the design process, characterization and a psychophysical validation of this particular light source. The information and results provided in this chapter are based on Paper **I**, Patent **VIII** and Conf. Works **IX**.

3.1 Literature review

This sections gives a more comprehensive review on the colour science and introduces a variety of metrics used for the evaluation of the colour rendition parameters of light sources with the emphasis on the advanced statistical colour rendition evaluation approach. Afterwards the PL band shape of different phosphors is discussed and the criteria for choosing a suitable phosphor family for the modelling are presented.

3.1.1 Advanced colour rendition metric

As it was discussed in the previous chapter, the diversity of SPDs resulting from the variety of solid-state light sources, caused the disruption of the common colour quality and rendition ability evaluation metric CRI. The simplest remedy for the disadvantages of CRI is to establish a two-metric system which accounts not only for the light source ability to make colours look realistic but also to make them appear "vivid" and easy to distinguish, i.e. colour saturating [95]. A method that quantifies the ability of a light source to render colours with high fidelity as well as discriminates colours within a figure of merit is the Colour quality scale (CQS) [96]. The general

CQS (Q_a) is estimated using 15 test colour samples and is based on the disregard of the colour saturating component in the colour shifts. The CQS metric contains additional scales such as colour fidelity scale (C_f), gamut area scale (Q_g) and colour preference scale (Q_p), but nevertheless suffers from a small number of test colour samples covering a small part of the colour space and make the results dependent on the chosen sample set.

A more comprehensive approach to the assessment of colour rendition parameters and quality of light sources is to analyse the shifts vectors of the entire colour palette (e.g. for 1269 Munsell samples) and, depending on the type of the colour distortion that occurs when the reference source is switched by that under assessment, to sort the test samples to several different groups [97]. This statistical method clearly distinguishes between the different types of colour distortions. The computational sorting of the colour shift vectors is based on the experimentally established just perceived differences of chromaticity and luminance. Afterwards, the relative numbers (percentages) of test colour samples exhibiting different types of colour distortions are defined as statistical colour quality indices, which include the Colour Fidelity Index (CFI, percentage of the test samples having the colour shifts smaller than perceived chromaticity differences), the Colour Saturation Index (CSI, percentage of the test samples having the colour shift vectors with a perceivable increase in chromatic saturation), the Coulor Dulling Index (CDI, percentage of the test samples having the colour shift vectors with a perceivable decrease in chromatic saturation), and the Hue Distortion Index (HDI, percentage of the test samples having the colour shift vectors with perceivable distortion of hue). The SPDs of light sources can be evaluated using the statistical method and compared to CRI and CQS using an online tool [98].

The most recent and widely used colour rendition metrics is a two-measure system having parameters R_f and R_g that correspond to the colour fidelity and gamut area, respectively [9] This metric that was proposed in the year 2015 is based on 99 colour samples with colour space and spectral uniformity that are taken from a real world environment. Although the R_f R_g metric has many advantages over CRI or CQS, it is not very suitable for defining the preferred lighting since in some cases two different metameric SPDs might have the exact R_f R_g values [99].

It is of importance that the colour quality of illumination should not be confined only by colour fidelity. In fact, it is widely known that the increased colour saturation improves the colour discrimination ability and agrees with the visual preference [100, 12]. For sophisticated objects such as artwork even more complex colour rendition properties may be required [70].

3.1.2 Optimization of direct emission LEDs

The optimization of direct emission LED SPDs, consisting of distinct single-band components (FWHM around 30 nm) and characterized by different colour rendition properties measured by statistical colour rendition indices CFI, CSI, and CDI, is described in [6, 101, 102], respectively. These results led to the construction of a Colour rendition engine – a tetrachromatic (RAGB – red, amber, green and blue) LED cluster with the ability to continuously traverse all possible metameric SPDs including those with the highest CFI, CSI, and CDI [15]. The highest values of the statistical indices as well as the conditions of preference lighting have been validated by the psychophysical experiment. The experiment has shown that most of the subjects give preference for SPDs with the CSI to CFI ratio varying between 0.3 and 3. This means that the direct emission LED cluster can be used to obtain not only the hight fidelity SPDs, but also those characterized by colour dulling, colour saturation or preference. However, the colour rendition engineering of SPDs composed of phosphor PL components is a more complex problem due to the the large diversity of phosphor emission spectra with different shapes, widths or even numbers of bands.

3.1.3 Selection of phosphor family for the model

One of the first attempts to determine the trade-off between the general CRI and LER for Gaussian shape SPDs was performed by Thornton in 1971 when the phosphor blends of both high and low fidelity used for fluorescent lamps were already known [103, 104]. The number and width of Gaussian components composing pcLED SPD of ultimate colour rendition (CFI = 100%) were determined later [105]. However, a general approach to the composition of practical phosphor blends for pcLEDs that emit light with different colour rendition properties has not been established so far. Due to a large diversity of phosphors considered for the application in solid-state lighting technology [7, 31, 44, 106, 107, 108], the first step towards the colour rendition engineering requires establishing model phosphor SPDs. Such component SPDs should meet the following requirements:

1. the SPDs should be related to a family of practical phosphors that have peak wavelengths within the entire visible spectrum;

2. the SPDs should be described with an appropriate accuracy by a single analytical expression containing a small number of parameters (e.g., just the peak wavelength).

Once the general approaches were established for a particular model component SPD, phosphors with SPDs that considerably differ from the model ones could be considered.

Taking into account the above requirements, the search of model phosphors was restricted to those having a single emission band with a predictable width. Phosphors characterized by multiband SPDs due to the spin-orbit split ground state (e.g. Ce^{3+} phosphors with $5d - 4f$ transitions [109]) or due to co-doping with several types of ions were not considered. Phosphors emitting due to shielded $4f - 4f$ transitions, which have SPDs with multiple narrow-band structure (e.g., Eu^{3+}, Sm^{3+}, and Tb^{3+} activated phosphors [53]) were also rejected.

The most appropriate and versatile model phosphor components for the use in colour rendition engineered SPDs are phosphors that emit due to $4f^6 5d^1 - 4f^7$ transitions in Eu^{2+} ions occupying similar sites within the host lattice. Such phosphors have distinct single bands with the width that on the wavelength scale has a tendency to increase with increasing peak wavelength. Depending on the crystal field splitting of the $5d$ level, the peaks of the spectral bands due to Eu^{2+} emission are available within the entire visible spectrum [110].

3.2 Experimental method

The experimental part of this chapter introduces the PL band model used for the optimization process and presents it's approval based on the comparison to the real phosphor PL bands. Also, the design process of the solid state luminaire of preferential colour rendition (PrefLED) is described and the guidelines of the psychophysical experiment carried in order to validate the PrefLED luminaire are given.

3.2.1 Choosing the suitable PL band model

There are several different methods that analytically describe the PL bands of phosphors [103, 105, 111, 112]. The model employed in this work was

determined by the authors of Paper **I**. This model describes a single PL band belonging to the Eu^{2+} doped phosphor family by Gaussian distribution in the photon energy scale [113]:

$$S_i(h\nu)\mathrm{d}\nu = 2\sqrt{\ln(2)/\pi}/W \exp[-4\ln(2)(h\nu - h\nu_i)^2/W^2]\mathrm{d}\nu, \qquad (3.1)$$

here $h\nu_i$ is a photon energy at the peak value, W - the full width of the spectrum at half maximum (FWHM) that depends on a phosphor matrix and is expressed in energy units. In the wavelength scale, the equation 3.1 is expressed as:

$$S_i\mathrm{d}\lambda = k(\lambda/\lambda_{0i})^{-2} \exp[-4\ln(2)h^2c^2(\lambda^{-1} - \lambda_{oi}^{-1})^2/W^2]\mathrm{d}\lambda, \qquad (3.2)$$

here $\lambda_{0i} = c/\nu_i$ (in the wavelength scale λ_i does not necessarily indicates the peak value), and k – normalization multiplier that does not have an analytical expression.

In order to develop a versatile model SPD a single value of energy FWHM to a variety of single-band Eu^{2+} phosphors described in literature and patents was attempted to apply. Figure 3.1 presents the dependence of FWHM in nm on the PL peak wavelength for various phosphors activated by Eu^{2+} ions. The circles, squares, diamonds, upward and downward triangles, and stars show the data for chalcogenides (sulphides [114, 32, 115] and selenides [88] of alkaline earth metals as well as thiochalcogenides [114, 86]), silicates [116, 117], aluminates [32, 118], nitridosilicates [119, 120], oxonitridosilicates (SiONs) [121, 122, 123], and oxonitridoaluminosilicates (SiAlONs) [124, 125]. Since the Eu^{2+} ions in some of these phosphors occupy different positions yet causing a dual structure of PL bands (e.g. ortho- and pentha-silicates [126] and nitridosilicates [127]) the data was sorted in respect to the appropriateness of the single-band model. The PL spectra of the above mentioned phosphors were digitized and fitted with the equation 3.2. Afterwards the fitting parameter R^2 was calculated which can possess the maximum value of 1 meaning a perfect fit. The open and solid points in Fig. 3.1 show data for phosphor PL bands with $R^2 < 0.99$ and $R^2 > 0.99$, respectively.

The line in Fig. 3.1 demonstrates the FWHM values in nm of spectra described by the equation 3.2. The FWHM in energy range was fixed and equal to 0.27 eV. Figure shows that the model FWHM monotonously increases from 44 to 93 nm in the peak wavelength range between 450 and 650 nm. The FWHM values of most Eu^{2+} activated phosphors PL spectra that are characterized by a single-band model ($R^2 > 0.99$) deviate from the

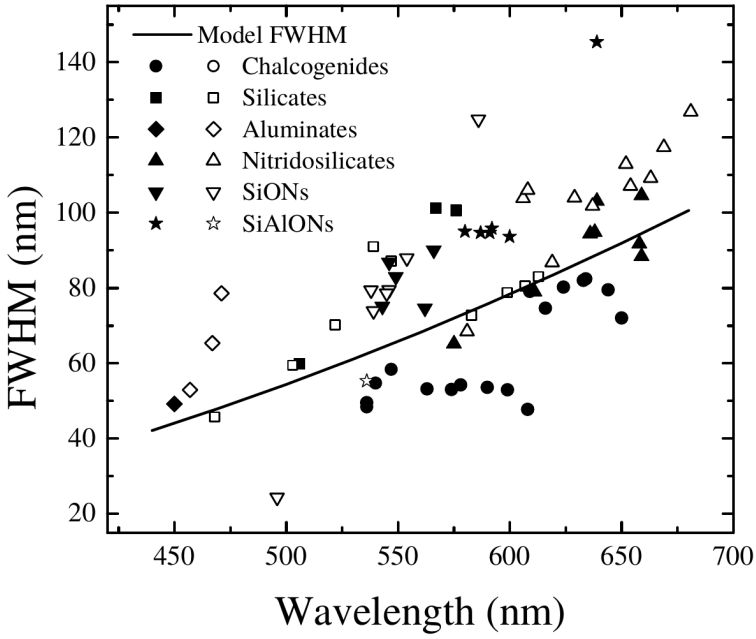

Figure 3.1: Dependence of FWHM in nm on the PL peak wavelength for various phosphors activated by Eu^{2+} ions. The open and solid points show data for phosphor PL bands that can be approximated by the equation 3.2 with $R^2 < 0.99$ and $R^2 > 0.99$, respectively [**I**].

solid line by no more than 20 nm. Chalcogenide phosphors have smaller FWHM values due small phonon frequencies [110]. However, SPDs of these phosphors are well described by the equation 3.2 ($R^2 > 0.99$). Most silicates, aluminates and nitrides have FWHM values that are equal or slightly larger than those of the model, nevertheless, many of them cannot be well fitted with the single band model ($R^2 < 0.99$).

Fig. 3.2 demonstrates SPDs of some Eu^{2+} activated phosphors (solid lines) as well as model SPDs of the same widths (dashed lines). The PL spectra from left to right belong to corresponding phosphors: blue $Ba_{0.6}Eu_{0.4}MgAl_{10}O_{17}$ (BAM, peak wavelength – 457 nm FWHM – 57 nm [118]), cyan Ba_2SiO_4:Eu^{2+} (peak wavelength – 503 nm, FWHM – 59 nm [116]), yellow $EuSi_2O_2N_2$ (peak wavelength – 586 nm, FWHM – 125 nm) and red SrS:Eu^{2+} (peak wavelength – 616 nm, FWHM – 75 nm [114]). The SPDs of blue, cyan and red phosphors are well described with the equation 3.2 and have the R^2 values greater than 0.99. However, the yellow phosphor deviates from the model and in this case $R^2 = 0.978$.

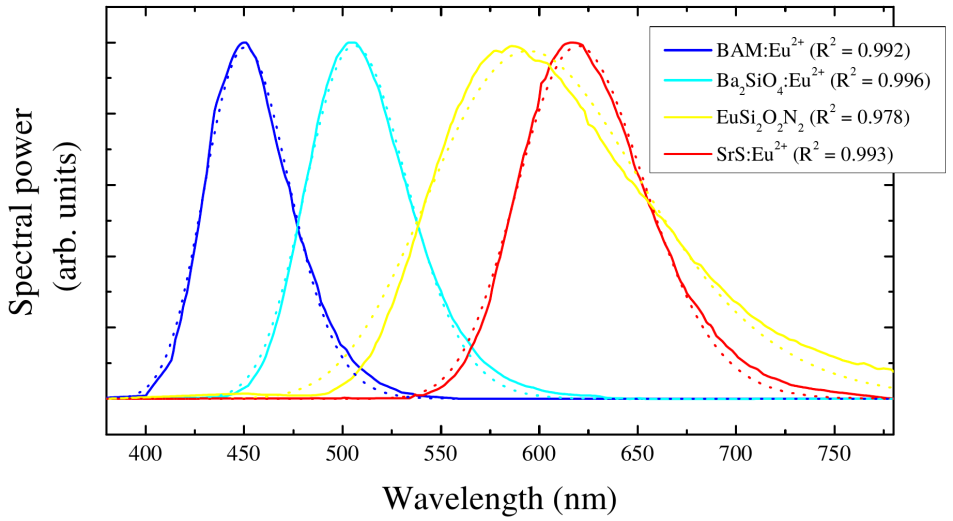

Figure 3.2: Some examples of the Eu^{2+} activated phosphor PL bands (solid lines) and the PL band fitted using the equation 3.2 (dashed lines) [**I**].

3.2.2 Optimization procedure

Computer optimization procedure was performed by prof. R. Vaicekauskas from the Vilnius University Faculty of Mathematics and Informatics. In order to optimize SPDs for pcLEDs three different components described by the equation 3.2 were combined to form trichromatic blends of different CCTs (3000, 4500, and 6500 K) using colour mixing equations described in subsec. 2.1.2. The optimal composite spectra were separately calculated for each CCT as functions of LER by maximizing an objective function for each of four colour parameters.

The objective function for colour fidelity blends is expressed as follows:

$$F_{CCT,LER}(\lambda_1, \lambda_2\lambda_3, p_1, p_2, p_3) = CFI, \tag{3.3}$$

here λ_1, λ_2, λ_3 and p_1, p_2, p_3 are the peak wavelengths and partial radiant fluxes of the three model phosphors spectra, respectively. For the colour saturation blend the objective function is:

$$F_{CCT,LER}(\lambda_1, \lambda_2\lambda_3, p_1, p_2, p_3) = CSI|_{HDI \leq 50\%}. \tag{3.4}$$

In the expressions here and bellow the constraint $\leq 50\%$ prevents high hue distortions. The objective functions for the colour dulling and colour

preference blends are, respectively, expressed as:

$$F_{CCT,LER}(\lambda_1, \lambda_2\lambda_3, p_1, p_2, p_3) = CDI|_{HDI \leq 50\%}, \quad (3.5)$$

$$F_{CCT,LER}(\lambda_1, \lambda_2\lambda_3, p_1, p_2, p_3) = CSI/CFI|_{HDI \leq 50\%, CDI \leq 10\%}. \quad (3.6)$$

In this case the constraint CDI $\leq 10\%$ prevents the solutions with low CSI and CFI values.

In all cases the six objective functions variables must satisfy the aforementioned colour mixing equations. For this reason the objective functions were maximized in the optimization region which is a parametric space with three degrees of freedom. The objective functions are maximized with a computer program that stochastically searches for the solution on a 3 dimensional parametric surface for the chosen CCT and LER values [78].

3.2.3 Modelling of SPDs and temperature measurements.

For the SPD modelling the PL spectra of the following Eu^{2+} activated commercial phosphors were used: blue BAM (*Intematix* B101C-2, 446 nm peak wavelength, 45 nm FWHM), cyan, green and orange silicates (*Intematix* G1758, 507 nm peak wavelength, 59 nm FWHM; EG3264, 528 nm peak wavelength, 71 nm FWHM, and O6040, 606 nm peak wavelength, 81 nm FWHM, respectively), as well as red and deep red nitrides (*PhosphorTech* HTR620, 617 nm peak wavelength, 83 nm FWHM, and *Intematix* ER6436; 625 nm peak wavelength, 87 nm FWHM, respectively). The modelling procedure was performed using *MathWorks® MATLAB* in the same way as described in subsec. 2.2.1. Phosphor PL for the SPDs modelling were measured using the method described in subsec. 2.2.1, except for BAM phosphor, were a near UV LED was used as an excitation source (peak wavelength 378 nm).

The temperature dependence was measured separately for each phosphor using a *LabSphere* Peltier element in the 0–80 °C temperature range.

3.2.4 Design process of a PrefLED luminaire

Figure 3.3 presents the drawing and the picture of the designed PrefLED luminaire. Eight blue light-emitting diodes (*Cree Royal Blue XP-E2*, EL peak value 453 nm) (1) were connected in series and soldered on a custom metal-core PCB board attached to a heat sink (2). As it is shown in the figure, one part of the blue EL is absorbed and converted by a 1 mm thickness, 25 wt% concentration green phosphor converter (3) made of silicone (*Dow*

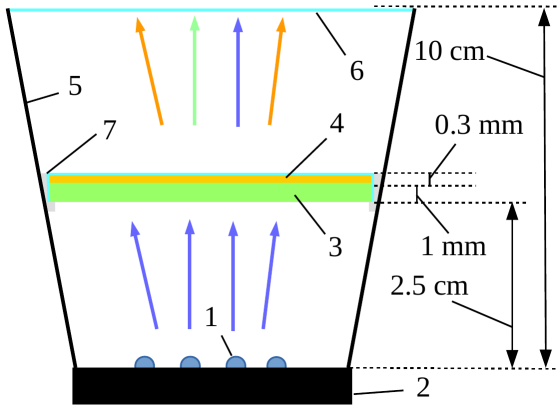

Figure 3.3: Scheme of the PrefLED luminaire [**IX**].

Corning AS 7096) and the aforementioned *Intematix G1758* phosphor mixture. The second part of the blue EL is converted by a 0.3 mm thickness, 15 wt% concentration red phosphor converter (4) made of the same silicone and *Intematix ER6436* phosphor mixture. The phosphor converter layers were sandwiched instead of intermixing so as to avoid the reabsorption and quenching of the less efficient phosphor. The luminaire was placed in a reflecting case (5) and covered with a round glass plate (6). The converter case (7) was milled using *ROLAND Modela 4 MDX – 40* milling machine of white PVC foam and PMMA. The thicknesses and concentrations of the phosphor converters were optimized prior the manufacturing process in collaboration with VU FF bachelor student Henrikas Dapkus, see ref. [91] for the optimization details. The blue LED as well as green and orange phosphors for the PrefLED prototype were selected according to the optimization results for pcLEDs of preferential colour rendition described in section 3.3 and Paper **I**. The spectral properties of the designed luminaire were measured using *LabSphere IllumiaPro 500-050* system.

3.2.5 Psychophysical experiment

Due to reliability in terms of psychophysics a side-by-side arrangement was chosen for the psychophysical experiment [128]. The experimental cabinet which is presented in Fig. 3.4 was divided in two equal parts each containing quasi-identical scenes that were composed of familiar objects such as fruits and soft drink cans of well-known brands and was mounted in a dark room. Cabinet scenes were illuminated with a diffused 2912 K CCT halogen lamp (MR16, Gu5.3 20 W, 12 V) and the developed PrefLED (0.5 A, 24 V) luminaire. The illuminance of both sides was set to 125 lx (illuminance

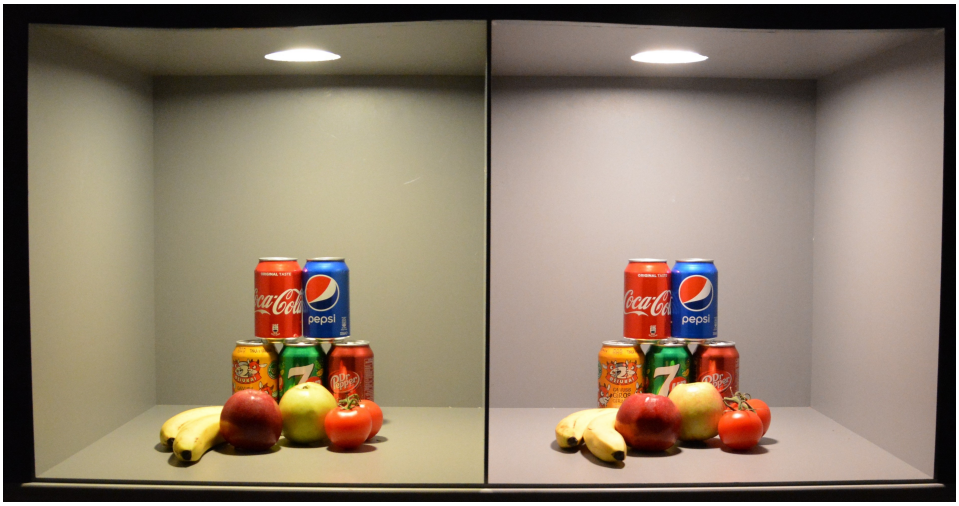

Figure 3.4: Experimental cabinet for the psychophysical validation (left – halogen lamp, right – PrefLED) [**IX**].

meter *Konica Minolta* T-10) by smoothly variable iris diaphragm and precise driving current control of halogen and PrefLED sources, respectively. The lamps were preheated for at least 30 min prior the experiment in order to ensure stable experimental conditions.

Prior to the experiment subjects were asked to take S. Ishihara Test for Colour Blindness, to check the colour-blindness related errors. No colour-blind participants were found. Further, the subjects have spent 5 min in a dark room in groups of 3 people for darkness-adaptation and afterwards they were one-by-one invited to the experimental room and seated in front of the cabinet. Due to the fact that the luminance was not changed during the experiment, the subjects were given 1 min to adapt to the cabinet lighting, which is enough under such experimental conditions [129]. Afterwards 20 questions where verbally introduced by the experimenter, present at the same room. The questions asked during the psychophysical experiment are numbered and provided in table 3.3 in subsec. 3.3.4. Subjects had to choose if the scene on the left or the right side represents the answer to the particular question. After the first set of the experiment subjects were escorted back to the dark room for another 5 minutes, the luminaires were swapped and the experiment was repeated, but subjects were not explained what was changed. Then the subjects had a 15 min break, while the scenes were swapped from the left to the right side while the luminaires were kept in place. After the brake both sets of the experiment were repeated. As a result, each subject has answered the questionnaire for four times. In total,

25 subjects (13 female and 12 male) of ages in between 18 and 34 with a mean value of 26 have voluntarily participated in the experiment. Three subjects were lighting experts working in a Lighting Research Group.

3.3 Results

This section presents the optimization results and gives the optimal wavelengths of theoretical phosphor PL bands for solid state light sources of different colour rendition properties – hight fidelity, colour dulling, saturating, and colour preference. Firstly, the section gives the theoretical SPDs modelled using real phosphor PL bands. Afterwards the solid state luminaire prototype of preferential colour rendition is characterized, compared to a conventional halogen lamp, and validated during the psychophysical experiment, which results are presented at the end of this section.

3.3.1 Model SPDs of pcLEDs and their spectral parameters

The results of the optimization process described in subsection 3.2.1 are presented in table 3.1 which gives the approximate optimal LED peak wavelengths for SPDs with different colour rendition properties: high fidelity, colour saturating, colour dulling, and colour preference. Table shows that the optimal peak wavelengths for the colour dulling blend are in the blue ($\sim$ 460 nm) and yellow regions ($\sim$ 535 and 580 nm). However, the commonly used cool white pcLED with YAG:Ce phosphor are characterized by a very similar SPD and for this reason the colour dulling blends will not be discussed further.

Table 3.1: Proposed approximate peak wavelengths of Eu^{2+} activated phsphors required for the trichromatic pcLEDs with different colour rendition properties [**I**].

Colour rendition property	Deep blue	Blue	Cyan	Green	Yellow	Red	Deep red
High fidelity		460		530		615	
Colour saturating	445		510				625
Colour dulling		460		535	580		
Colour preference		460	510			610	

Figure 3.5 shows the SPDs of full-conversion LEDs characterized by a

high colour fidelity for different CCTs. All three SPDs were composed of the same phosphors: blue aluminate ($BaMgAl_{10}O_{17}$ BAM, Intematix B101C-2; λ_{peak} = 446 nm, FWHM = 45 nm), green silicate (Intematix EG3264, λ_{peak} = 528 nm, FWHM = 71 nm), and red nitride (PhosphorTech HTR620; λ_{peak} = 617 nm, FWHM = 83 nm). The modelled SPDs have CFIs of 88%, 73%, 56% and LER values of 307, 300, and 289 lm/W for CCTs of 3000, 4500, and 6500 K, respectively. The spectral parameters of the SPD at 3000 K are very close to the optimal ones that are presented in Paper **I** Fig. 3. However, due to the longer then required peak wavelengths of commercial phosphors, the CFI and LER values, for higher CCTS, are somewhat lower than the optimal ones.

If a broad BAM PL spectral component is replaced by the same peak wavelength but narrower blue InGaN LED (FWHM = 24 nm) EL band, the value of CFI is reduced by 3–10%. However, the value of LER increases by 3–9 lm/W depending on the CCT. The limiting radiant efficiency of such LEDs (with CFI of ∼80%) accounting for the Stokes shift is about 80% assuming the radiant efficiency of the blue emitter and the QE of the phosphors of 100% This means that the high colour fidelity blends can be achieved using InGaN LEDs as blue light sources.

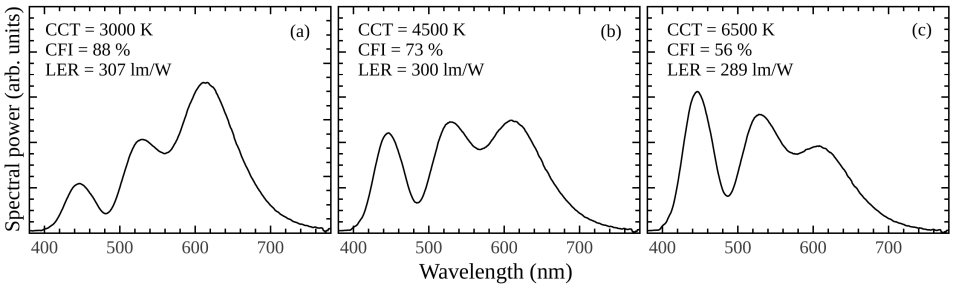

Figure 3.5: (a), (b), and (c) examples of high colour fidelity trichromatic SPDs composed of commercial blue BAM (Intematix B101C-2), green silicate (Intematix EG3264), and red nitride (PhosphorTech HTR620) Eu^{2+} phosphors for CCTs of 3000, 4500, and 6500 K, respectively. The values of CFI and LER are indicated [**I**].

Figure 3.6 shows the SPDs of full-convertion LEDs characterized by a high colour saturation for different CCTs. All SPDs were composed of the same phosphors: the aforementioned blue BAM, cyan silicate (Intematix G1758, λ_{peak} = 507 nm, FWHM = 59 nm), and deep red nitride (Intematix ER6436; λ_{peak} = 625 nm, FWHM = 87 nm). The modelled SPDs have CSIs of 59%, 61%, 62% and LER values of 255, 249, and 241 lm/W for CCTs

of 3000, 4500, and 6500 K, respectively. These values are very close to the theoretical ones presented in Paper **I** Fig. 5.

If BAM PL spectral component is replaced by the InGaN LED EL band the spectral parameters remain almost unchanged for all CCT values. The limiting radiant efficiency of such LEDs (with CSI of ∼60%) accounting for the Stokes shift is 82% for all considered CCTs assuming the radiant efficiency of the blue emitter and the quantum efficiency of the phosphors of 100%. This means that the colour saturating blends can be achieved using InGaN LEDs as blue light sources.

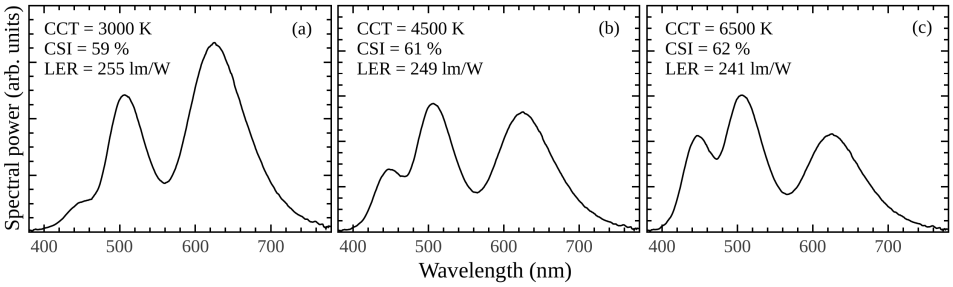

Figure 3.6: (a), (b), and (c) examples of colour-saturating trichromatic SPDs composed of commercial blue BAM (Intematix B101C-2), cyan silicate (Intematix EG1758), and deep red nitride (Intematix ER6436) Eu^{2+} phosphors for CCTs of 3000, 4500, and 6500 K, respectively. The values of CSI and LER are indicated [**I**].

Figure 3.7 shows the SPDs of full-convertion LEDs characterized as high preference for different CCTs. All SPDs were composed of the same phosphors: the aforementioned blue BAM, cyan silicate and orange silicate (Intematix O6040; $\lambda_{peak} = 606$ nm, FWHM = 81 nm). The modelled SPDs have CSI/CFI ratios of 0.6, 0.97, 1.22, and LER values of 304, 286, and 268 lm/W for CCTs of 3000, 4500, and 6500 K, respectively. The CSI/CFI ratio of the composed SPDs are within the preference interval which is 0.3–3. The LERs are somewhat lower than theoretical shown in Paper **I** Fig. 8 due to the slightly different than required peak wavelengths of commercial phosphors.

If a broad BAM spectral component is replaced by a narrow InGaN LED EL band, the CSI/CFI ratio is reduced by 0.03-0.14 and LER values increase by 2–6 lm/W depending on the CCT. The limiting radiant efficiency of such LEDs (with CSI/CFI of ∼1) accounting for the Stokes shift is 83% for all considered CCTs assuming the radiant efficiency of the blue emitter and the quantum efficiency of the phosphors of 100%. This means that the

colour preference blends can also be achieved using InGaN LEDs as blue light sources.

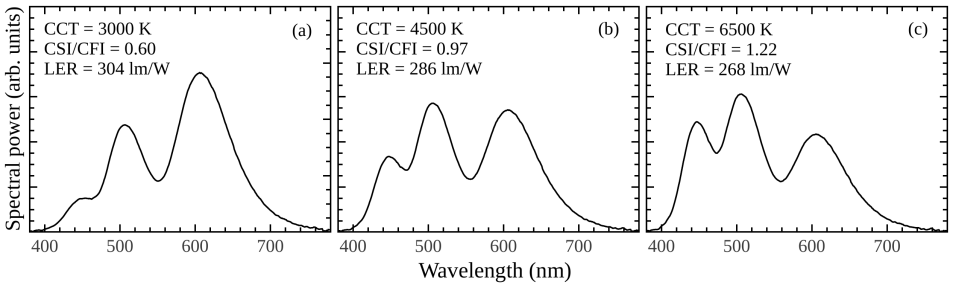

Figure 3.7: (a), (b) and (c) examples of colour-preference trichromatic SPDs composed of commercial blue BAM (Intematix B101C-2), cyan silicate (Intematix EG1758), and red-orange silicate (Intematix O6040) Eu^{2+} phosphors for CCTs of 3000 K, 4500 K, and 6500 K, respectively. The values of CSI/CFI and LER are indicated [**I**].

3.3.2 Temperature dependence

Figure 3.8 (a), (b), and (c) show the dependence of colour parameters on ambient temperature for the SPDs characterized by high colour fidelity, colour saturation and colour preference, respectively. The red line indicates the limits beyond the SPD looses the dominant colour properties. Figure shows that the 3000 and 4500 K CCTs colour fidelity blends are quite resistant to the heat and the colours are not distorted within the measured temperature range (0–80 °C). However, 6500 K blend is very sensitive to the ambient temperature and as soon as 30 °C are reached the SPD starts to distort colours due to the decrease of CFI and the increase of CDI and HDI. Colour saturating blends are the most resistant to heat since the SPDs at all CCTs sustain the colour saturation ability within the measured temperature range. The most sensitive to the heat are colour preference blends. When the temperature is increased the SPDs change their shapes, and the value of CSI is reduced in favour of CFI. Above 50 and 80 °C, the 3000 K as well as 4500 and 6500 K colour preference blends, respectively, become high fidelity blends.

The results show that it is of importance to take into account the temperature dependence of phosphors while composing the SPDs so as the designed light source would be characterized by a desirable colour rendition property.

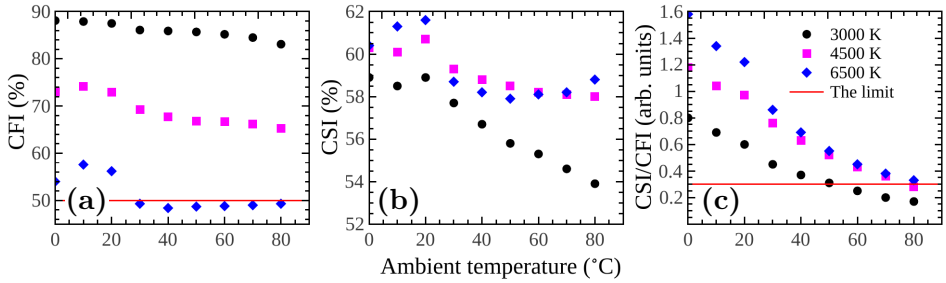

Figure 3.8: (a), (b), and (c) dependences of colour parameters on the ambient temperature at different CCTs for the colour fidelity, colour saturation and colour preference blends, respectively. The red line indicates the limit, upon which the dominant colour properties are lost.

3.3.3 Characterization of the designed PrefLED prototype

The SPDs for the colour preference luminaire and the halogen lamp are presented in Fig. 3.9. The pcLED SPD is characterized by three components in the blue (455 nm), green (517 nm), and deep red (621 nm) spectral regions. A deep red component of the PrefLED gives the ability to saturate colours of illuminated objects. The spectrum of MR16 halogen lamp is similar to the black body radiator emission, with a slight distortion in the red part due to a multifaceted reflector.

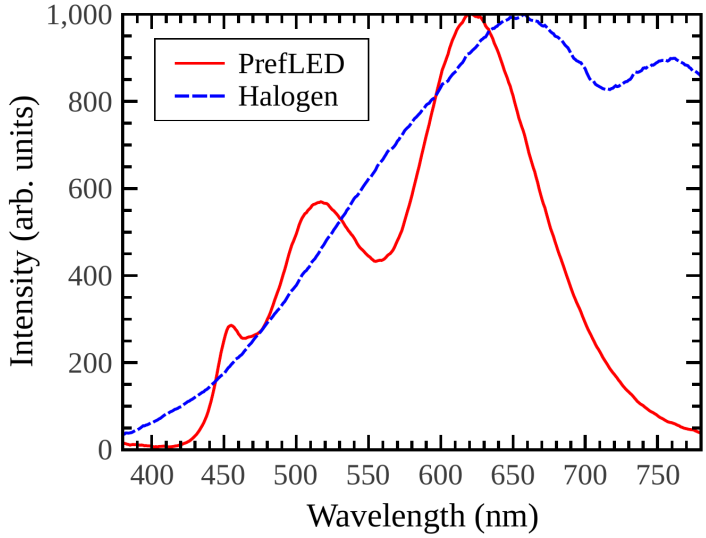

Figure 3.9: SPDs of the designed PrefLED and the halogen lamp used for the reference [**IX**].

Figure 3.10 (a) presents the *xy* chromaticity coordinates of the blue

LED and phosphors used for the design of the luminaire as well as those of PrefLED and Halogen lamp, in CIE 1931 chromaticity diagram. It is clearly seen in Fig. 3.10 (b) that both SPDs and the 2900 K illuminant are confined by the 3-step MacAdam ellipse, which means that the test and reference luminaires are close to the Planckian locus and can be described by a similar CCT.

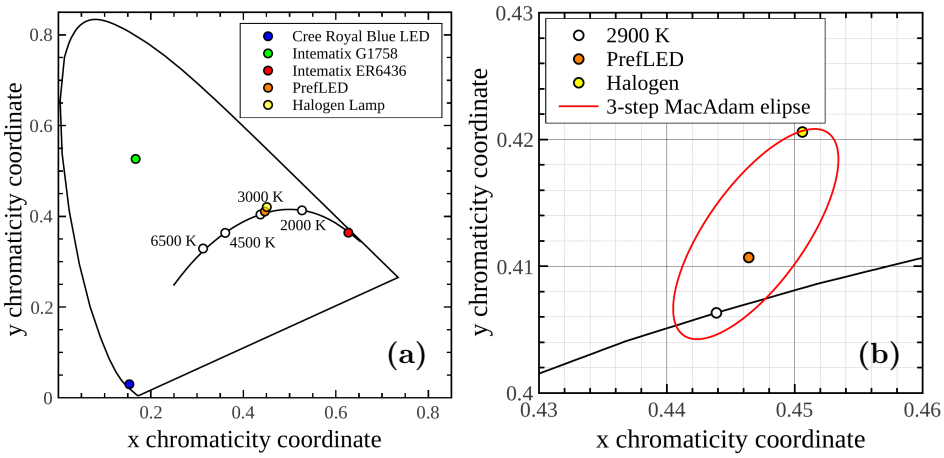

Figure 3.10: (a) Chromaticity coordinates of the PrefLED and the halogen lamp in the CIE 1931 chromaticity diagram; (b) the enlarged view of the CIE 1931 chromaticity diagram containing 3-step MacAdam ellipse [**IX**].

Table 3.2 presents the colourimetric parameters of the aforementioned SPDs along with the CIE A standard illuminant. The developed LED has a 0.0014 D_{uv} value which is within the dimensions of double MacAdam ellipse with the black body radiation chromaticity, and thus satisfies the requirements for white light. It is also seen that the halogen lamp has high CFI (97%) and R_a (96), whereas the PrefLED exhibit somewhat lower values of 47% and 87, respectively. However, CSI value for halogen lamp and PrefLED is 0 and 30%, respectively. This means that for the designed PrefLED prototype the CSI to CFI ratio is 0.64, and falls into the colour preference interval which is between 0.3 and 3 as was discussed previously. LERs of PrefLED and halogen lamp are 271 and 170 lm/W, respectively, meaning that the PrefLED SPD is 1.6 times more efficient. Table 3.2 also presents photopic CAF values which are 0.851 and 1.01 for PrefLED and Halogen lamp, respectively, and therefore make a small difference if compared to CIE A illuminant (1).

Table 3.2: Properties of the designed pcLED and of reference light sources [**IX**].

Name	**CCT, K**	$\mathbf{D}_{uv}$	**LER, lm/W**	**CFI, %**	**CSI, %**	$\mathbf{R}_a$	$\mathbf{R}_f$	$\mathbf{R}_g$	**CAF**
PrefLED	2900	0.0014	271	47	29	87	82	96	1.01
Halogen	2912	0.0046	170	97	0	96	95	96	0.851
CIE A	2856	0	155	100	0	100	100	100	1

3.3.4 Results of the psychophysical experiment

The results of the psychophysical experiment are presented in Fig. 3.11. The numbers on the x axis represent question numbers in the questionnaire given in tab. 3.3, while the mean values of the selections are indicated on the y axis. As it is seen in the histogram, the subjects were tend to give preference for the PrefLED luminaire – it was claimed to be more bright, colourful, vivid, attractive, picturesque and luxurious. Also, it was more preferred for the use in the offices, grocery stores, restaurants, shopping malls and certain places at home, in particularly, kitchen or bathroom. However, with the confidence intervals taken into account, both luminaires were claimed to be cosy. Halogen lamp was perceived as more natural and peaceful, thus, as a result it was claimed to be more suitable for the illumination at home, in particular, sleeping room. Probably lower CAF value of the MR16 halogen was unconsciously noticed by the subjects, prompting for more peaceful sensation.

However, the results represent only mono-cultural (Lithuanian) and relatively young age distribution of subjects leaving the space for further investigation of subjects of different cultures and countries of origin/residence. At the moment of writing this dissertation the psychophysical experiment on the perceived brightness of the PrefLED and halogen luminaires is being carried on.

3.4 Summary

To sum up, in this part, according to the theoretical optimization results, the pcLED SPDs, composed of commercial phosphor PL spectral components, and characterized by hight colour fidelity, colour saturation and colour preference, for different CCTs were modelled. Afterwards, the pcLED luminaire prototype of preferential colour rendition was designed and validated during a psychophysical experiment. The experiment has revealed that the designed prototype is described as a more bright, vivid, colourful, and at-

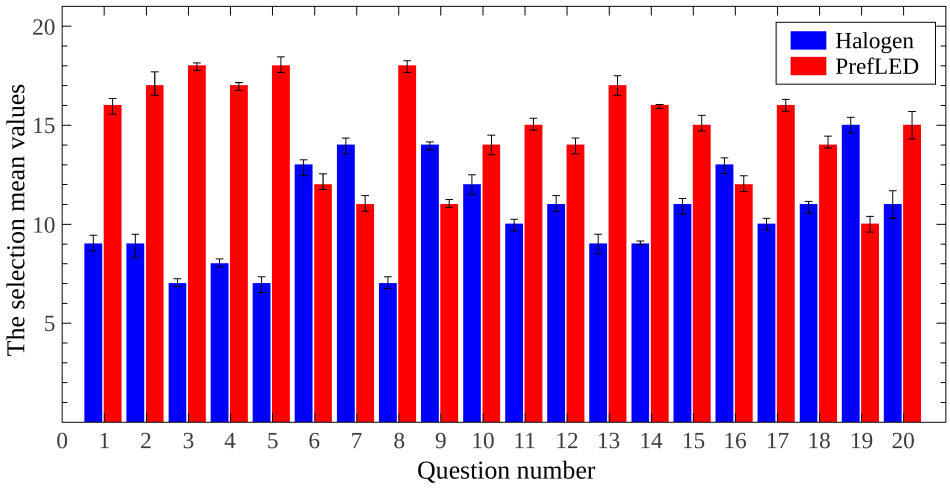

Figure 3.11: Results of a psychophysical experiment. Numbers on the x axis represent question numbers in the questionnaire presented in tab. 3.3, the mean values of selected luminaires are indicated on the y axis [**IX**].

tractive. Moreover it is claimed to be more suitable for the illumination of active environments, suitable for work (office, factory) or free-time (shopping mall, grocery store, restaurant). However, a conventional halogen lamp of the same CCT value was chosen as a more favourable light source for the use at home, in particular for the illumination of the sleeping room.

Table 3.3: Questionnaire used during the psychophysical experiment [**IX**].

Which illuminated scene appears more...	
1 Bright	6 Cosy
2 Vivid	7 Peaceful
3 Colourful	8 Luxurious
4 Attractive	9 Natural
5 Picturesque	10 Preferred(in general)
Which illumination would you choose for...	
11 Office	16 Home
12 Factory	17 Kitchen
13 Shopping mall	18 Living-room
14 Grocery store	19 Sleeping-room
15 Restaurant	20 Bathroom

Conclusions

During this work the spectral engineering of pcLEDs for three niche applications was performed. The first chapter was dedicated to pcLEDs meeting the photobiological processes of plants. In this chapter, different gallium garnet phosphors doped with Cr^{3+} were investigated, optimized and applied for solid state lighting.

The second chapter covered the photobiologically friendly mesopic sources of light that are characterized by low CCT and minimized CAF value. In this chapter photobiologically friendly dichromatic pcLED SPDs were modelled and their photometric properties were evaluated. Also, two sets of pcLED firelight prototypes were designed and characterized.

The final third chapter presented the optimization of theoretical pcLED SPDs of different colour rendition properties in respect to LER. The optimization results were used to model pcLED SPDs characterized by high colour fidelity, colour saturation and colour preference for different CCTs. Finally, the pcLED prototype of preferential colour rendition was characterized and validated by a psychophysical experiment.

The conclusions from these three parts of the dissertation work are drawn and presented as follows:

1. Ce^{3+} ions (co)doped along with Cr^{3+} ions cause a strong quenching of Cr^{3+} PL in gadolinium gallium garnet phosphor synthesized by a sol-gel method, and, therefore, do not give an advantage.

2. Sol-gel derived gadolinium, yttrium, lutetium and gadolinium scandium garnets doped with Cr^{3+} ions are characterized by a broad PL band in the far-red spectral region which overlaps the absorption of P_{fr} plant pigment, and therefore, are suitable for the horticultural applications.

3. The PL intensity and quantum efficiency of sol-gel derived gallium garnets phosphor powders can be effectively enhanced by optimizing the concentration of Cr^{3+} ions and calcination temperature.

4. The measurements of PL dependence on the temperature have revealed that up to 90 °C, no thermal quenching is observed for gallium

garnets doped with Cr^{3+}, which makes these phosphors feasible for the pcLED applications.

5. Sol-gel derived YGG doped with 8 mol% Cr^{3+} ions and calcined at 1400 °C was characterized by the highest QE that reached 46%, and, therefore, was used for the design of pcLED luminary prototype meeting the photomorphogenetic needs of plants.

6. Most of the proposed theoretical *firelight* LED SPDs as well as the designed *firelight* LED prototypes have the mesopic equivalent of the general CRI comparable to the general CRI of common LEDs under photopic conditions, which makes them suitable for the outdoor lighting applications under low illuminance levels.

7. The proposed theoretical *firelight* LED SPDs as well as the designed *firelight* LED prototypes are advantageous in respect of conventional white light sources in terms of circadian action, and, therefore, can be used in outdoor environments, where a part of efficacy can be traded for photobiological safety, reduced light pollution, and visual comfort.

8. SPDs containing PL components of Eu^{2+} doped silicate phosphors are characterized by a relatively high LER and general mesopic CRI as well as low CAF, if compared to conventional light sources, and are thus claimed as the most suitable phosphors for *firelight* LED sources of low circadian action.

9. SPDs composed of PL bands of Eu^{2+} doped phosphors were optimized for different colour rendering properties (high fidelity, colour saturating or colour preference) using model spectral components approximated by Gaussian shapes on the photon energy scale.

10. A psychophysical experiment revealed that the designed PrefLED prototype is perceived as more bright, vivid, colourful and attractive if compared to a conventional halogen lamp of the same CCT. Therefore it is advantageous for lighting in the most of active environments. However, the halogen lamp was perceived as more peaceful, and, therefore, it is preferable for the illumination of calm environments, such as home, in particular, sleeping room.

Bibliography

[1] P. Mottier, *LEDs for Lighting Applications* (John Wiley & Sons, Inc, London, 2009).

[2] A. Nardelli, E. Deuschle, L. D. de Azevedo, J. L. N. Pessoa, E. Ghisi, Assessment of light emitting diodes technology for general lighting: A critical review, Renew. Sust. Energ. Rev. **75**, 368–379 (2017).

[3] D. Tsonev, S. Videv, H. Haas, Light fidelity (li-fi): towards all-optical networking, Proc.SPIE **9007**, 9007–10 (2014).

[4] A. Žukauskas, *Puslaidininkiniai Šviestukai* (Progretus, Vilnius, 2008).

[5] E. F. Schubert, *Light-emitting diodes* (Cambridge University Press, 2018), 3rd edition.

[6] A. Žukauskas, R. Vaicekauskas, F. Ivanauskas, H. Vaitkevičius, M. Shur, Rendering a color palette by light-emitting diodes, Appl. Phys. Lett. **93**, 021109 (2008).

[7] S. Ye, F. Xiao, Y. Pan, Y. Ma, Q. Zhang, Phosphors in phosphor-converted white light-emitting diodes: Recent advances in materials, techniques and properties, Mater. Sci. Eng. R **71**, 1–34 (2010).

[8] Luxeon, *LUXEON C Color Line Datasheet*, https://www.lumileds.com/uploads/571/DS144-pdf.

[9] A. David, P. T. Fini, K. W. Houser, Y. Ohno, M. P. Royer, K. A. G. Smet, M. Wei, L. Whitehead, Development of the ies method for evaluating the color rendition of light sources, Opt. Express **23**(12), 15888–15906 (2015).

[10] Commission Internationale de l'Éclairage, *Method of measuring and specifying colour rendering properties of light sources*, pub. CIE 13.3:1995.

[11] J. Zhang, R. Hu, X. Yu, B. Xie, X. Luo, Spectral optimization based simultaneously on color-rendering index and color quality scale for white led illumination, Opt. Laser Technol. **88**, 161 – 165 (2017).

[12] W. A. Thornton, A validation of the color-preference index, J. Illum. Eng. Soc. **4**(1), 48–52 (1974).

[13] A. Liu, A. Tuzikas, A. Žukauskas, R. Vaicekauskas, P. Vitta, M. Shur, Cultural preferences to color quality of illumination of different artwork objects revealed by a color rendition engine, IEEE Photonics J. **5**(4), 6801010–6801010 (2013).

[14] Y. Ohno, Color quality metrics–recent progress and future perspective, in *The 15th International Symposium of Science and Technology of Lighting* (2016).

[15] A. Žukauskas, R. Vaicekauskas, P. Vitta, A. Tuzikas, A. Petrulis, M. Shur, Color rendition engine, Opt. Express **20**, 5356–5367 (2012).

[16] F. Falchi, P. Cinzano, C. D. Elvidge, D. M. Keith, A. Haim, Limiting the impact of light pollution on human health, environment and stellar visibility, J. Environ. Manage. **92**(10), 2714–2722 (2011).

[17] G. C. Brainard, J. P. Hanifin, J. M. Greeson, B. Byrne, G. Glickman, E. Gerner, M. D. Rollag, Action spectrum for melatonin regulation in humans: Evidence fora novel circadian photoreceptor, J. Neurosci. **21**(16), 6405–6412 (2001).

[18] K. Thapan, J. Arendt, D. J. Skene, An action spectrum for melatonin suppression: evidence for a novel non-rod, non-cone photoreceptor system in humans, J. Physiol. **535**(1), 261–267 (2001).

[19] S. Davis, D. K. Mirick, Circadian disruption, shift work and the risk of cancer: a summary of the evidence and studies in Seattle, Cancer Causes Control **17**(4), 539–545 (2006).

[20] M. Hatori, C. Gronfier, R. N. Van Gelder, P. S. Bernstein, J. Carreras, S. Panda, F. Marks, D. Sliney, C. E. Hunt, T. Hirota, et al., Global rise of potential health hazards caused by blue light-induced circadian disruption in modern aging societies, NPJ Aging Mech. Disease **3**(1), 9 (2017).

[21] https://www.nobelprize.org/prizes/medicine/2017/press-release/.

[22] D. Singh, C. Basu, M. Meinhardt-Wollweber, B. Roth, Leds for energy efficient greenhouse lighting, Renew. Sust. Energy Rev. **49**, 139–147 (2015).

[23] N. Yeh, J. Chung, High-brightness LEDs - energy efficient lighting sources and their potential in indoor plant cultivation, Renew. Sust. Energy Rev. **13**, 2175 (2003).

[24] D. Despommier, Farming up the city: the rise of urban vertical farms, Trends biotechnol. **31**(7), 388–389 (2013).

[25] P. Daukantas, Optics in agriculture, Opt. Photonics News **28**(11), 42–49 (2017).

[26] S. Kim, E. Hahn, J. Heo, K. Paek, Effects of LEDs on net photosynthetic rate, growth and leaf stomata of chrysanthemum plantlets in vitro, Sci. Hort. **101**, 143–151 (2004).

[27] E. Taulavuori, K. Taulavuori, J. K. Holopainen, R. Julkunen-Tiitto, C. Acar, I. Dincer, Targeted use of LEDs in improvement of production efficiency through phytochemical enrichment, J. Sci. Food Agric. **97**(15), 5059–5064 (2017).

[28] A. Viršilė, M. Olle, P. Duchovskis, *LED Lighting in Horticulture* (Springer Singapore, Singapore, 2017), 113–147.

[29] G. Tamulaitis, P. Duchovskis, Z. Bliznikas, K. Breivė, R. Ulinskaitė, A. Brazaitytė, A. Novičkovas, A. Žukauskas, High-power light-emitting diode based facility for plant cultivation, J. Phys D: Appl. Phys. **38**, 3182–3187 (2005).

[30] H. Kajii, K. Kimpara, Y. Ohmori, Visible to near-infrared organic light-emitting diodes using phosphorescent materials by solution process, Thin Solid Films **518**, 551–554 (2009).

[31] P. Smet, A. Parmentier, D. Poelman, Selecting conversion phosphors for white light-emitting diodes, J. Electrochem. Soc. **158**, R37–R54 (2011).

[32] W. Yen, M. Weber, *Inorganic Phosphors: Compositions, Preparation and Optical Properties* (CRC Press, Boca Raton, 2004).

[33] L. Ma, D. J. Wang, Z. Y. Mao, Q. F. Lu, Z. H. Yuan, Investigation of Eu–Mn energy transfer in $A_3MgSi_2O_8$:Eu^{2+}, Mn^{2+} (A=Ca,Sr,Ba) for light-emitting diodes for plant cultivation, Appl. Phys. Lett. **93**(14), 144101 (2008).

[34] A. Speghini, F. Piccinelli, M. Bettinelli, Synthesis, characterization and luminescence spectroscopy of oxide nanopowders activated with trivalent lanthanide ions: The garnet family, Opt. Mater. **33**(3), 247–257 (2011).

[35] W. Wang, J. Tang, S. T. V. Hsu, J. Wang, B. P. Sullivan, Energy transfer and enriched emission spectrum in Cr and Ce co-doped $Y_3Al_5O_{12}$ yellow phosphors, Chem. Phys. Lett. **457**(1), 103 – 105 (2008).

[36] L. M. Shao, X. P. Jing, Energy transfer and luminescent properties of Ce^{3+}, Cr^{3+} co-doped $Y_3Al_5O_{12}$, J. Lumin. **131**(6), 1216 – 1221 (2011).

[37] K. Al-Kodmany, The vertical farm: A review of developments and implications for the vertical city, Buildings **8**(2), 24 (2018).

[38] L. Poulet, G. Massa, R. Morrow, C. Bourget, R. Wheeler, C. Mitchell, Significant reduction in energy for plant-growth lighting in space using targeted LED lighting and spectral manipulation, Life Sci. Space Res. **2**, 43–53 (2014).

[39] M. McDonald, *Photobiology of Higher Plants* (John Wiley & Sons Ltd, 2003).

[40] C. Brown, A. Schuerger, J. Sager, Growth and photomorphogenesis of pepper plants under red light-emitting diodes with supplemental blue or far-red lighting, J. Amer. Soc. Hort. Sci. **120**(5), 808–813 (1995).

[41] R. Bula, R. Morrow, T. Tibbitts, D. Barta, Light-emitting diodes as a radiation source for plants, HortScience **26**(2), 203–205 (1991).

[42] E. G. Víllora, S. Arjoca, D. Inomata, K. Shimamura, Single-crystal phosphors for high-brightness white LEDs/LDs, Proc. SPIE **9768**, 9768 – 9768 – 11 (2016).

[43] G. Zhao, T. Li, X. He, J. Xu, Preparation of gadolinium gallium garnet polycrystalline material by coprecipitation method, Mater. Lett. **56**, 1098–1102 (2002).

[44] R. Xie, Y. Li, N. Hirosaki, H. Yamamoto, *Nitride Phosphors and Solid-State Lighting* (CRC/Taylor & Francis, New York, 2011).

[45] M. Raukas, J. Kelso, Y. Zheng, K. Bergenek, D. Eisert, A. Linkov, F. Jermann, Ceramic phosphors for light conversion in leds, ECS J. Solid State Sci. Technol. **2**(2), R3168–R3176 (2013).

[46] Y. H. Song, E. K. Ji, B. W. Jeong, M. K. Jung, E. Y. Kim, D. H. Yoon, High power laser-driven ceramic phosphor plate for outstanding efficient white light conversion in application of automotive lighting, Sci. Rep. **6**, 31206 (2016).

[47] S. M. Sze, *Semiconductor devices: physics and technology* (John Wiley & Sons, 2008).

[48] B. Struve, G. Huber, The effect of the crystal field strength on the optical spectra of Cr^{3+} in gallium garnet laser crystals, Appl. Phys. B **36**, 195–201 (1985).

[49] H. Orucu, G. Ozen, J. Collins, B. D. Bartolo, Temperature dependence of the luminescence spectra of garnet crystals doped with chromium ions, Opt. Mater. **31**(7), 1065–1070 (2009).

[50] R. Nobes, E. Akhmatskaya, V. Milman, B. Winkler, C. Pickard, Structure and properties of aluminosilicate garnets and katoite: an ab initio study, Comput. Mater. Sci. **17**(2-4), 141–145 (2000).

[51] B. Struve, G. Huber, Laser performance of Cr^{3+}:Gd(Sc,Ga) garnet, J. Appl. Phys. **57**, 45–48 (1985).

[52] C. Greskovich, S. Duclos, Ceramic scintilators, Annu. Rev. Mater. Sci. **27**, 69–88 (1997).

[53] S. Shinoya, W. Yen, *Phosphor Handbook* (CRC Press, Boca Raton, 1999).

[54] Y. Tanabe, S. Sugano, On the absorption spectra of complex ions ii, J. Phys. Soc. Jpn. **9**(5), 766–779 (1954).

[55] M. Seltzer, Interpretation of the emission spectra of trivalent chromium-doped garnet crystals using Tanabe-Sugano diagrams, J. Chem. Educ. **72**(10), 886–888 (1995).

[56] K. Petermann, G. Huber, Broad band fluorescence of transition metal doped garnets and tungstates, J. Lumin. **31, 32**, 71–77 (1984).

[57] B. Malysa, A. Meijerink, T. Jüstel, Temperature dependent Cr^{3+} photoluminescence in garnets of the type $X_3Sc_2Ga_3O_{12}$ (X = Lu, Y, Gd, La), J. Lumin. **202**, 523 – 531 (2018).

[58] N. Greenham, I. W. Samuel, G. Hayes, R. Phillips, Y. Kessener, S. Moratti, A. Holmes, R. Friend, Measurement of absolute photoluminescence quantum efficiencies in conjugated polymers, Chem. Phys. Lett. **241**, 89–96 (1995).

[59] J. de Mello, H. Wittmann, R. Friend, An improved experimental determination of external photoluminescence quantum efficiency, Adv. Mater. **9**(3), 230–232 (1997).

[60] A. Katelnikovas, T. Bareika, P. Vitta, T. Jüstel, H. Winkler, A. Kareiva, A. Žukauskas, G. Tamulaitis, $Y_{3-x}Mg_2AlSi_2O_{12}$:Ce_x^{3+} phosphors – prospective for warm-white light emitting diodes, Opt. Mater. **32**(9), 1261–1265 (2010).

[61] A. Katelnikovas, P. Vitta, P. Pobedinskas, G. Tamulaitis, A. Žukauskas, J. E. Jørgensen, A. Kareiva, Photoluminescence in sol–gel-derived YAG:Ce phosphors, J. Cryst. Growth **304**(2), 361–368 (2007).

[62] J. R. Lakowicz, *Principles of Fluorescence Spectroscopy* (Springer, Berlin, 2006).

[63] P. Vitta, *Fluorescencijos Gesimo Trukmės Matavimai Dažninės Skyros Metodu*, Vilnius University, lab manual (2007).

[64] S. Butkutė, *Synthesis and characterization of novel luminescent materials: typical oxide phosphors and possible inert host lattices*, Ph.D. thesis, Vilnius University (2018).

[65] G. Blasse, B. Grabmaier, M. Ostertag, The afterglow mechanism of chromium-doped gadolinium gallium garnet, J. Alloy. Compd. **200**, 17–18 (1993).

[66] S. Butkute, E. Gaigalas, A. Beganskiene, F. Ivanauskas, R. Ramanauskas, A. Kareiva, Sol-gel combustion synthesis of high-quality chromium-doped mixed-metal garnets $Y_3Ga_5O_{12}$ and $Gd_3Sc_2Ga_3O_{12}$, J. Alloys Compd. **739**, 504 – 509 (2018).

[67] L. Kostyk, A. Luchechko, Y. Zakharko, O. Tsvetkova, B. Kukliński, Cr-related centers in $Gd_3Ga_5O_{12}$ polycrystals, J. Lumin. **129**, 312–316 (2009).

[68] A. Katelnikovas, J. Jurkevičius, K. Kazlauskas, P. Vitta, T. Jüstel, A. Kareiva, A. Žukauskas, G. Tamulaitis, Efficient cerium-based sol–gel derived phosphors in different garnet matrices for light-emitting diodes, J. Alloys Compd. **509**(21), 6247 – 6251 (2011).

[69] S. Healy, C. Donnelly, T. Glynn, G. Imbusch, G. Morgan, Temperature dependence of the luminescence of GSGG:Cr^{3+}, J. Lumin. **46**, 1–7 (1990).

[70] W. Liu, Q. Zhang, L. Ding, D. Sun, J. Xiao, S. Yin, Preparation and luminescence properties of nano-polycrystalline Cr^{3+}:$Lu_3Ga_5O_{12}$, Physica B **403**, 3403–3405 (2008).

[71] R. Martín-Rodríguez, R. Valiente, F. Rodríguez, M. Bettinelli, Temperature and pressure dependence of the optical properties of Cr^{3+}–doped $Gd_3Ga_5O_{12}$ nanoparticles, Nanotechnology **22**(26), 265707 (2011).

[72] Commission Internationale de l'Éclairage, *CIE 2-deg photopic luminosity curve*, CIE Proceedings (1924).

[73] A. Žukauskas, R. Vaicekauskas, P. Vitta, Optimization of solid-state lamps for photobiologically friendly mesopic lighting, Appl. Optics **51**(35), 8423–8432 (2012).

[74] Commission Internationale de l'Éclairage, *CIE Scotopic luminosity curve*, CIE proceedings (1951).

[75] Commission Internationale de l'Éclairage, *Recommended system for mesopic photometry based on visual performance*, pub. CIE 191:2010 (2010).

[76] D. Gall, Circadiane Lichtgrößen und deren messtechnische Ermittlung, Licht **54**, 1292–1297 (2002).

[77] National Electrical Manufacturers Association, *American National Standard for Electric Lamps – Specifications for the Chromaticity of Solid State Lighting (SSL) Products*, ANSI C78.377-2008 (2008).

[78] A. Žukauskas, R. Vaicekauskas, F. Ivanauskas, R. Gaska, M. Shur, Optimization of white polychromatic semiconductor lamps, Appl. Phys. Lett. **80**, 234–236 (2002).

[79] D. L. MacAdam, Visual sensitivities to color differences in daylight∗, J. Opt. Soc. Am. **32**(5), 247–274 (1942).

[80] G. Wyszecki, W. S. Stiles, *Color science: concepts and methods, quantitative data and formulas* (Wiley, 2000).

[81] Y. Ohno, Practical Use and Calculation of CCT and Duv, LEUKOS **10**(1), 47–55 (2014).

[82] Commission Internationale de l'Éclairage, *Colour rendering of white LED sources*, pub. CIE 177:2007.

[83] K. E. West, M. R. Jablonski, B. Warfield, K. S. Cecil, M. James, M. A. Ayers, J. Maida, C. Bowen, D. H. Sliney, M. D. Rollag, J. P. Hanifin, G. C. Brainard, Blue light from light-emitting diodes elicits a dose-dependent suppression of melatonin in humans, J. Appl. Physiol. **110**(3), 619–626 (2011).

[84] D. Lang, Energy efficient illumination for the biological clock, Proc. of SPIE **7954**, 795402–1–12 (2011).

[85] *Patrick J. Lynch, medical illustrator*, creative Commons Attribution 2.5 License (2006).

[86] H. Menkara, C. Summers, B. Wagner, Light-emitting device having thio-selenide fluorescent phosphor, US Patent 7,109,648 (2006).

[87] R. Mueller-Mach, G. O. Mueller, M. R. Krames, O. B. Shchekin, P. J. Schmidt, H. Bechtel, C.-H. Chen, O. Steigelmann, All-nitride monochromatic amber-emitting phosphor-converted light-emitting diodes, Phys. Status Solidi-R **3**(7-8), 215–217 (2009).

[88] X. Zhang, L. Liang, Q. Su, Luminescence properties of $(Ca_{1-x}Sr_x)S:Eu^{2+}$ phosphors for white LEDs application, Mater. Lett. **59**, 749–753 (2005).

[89] R. J. Xie, N. Hirosaki, K. Sakuma, Y. Yamamoto, M. Mitomo, Eu^{2+} -doped Ca-α-SiAlON: a yellow phosphor for white light-emitting diodes, Appl. Phys. Lett. **84**(26), 5404–5406 (2004).

[90] I. Reklaitis, T. Grinys, R. Tomašiūnas, T. Puodžiūnas, L. Mažulė, V. Sirutkaitis, C. Lin, C. Yang, A new geometrical approach for rapid LED processing by using femtosecond laser, Opt. Laser. Eng. **74**, 17–21 (2015).

[91] H. Dapkus, *Kietakūnių konversijos fosfore šviesos šaltinių nišiniams taikymams kūrimas ir charakterizavimas*, Bachelor's thesis, Vilnius University, Vilnius (2017).

[92] H. F. Ivey, Color and efficiency of luminescent light sources, J. Opt. Soc. Am. **55**(5), 576–576 (1965).

[93] A. A. Kruithof, Tubular luminescence lamps for general illumination, Philips Tech. Rev. **6**, 65–96 (1941).

[94] A. Petrulis, L. Petkevičius, P. Vitta, R. Vaicekauskas, A. Žukauskas, Exploring preferred correlated color temperature in outdoor environments using a smart solid-state light engine, LEUKOS **14**(2), 95–106 (2018).

[95] M. S. Rea, J. P. Freyssinier-Nova, Color rendering: A tale of two metrics, Color Res. Appl. **33**(3), 192–202 (2008).

[96] W. Davis, Y. Ohno, Color quality scale, Opt. Eng. **49**, 033602 (2010).

[97] A. Žukauskas, R. Vaicekauskas, F. Ivanauskas, H. Vaitkevičius, P. Vitta, M. Shur, Statistical approach to color quality of solid-state lamps, IEEE J. Sel. Top. Quantum Electron. **15**, 1753–1762 (2009).

[98] http://demo.lrg.projektas.vu.lt/lcq/en/.

[99] Y. Ohno, CIE Reserch Strategy – Future of Color Quality Metrics for Lighting, in *13th AIC Congress: Being color with health Book of abstracts* (Jeju, Republic of Korea, 16th–20th October 2017), 158.

[100] D. B. Judd, A flattery index for artificial illuminants, Illum. Eng. **62**, 593–598 (1967).

[101] A. Žukauskas, R. Vaicekauskas, M. Shur, Solid-state lamps with optimized color saturation ability, Opt. Express **18**, 2287–2295 (2010).

[102] A. Žukauskas, R. Vaicekauskas, M.Shur, Color-dulling solid-state sources of light, Opt. Express **20**, 9755–9762 (2012).

[103] W. A. Thornton, Luminosity and color-rendering capability of white light, J. Opt. Soc. Am. **61**(9), 1155–1163 (1971).

[104] W. A. Thornton, Color-discrimination index, J. Opt. Soc. Am. **62**(2), 191–194 (1972).

[105] A. Žukauskas, R. Vaicekauskas, F. Ivanauskas, H. Vaitkevičius, M. Shur, Spectral optimization of phosphor-conversion light-emitting diodes for ultimate color rendering, Appl. Phys. Lett **93**, 051115 (2008).

[106] M. Shur, A. Žukauskas, Solid-state lighting: Toward superior illumination, Proc. IEEE **93**, 1691–1703 (2005).

[107] T. Jüstel, Luminescent materials for phosphor-converted LEDs, in C. Ronda (ed.), *Luminescence* (Wiley, Weinheim, 2008), 179–190.

[108] Z. Xia, Q. Liu, Progress in discovery and structural design of color conversion phosphors for leds, Prog. Mater. Sci. **84**, 59–117 (2016).

[109] R. Jacobs, W. Krupke, M. Weber, Measurement of excited-state-absorption loss for Ce^{3+} in $Y_3Al_5O_{12}$ and implications for tunable $5d \rightarrow 4f$ rare-earth lasers, Appl. Phys. Lett. **33**, 410–412 (1978).

[110] P. Dorenbos, Energy of the first $4f^7 \rightarrow 4f^6 5d$ transition of Eu^{2+} in inorganic compounds, J. Lumin. **104**, 239–260 (2003).

[111] G. He, L. Zheng, White-light clusters with high color rendering, Opt. Lett. **35**, 2955–2957 (2010).

[112] M. Chien, C. Tien, Multispectral mixing scheme for LED clusters with extended operational temperature window, Opt. Express **20**, A245–A254 (2012).

[113] B. Ridley, *Quantum Processes in Semiconductors* (Oxford University Press, New York, 2006).

[114] R. Mueller-Mach, G. Mueller, M. Krames, T. Trottier, High-power phosphor converted light-emitting diodes based on III-nitrides, IEEE J. Sel. Top. Quantum Electron. **8**, 339–345 (2002).

[115] Y. Hu, W. Zhuang, H. Ye, S. Zhang, Y. Fang, X. Huang, Preparation and luminescent properties of $(Ca_{1-x}Sr_x)S{:}Eu^{2+}$ red-emitting phosphor for white LED, J. Lumin. **111**, 139–145 (2005).

[116] T. Barry, Fluorescence of Eu^{2+}-activated phases of binary alkaline earth orthosilicate systems, J. Electrochem. Soc. **115**, 118–1184 (1968).

[117] S. Liu, S. Cheng, Y. Li, Aluminum-silicate based orange-red phosphors with mixed divalent and trivalent cations, US Patent 7,648,650 (2010).

[118] Y. Dong, N. Wang, S. Cheng, Y. Li, Aluminate based blue phosphors, US Patent 7,390,437 (2008).

[119] M. Yamada, T. Naitou, K. Izuno, H. Tamaki, Y. Murazaki, M. Kameshima, T. Mukai, Red-enhanced white-light-emitting diode using a new red phosphor, Jpn. J. Appl. Phys. **42**, L20 (2003).

[120] S. Liu, D. Tao, X. Yuan, Y. Li, Nitride based red-emitting phosphors, US Patent 8,274,215 (2012).

[121] R. Mueller-Mach, G. Mueller, M. Krames, H. Höppe, F. Stadler, W. Schnick, T. Juestel, P. Scmidt, Highly efficient all-nitride phosphor-converted white light-emitting diode, Phys. Status Solidi A **202**, 1727–1732 (2005).

[122] F. Stadler, O. Oeckler, H. Höppe, M. Möller, R. Pöttgen, B. Mosel, P.Scmidt, V.Duppel, A.Simon, W.Schnick, Crystal structure, physical properties and HRTEM investigation of the new oxonitridosilicate $EuSi_2O_2N_2$, Chem. Eur. J. **12**, 6984–6990 (2006).

[123] V. Bachmann, C. Ronda, O. Oeckler, W. Schnick, A. Meijerink, Color pint tuning for (Ca,Sr,Ba)$Si_2O_2N_2$:Eu^{2+} for white LEDs, Chem. Mater. **21**, 316–325 (2009).

[124] J. van Krevel, J. van Rutten, H. Mandal, H. Hintzen, R. Metselaar, Luminescence properties of terbium-, cerium-, or europium-doped α-sialon materials, J. Solid State Chem. **165**, 19–24 (2002).

[125] N. Hirosaki, R. Xie, K. Kimoto, T. Sekiguchi, Y. Yamamoto, T. Suehiro, M. Mitomo, Characterization and properties of green-emitting β-SiAlON:Eu^{2+} powder phosphors for white light-emitting diodes, Appl. Phys. Lett. **86**, 211905 (2005).

[126] X. Luo, W. Cao, F. Su, The development of silicate matrix phosphors with broad excitation band for phosphor-converted white LED, Chin. Sci. Bull. **53**, 2923–2930 (2008).

[127] H. Höppe, H. Lutz, P. Morys, W. Schnick, A. Seilmeier, Luminescence in Eu^{2+}-doped $Ba_2Si_5N_8$: fluorescence, thermoluminescence, and upconversion, J. Phys. Chem. Sol. **61**, 2001–2006 (2000).

[128] K. Houser, S. Fotios, M. Royer, A test of the s/p ratio as a correlate for brightness perception using rapid-sequential and side-by-side experimental protocols, Leukos **6**(2), 119–137 (2009).

[129] M. D. Fairchild, L. Reniff, Time course of chromatic adaptation for color-appearance judgments, J. Opt. Soc. Am. A **12**(5), 824–833 (1995).

Notes

Notes

Vilniaus universiteto leidykla
Universiteto g. 1, LT-01513 Vilnius
El. p. info@leidykla.vu.lt,
www.leidykla.vu.lt
Tiražas 20 egz.